UNIVERSIDADE DE LISBOA
FACULDADE DE CIÊNCIAS
DEPARTAMENTO DE FÍSICA

One-loop corrections to Higgs decay to dark matter

Pedro Tiago Lopes Gabriel

Mestrado em Física
Especialização em Física Nuclear e Partículas

Dissertação orientada por:
Prof. Dr. Rui Alberto Serra Ribeiro dos Santos

2021

Acknowledgements

First of all, I would like to thank my supervisor, Dr. Rui Santos, for his guidance, support and patience throughout the course of this project. I would also like to acknowledge the other members of the project, Duarte Azevedo, Kodai Sakurai and Margarete Mühlleitner for all their work and dedication which was essential to the success of the project. I want to thank my family for always being supportive and understanding. I also want to thank my friend Manuel Xarepe for the companionship, the discussions and the laughs over the past 6 years of our academic life. Finally, I would like to offer a very special thanks to Sandra Caeiro for her unconditional love and support.

Resumo

À medida que as medições dos acoplamentos do bosão de Higgs se tornam cada vez mais precisas, a sua largura de decaimento poderá tornar-se numa ferramenta poderosa no estudo de extensões ao Modelo Padrão (SM) com sectores escuros, no *Large Hadron Collider* (LHC). Neste trabalho, queremos calcular as correcções electrofracas a 1-loop à amplitude de decaimento do bosão de Higgs para um par de partículas candidatas a matéria escura, no contexto da fase de dubleto escuro do *Next-to-minimal 2-Higgs-doublet Model* (N2HDM), com o objectivo de limitar o espaço de parâmetros do modelo.

Começamos por apresentar os sectores escalar e de Yukawa do N2HDM geral. O N2HDM é uma extensão simples do Modelo Padrão da Física de Partículas (SM) com dois dubletos e um singleto de isospin fraco. O potencial do N2HDM contém duas simetrias $\mathbb{Z}_2$ para além da simetria de CP. Existem várias configurações de vácuo (fases) possíveis no N2HDM, nas quais se inclui a fase de dubleto escuro (DDP). Nesta fase, um dos dubletos e o singleto obtêm um valor de expectação de vácuo (VEV) não-nulo, quebrando uma das simetrias $\mathbb{Z}_2$ do potencial e resultando em dois sectores escalares diferentes: um sector visível composto por dois bosões de Higgs neutros CP-par e um sector escuro composto por um escalar neutro CP-par, um escalar neutro CP-ímpar e dois escalares carregados. No âmbito da DDP, existem quatro processos de decaimento distintos que podem representar o decaimento do bosão de Higgs do Modelo Padrão para um par de partículas de matéria escura.

Para que possamos calcular as correcções radiativas a 1-loop às amplitudes de decaimento destes processos, é necessário proceder à renormalização dos sectores escalar e de gauge do modelo. As massas e as funções de onda são renormalizadas recorrendo ao esquema de renormalização *on-shell* (OS), no qual a forma dos propagadores das partículas a ordens superiores é fixada como sendo igual à do nível-árvore. Em conjunto com o esquema OS, também utilizamos o esquema alternativo de *tadpoles* (AT), através do qual são renormalizados os VEVs. Neste esquema de renormalização, os VEVs sofrem um desvio que resulta em diagramas de Feynman adicionais que contribuem para as correcção a 1-loop dos processos. A carga eléctrica é renormalizada recorrendo ao esquema G_μ. Este esquema trata de correcções logarítmicas que surgem devido às baixas massas dos fermiões em relação à escala de energia electrofraca. O ângulo de mistura dos escalares CP-par, é renormalizado recorrendo ao esquema KOSY, assim denominado em honra a Shinya Kanemura, Yasuhiro Okada, Eibun Senaha, C.-P. Yuan. Juntamente com o esquema KOSY, utilizamos a *pinch technique* de modo a garantir a independência de gauge das amplitudes corrigidas. Os parâmetros restantes do potencial, são renormalizados utilizando três esquemas de renormalização distintos: o esquema $\overline{\text{MS}}$ e dois esquemas dependentes de processos físicos

(*process-dependent*). Em ambos os esquemas *process-dependent*, o processo $H_i \to A_D A_D$ é utilizado como processo auxiliar para renormalizar o processo $H_i \to H_D H_D$. Um dos esquemas é denominado *OS process-dependent* onde as partículas externas que participam no processo auxiliar estão *on-shell*. O outro esquema é denominado *ZEM process-dependent* onde as partículas externas que participam no processo auxiliar têm momento linear nulo.

Neste trabalho definimos também os observáveis que pretendemos calcular. Começamos por definir os conceitos de largura parcial e largura total de decaimento, derivando a sua forma a *leading order* (LO) e a *next-to-leading order* (NLO). Por fim, definimos o conceito de fracção de decaimento, apresentando também a sua forma a LO e a NLO.

Apresentamos dois cenário possíveis para o decaimento do bosão de Higgs para um par de partículas de matéria escura, no contexto da DDP. Estes cenários resultam da hierarquia entre as massas das duas partículas escalares do sector visível do DDP. No primeiro cenário, o cenário do Higgs leve, o bosão de Higgs do modelo padrão corresponde ao escalar visível mais leve, identificado como H_1. No segundo cenário, o cenário do Higgs pesado, o bosão de Higgs corresponde ao escalar visível mais pesado na DDP, identificado como H_2. Para cada cenário, apresentamos a forma explícita das correcções a 1-loop à amplitude do processo de decaimento. Também são apresentadas de forma explícita, as expressões para a largura parcial de decaimento e a fracção de decaimento a NLO. São apontadas algumas diferenças entre os dois cenários, nomeadamente o maior espaço de parâmetros e a contribuição adicional para a largura total de decaimento do processo $H_2 \to H_1 H_1$, ambas no cenário do Higgs pesado.

Relativamente a resultados numéricos, são apresentados dois estudos. No primeiro estudo, observamos como os diferentes esquemas de renormalização utilizados para fixar os contra-termos dos parâmetros m_{22}^2 e λ_8 se comportam relativamente a alguns parâmetros do modelo. Primeiro, abordamos a relação entre a largura parcial de decaimento e o acoplamento escuro $\lambda_{H_1 H_D H_D}$, no limite do modelo do dubleto inerte (IDM). Observamos que o esquema $\overline{\text{MS}}$ é muito sensível à massa do escalar carregado, produzindo correcções muito grandes à largura parcial de decaimento para valores mais altos da massa do escalar carregado. No caso dos esquemas *process-dependent* isto não ocorre, sendo que estes esquemas produzem correcções muito mais pequenas mesmo para valores mais altos da massa do escalar carregado. Estudamos também a relação entre o tamanho das correcções à largura parcial de decaimento e a diferença entre as massas dos escalares neutros do sector escuro. Concluímos que as correcções a 1-loop nos esquemas *process-dependent* são tanto maiores quanto maior é a diferença entre as massas. No caso do esquema $\overline{\text{MS}}$ isto não ocorre, mantendo-se o tamanho das correcções constante relativamente à diferença de massas.

No segundo estudo numérico, realizamos um *scan* no espaço de parâmetros da DDP. Utilizamos o código `ScannerS` para gerar pontos do espaço de parâmetros para cada cenário, considerando constrangimentos teóricos e experimentais. Para cada ponto, é calculada a fracção de decaimento a NLO para o decaimento do bosão de Higgs para um par de partículas de matéria escura, no esquema $\overline{\text{MS}}$ e nos dois esquemas *process-dependent*. Concluímos que o esquema OS *process-dependent* é o mais estável dos três, enquanto que o esquema $\overline{\text{MS}}$ é o mais instável. Concluímos que a instabilidade do esquema $\overline{\text{MS}}$ não pode ser atribuída à escolha de escala de renormalização e que este esquema de renormalização simplesmente não é adequado a este caso em particular. Concluímos também que a estabilidade dos esquemas *process-*

dependent está relacionada com o limite superior de 10 GeV para a diferença entre as massas dos escalares neutros do sector escuro. Por fim, comparamos as fracções de decaimento dos pontos com o actual limite experimental dos decaimentos invisíveis do bosão de Higgs, $BR(h_{125} \to \text{invisible}) < 0.11$, excluindo todos os pontos com correcções à largura parcial de decaimento maiores do que 100%. Concluímos que, se impusermos limites às correcções a 1-loop de modo a que a teoria de perturbações seja válida, a maioria das fracções de decaimento a NLO para os esquemas de renormalização *process-dependent* estão abaixo do limite experimental. Desta forma, ainda não é possível obter constrangimentos para o espaço de parâmetros da DDP do N2HDM a *next-to-leading order*. No entanto, à medida que as medições dos acoplamentos do bosão de Higgs e dos seus decaimentos invisíveis se tornam cada vez mais precisas, estamos certos de que no futuro poderemos utilizar este método para restringir o espaço de parâmetros do modelo.

Palavras Chave: Matéria Escura, Bosão de Higgs, Extensões ao Modelo Padrão, N2HDM, Renormalização.

Abstract

With the measurements of the Higgs boson couplings becoming more and more precise, its invisible decay width may prove to be a powerful tool in probing Standard Model extensions with dark sectors at the Large Hadron Collider (LHC). In this work, we calculate the one-loop electroweak corrections to the partial decay width of the Higgs boson decay into a pair of dark matter particles, in the context of the Next-to-minimal 2-Higgs-doublet model in its dark doublet phase. We start by performing the renormalization of the scalar and gauge sectors of the N2HDM. With the renormalized model, we calculate the expressions for the one-loop corrected partial decay width and branching ratio of the Higgs boson decay into a pair of dark matter particles. In the end, we show that the current measurement on the Higgs-to-invisible branching ratio, $BR(h_{125} \to \text{invisible}) < 0.11$, does not constrain the parameter space of the N2HDM at leading order. We also conclude that, by requiring the one-loop corrections to not be unphysically large, no constraints on the parameter space can be extracted yet at next-to-leading order.

Keywords: Dark Matter, Higgs Boson, Standard Model Extensions, N2HDM, Renormalization.

Contents

List of Figures

List of Abbreviations

1PI	One-particle Irreducible
ATS	Alternative Tadpole Scheme
CP	Charge-Parity
DDP	Dark Doublet Phase
DM	Dark Matter
EW	Electroweak
EWSB	Electroweak Symmetry Breaking
FCNC	Flavour-changing Neutral Current
IDM	Inert Doublet Model
IR	Infrared
LO	Leading Order
MS	Minimal Subtraction
N2HDM	Next-to-Minimal 2-Higgs Doublet Model
NLO	Next-to-Leading Order
OS	On-Shell
QFT	Quantum Field Theory
SM	Standard Model of Particle Physics
UV	Ultraviolet
VEV	Vacuum Expectation Value
WFRC	Wave-function Renormalization Constant
WIMP	Weakly Interacting Massive Particle
ZEM	Zero External Momentum

Chapter 1

Introduction

The discovery of the Higgs boson in 2012 at the Large Hadron Collider [1, 2], gave the world the missing piece of the puzzle that is the Standard Model of Particle Physics (SM). This discovery confirmed the validity of the SM and of the mechanism of electroweak symmetry breaking (EWSB), by which all massive particles in the SM acquire their masses. However, even though the SM is one of the most successful models in physics, it still does not provide the answers to some of particle physics biggest mysteries such as the matter and anti-matter asymmetry, the neutrino masses or the existence of dark matter.

With respect to dark matter (DM), while we do not know much about its nature, there is great evidence of its existence. From gravitational effects on astrophysical scales to cosmological calculations of the relic density of baryonic matter based on the cosmic microwave background radiation, there is overwhelming evidence that what we see is not the whole picture [3]. Currently, one of the most popular candidates for DM is the so-called weakly interacting massive particle (WIMP). The WIMP is described as an elementary particle that may interact through gravity and any force as weak or weaker than the weak interaction. In most models, the WIMP has a mass of the order of the electroweak scale. If we wish to merge the WIMP paradigm with the SM, we must turn to SM extensions. Due to the exceptional agreement between the SM and most of the experimental measurements, any SM extension is strongly constrained as it needs to contain the SM with at least the same experimental agreement than the SM.

One of the simplest SM extensions is the Next-to-minimal 2-Higgs Doublet model (N2HDM) [4–8]. In this model, the scalar sector of the SM is extended by a weak isospin doublet and a real weak isospin singlet [7]. The N2HDM allows for several vacuum configurations that generate DM candidate particles. One of these configurations is the so-called Dark Doublet Phase (DDP). This phase of the N2HDM, is very similar in construction to another SM extension, the Inert Doublet Model (IDM) [9–12]. However, the N2HDM presents a richer phenomenology, introduced by the additional singlet.

In this work, we explore the DDP of the N2HDM with the goal of probing its dark sector. To achieve this, we make use of the precise measurements of the Higgs boson couplings to the SM particles, which are becoming a very powerful tool in limiting the parameter space of SM extensions. When it comes to DM models, a specially useful measurement is the upper limit on the branching ratio of the Higgs boson

decay into invisible particles, which is currently constrained to be $BR(h_{125} \to \text{invisible}) < 0.11$ [13]. The main goal of this work is to calculate at next-to-leading order (NLO) the partial decay width and the branching ratio of the decays within the DDP of the N2HDM that may represent the Higgs boson decay to DM candidates. To calculate these observables at NLO, we must calculate their one-loop corrections which requires the renormalization of the model. In the end, we compare the numerical values of the corrected observables, for the allowed parameter space, to the experimental upper limit. The discussion presented in this thesis is based on the work developed in [14].

This thesis is structured as follows: in chapter 2 we introduce the N2HDM and its DDP. In chapter 3, we discuss the full process of renormalization of the scalar and gauge sectors of the N2HDM. In chapter 4, we determine the expressions for the partial decay width and branching ratio at both LO and NLO. In chapter 5, we discuss two possible scenarios for the decay of the Higgs boson into DM candidates. In chapter 6, we present and discuss our numerical results. Finally, in chapter 7, we draw our final conclusions. This thesis also contains two appendices: in appendix A, we present some additional details related to the DDP of the N2HDM. In appendix B, we present some additional calculations related to the process of renormalization.

Chapter 2

The Next-to-Minimal 2-Higgs Doublet Model

The Next-to-Minimal 2-Higgs Doublet Model (N2HDM) [4–8] is a simple extension of the SM. The N2HDM scalar sector is composed of two complex $SU(2)_L$ doublets of hypercharge 1 and a real $SU(2)_L$ singlet of hypercharge 0. The addition of an extra doublet and an extra singlet, results in a rich phenomenology that allows for the existence of dark matter candidate fields. In the next sections, we discuss the construction of the N2HDM, as well as the specific vacuum configuration that is used in this project.

2.1 Scalar Sector

The scalar sector defines the scalar-scalar and the scalar-gauge interactions. The scalar Lagrangian $\mathcal{L}_{scalar}$ is defined as

$$\mathcal{L}_{scalar} = (D_\mu \Phi_i)^\dagger (D^\mu \Phi_i) + \frac{1}{2}(\partial_\mu \Phi_S)(\partial^\mu \Phi_S) - V_{scalar}, \tag{2.1}$$

with Φ_i ($i \in \{1, 2\}$) being the complex $SU(2)_L$ doublets and Φ_S being the real $SU(2)_L$ singlet. D_μ is the covariant derivative and is defined as

$$D_\mu = \partial_\mu + i g_L \frac{\sigma^a}{2} W_\mu^a + i g_Y \frac{Y}{2} B_\mu, \tag{2.2}$$

where σ^a ($a \in \{1, 2, 3\}$) are the Pauli matrices and Y is the hypercharge. g_L and g_Y are the $SU(2)_L$ and $U(1)_Y$ coupling constants respectively, and W_μ^a and B_μ are their corresponding gauge fields. The last term of equation 2.1 is the scalar potential V_{scalar}, that we will discuss further in the next subsection.

2.1.1 Scalar Potential

The most general renormalizable form of the N2HDM potential, includes all possible combinations of the fields Φ_1, Φ_2 and Φ_S up to the quartic terms that are compatible with the SM symmetries. In this

project, we impose additional constraints to the model in the form of two $\mathbb{Z}_2$ symmetries, defined as $\mathbb{Z}_2^{(1)}$ and $\mathbb{Z}_2^{(2)}$, which are given by

$$\mathbb{Z}_2^{(1)} : \Phi_1 \to \Phi_1,\ \Phi_2 \to -\Phi_2,\ \Phi_S \to \Phi_S, \tag{2.3a}$$

$$\mathbb{Z}_2^{(2)} : \Phi_1 \to \Phi_1,\ \Phi_2 \to \Phi_2,\ \Phi_S \to -\Phi_S. \tag{2.3b}$$

The resulting potential V_{scalar} is

$$\begin{aligned} V_{scalar} = {} & m_{11}^2(\Phi_1^\dagger\Phi_1) + m_{22}^2(\Phi_2^\dagger\Phi_2) - m_{12}^2(\Phi_1^\dagger\Phi_2 + h.c.) + \frac{\lambda_1}{2}(\Phi_1^\dagger\Phi_1)^2 + \frac{\lambda_2}{2}(\Phi_2^\dagger\Phi_2)^2 \\ & + \lambda_3(\Phi_1^\dagger\Phi_1)(\Phi_2^\dagger\Phi_2) + \lambda_4(\Phi_1^\dagger\Phi_2)(\Phi_2^\dagger\Phi_1) + \frac{\lambda_5}{2}[(\Phi_1^\dagger\Phi_2)^2 + h.c.] \\ & + \frac{1}{2}m_S^2\Phi_S^2 + \frac{\lambda_6}{8}\Phi_S^4 + \frac{\lambda_7}{2}(\Phi_1^\dagger\Phi_1)\Phi_S^2 + \frac{\lambda_8}{2}(\Phi_2^\dagger\Phi_2)\Phi_S^2, \end{aligned} \tag{2.4}$$

with m_{11}, m_{22}, m_{12} and m_S having dimension of mass and λ_i ($i \in \{1, 8\}$) being dimensionless coefficients. We take the model to be CP-conserving which means that all coefficients can be defined as real.

The doublet and singlet fields can be parameterized as

$$\Phi_1 = \begin{pmatrix} \phi_1^+ \\ \frac{1}{\sqrt{2}}(v_1 + \rho_1 + i\eta_1) \end{pmatrix}, \quad \Phi_2 = \begin{pmatrix} \phi_2^+ \\ \frac{1}{\sqrt{2}}(v_2 + \rho_2 + i\eta_2) \end{pmatrix}, \quad \Phi_S = v_S + \rho_S, \tag{2.5}$$

where ρ_1, ρ_2 and ρ_S are neutral CP-even fields, η_1 and η_2 are neutral CP-odd fields, ϕ_1^+ and ϕ_2^+ are charged complex fields. The most general non-charge breaking vacuum state has the form

$$\langle\Phi_1\rangle = \begin{pmatrix} 0 \\ \frac{v_1}{\sqrt{2}} \end{pmatrix}, \quad \langle\Phi_2\rangle = \begin{pmatrix} 0 \\ \frac{v_2}{\sqrt{2}} \end{pmatrix}, \quad \langle\Phi_S\rangle = v_S, \tag{2.6}$$

with v_1, v_2 and v_S being the vacuum expectation values (VEV) of Φ_1, Φ_2 and Φ_S respectively. These VEVs, spontaneously break the $SU(2)_L \otimes U(1)_Y$ symmetry to a $U(1)_{EM}$. The doublet VEVs are related to the SM VEV through the relation

$$v_{SM}^2 = v_1^2 + v_2^2. \tag{2.7}$$

We require the potential to be minimized at the VEV. Therefore, the following stationary conditions must be met

$$\left\langle \frac{\partial V}{\partial \Phi_1} \right\rangle = 0 \quad \Rightarrow \quad v_2 m_{12}^2 - v_1 m_{11}^2 = \frac{1}{2}v_1(v_1^2\lambda_1 + v_2^2\lambda_{345} + v_S^2\lambda_7), \tag{2.8a}$$

$$\left\langle \frac{\partial V}{\partial \Phi_2} \right\rangle = 0 \quad \Rightarrow \quad v_1 m_{12}^2 - v_2 m_{22}^2 = \frac{1}{2}v_2(v_1^2\lambda_{345} + v_2^2\lambda_2 + v_S^2\lambda_8), \tag{2.8b}$$

$$\left\langle \frac{\partial V}{\partial \Phi_S} \right\rangle = 0 \quad \Rightarrow \quad -v_S m_S^2 = \frac{1}{2}v_S(v_1^2\lambda_7 + v_2^2\lambda_8 + v_S^2\lambda_6), \tag{2.8c}$$

where $\lambda_{345} = \lambda_3 + \lambda_4 + \lambda_5$. These minimum conditions allow us to write m_{11}^2, m_{22}^2 and m_S^2 as functions of the VEVs and the λ parameters. The parameterizations presented in equations 2.5 and 2.6, represent the most general case of the N2HDM also know as the broken phase of the N2HDM. This phase does not contain a dark sector. However, by choosing different combinations for the values of the VEVs, we get different phases of the model, some of which feature dark sectors. In this project, we will be working with the Dark Doublet Phase (DDP) in which only one of the doublets and the singlet acquire non-vanishing VEV. This phase is discussed further in section 2.3. The remaining phases of the N2HDM are discussed with greater detail in [4–8].

2.2 The Yukawa Lagrangian

The Yukawa Lagrangian describes the interactions between the scalar fields and the fermions. The fermions are treated in the same way as in the SM. Fermions are grouped into triplets in flavour space

$$\psi \in \left\{ U \coloneqq \begin{pmatrix} u \\ c \\ t \end{pmatrix}, \quad D \coloneqq \begin{pmatrix} d \\ s \\ b \end{pmatrix}, \quad E \coloneqq \begin{pmatrix} e \\ \mu \\ \tau \end{pmatrix}, \quad N \coloneqq \begin{pmatrix} \nu_e \\ \nu_\mu \\ \nu_\tau \end{pmatrix} \right\}, \tag{2.9}$$

where U represents the up-type quarks, D represents the down-type quarks, E represents the charged leptons and N represents the neutrinos. All fermionic fields are also decomposed into their chiral projections

$$\psi = \psi_R + \psi_L, \tag{2.10}$$

where $\Psi_{R/L}$ represents the chiral right-hand/left-hand component of the fermion. All left-handed states are then grouped into $SU(2)_L$ doublets

$$Q_L \coloneqq \begin{pmatrix} U_L \\ D_L \end{pmatrix} = \begin{pmatrix} (u_L, c_L, t_L)^T \\ (d_L, s_L, b_L)^T \end{pmatrix}, \quad L_L \coloneqq \begin{pmatrix} N_L \\ E_L \end{pmatrix} = \begin{pmatrix} (\nu_{e,L}, \nu_{\mu,L}, \nu_{\tau,L})^T \\ (e_L, \mu_L, \tau_L)^T \end{pmatrix}, \tag{2.11}$$

while all the right-handed states are grouped into $SU(2)_L$ singlets[1]

$$U_R \coloneqq \begin{pmatrix} u_R \\ c_R \\ t_R \end{pmatrix}, \quad D_R \coloneqq \begin{pmatrix} d_R \\ s_R \\ b_R \end{pmatrix}, \quad E_R \coloneqq \begin{pmatrix} e_R \\ \mu_R \\ \tau_R \end{pmatrix}. \tag{2.12}$$

The most general Yukawa Lagrangian is composed of all possible combinations of the $SU(2)_L$ doublets ψ_L, the $SU(2)_L$ Higgs doublets Φ_1 and Φ_2 and the $SU(2)_L$ singlets ψ_R in such way that the Lagrangian remains invariant under $SU(2)_L \otimes U(1)_Y$ transformations. Thus, the Yukawa Lagrangian $\mathcal{L}_{Yukawa}$ is written as

$$\mathcal{L}_{Yukawa} = -\sum_i \bar{Q}_L^T Y_{U,i} \tilde{\Phi}_i U_R + \bar{Q}_L^T Y_{D,i} \Phi_i D_R + \bar{L}_L^T Y_{E,i} \Phi_i E_R + h.c., \tag{2.13}$$

[1] Just like in the SM, neutrinos are considered to only have LH chiral projection.

with $Y_{\psi,i}$ being the 3×3 Yukawa coupling matrices in flavour space, $\tilde{\Phi}_i$ being defined as $\epsilon_{ij}\Phi_j^*$ with ϵ_{ij} being the totally anti-symmetric tensor in two dimensions and $\bar{\psi}_L$ being the anti-fermionic field.

Since the Yukawa coupling matrices are not necessarily diagonal in flavour space, equation 2.13 allows for the occurrence of flavour-changing neutral currents (FCNC) at tree level which are very constrained by experimental observation. To prevent FCNCs at tree-level, the $\mathbb{Z}_2$ symmetry presented in equation 2.3a is extended to the fermions in such way that all fermions only couple to the Higgs doublet Φ_1 [15].

2.3 The Dark Doublet Phase

The Dark Doublet Phase (DDP), is one of the three phases of the N2HDM that allows for the existence of a dark sector. In the DDP, only one of the $SU(2)_L$ Higgs doublets and the singlet acquire non-vanishing VEVs. If we choose Φ_1 to be the doublet with non-null VEV, the $\mathbb{Z}_2^{(2)}$ symmetry in equation 2.3 is spontaneously broken while the $\mathbb{Z}_2^{(1)}$ symmetry is conserved. This means that the fields originating from Φ_2 form a dark sector of particles in the sense that they are odd under $\mathbb{Z}_2$ while all other fields are even. Therefore, the vacuum configuration in equation 2.6 becomes

$$\langle \Phi_1 \rangle = \frac{1}{\sqrt{2}} \begin{pmatrix} 0 \\ v \end{pmatrix}, \quad \langle \Phi_2 \rangle = \begin{pmatrix} 0 \\ 0 \end{pmatrix}, \quad \langle \Phi_S \rangle = v_S, \tag{2.14}$$

where we used the relation in equation 2.7 to set v_1 equal to the SM VEV v. Also, with this vacuum configuration, the minimum conditions in equation 2.8, become

$$m_{11}^2 = -\frac{1}{2}(v^2\lambda_1 + v_S^2\lambda_7), \tag{2.15a}$$

$$m_{12}^2 = 0, \tag{2.15b}$$

$$m_S^2 = -\frac{1}{2}(v^2\lambda_7 + v_S^2\lambda_6). \tag{2.15c}$$

From equation 2.15b we see that the parameter m_{12} is identically zero in this phase of the N2HDM, meaning that the DDP contains only 11 independent scalar parameters instead of the original 12. In this vacuum configuration, the CP-even fields ρ_1 and ρ_S are allowed to mix because they have the same quantum numbers. This includes the new "darkness" quantum number associated with the conserved $\mathbb{Z}_2^{(1)}$ symmetry.

2.3.1 Mass Eigenstates and Parametrization

The rotation to the mass basis, leads to a reparameterization of the potential. This happens because the mass matrices of the fields are required to be diagonal in the mass basis. With this constraint, we obtain expressions that allow us to write the gauge parameters as functions of the physical parameters. The mass

matrices are given by

$$M^{\rho}_{ij} = \frac{\partial^2 V_{scalar}}{\partial\rho_i \partial\rho_j}, \quad M^{\eta}_{kl} = \frac{\partial^2 V_{scalar}}{\partial\eta_k \partial\eta_l}, \quad M^{\pm}_{kl} = \frac{\partial^2 V_{scalar}}{\partial\phi^+_k \partial\phi^-_l}, \tag{2.16}$$

with $i, j \in \{1, 2, S\}$ and $k, l \in \{1, 2\}$ and where M^{ρ} represents the CP-even fields 3×3 mass matrix, M^{η} represents the CP-odd fields 2×2 mass matrix and $M^{\pm}$ represents the charged fields 2×2 mass matrix. Since there is no mixing in the CP-odd and charged sectors, their corresponding mass matrices are already diagonal, meaning that the CP-odd fields and the charged fields are already mass eigenstates. The same applies to the CP-even field ρ_2 which is a mass eigenstate as well. From this point onward, these fields will be relabeled as

$$H_D = \rho_2, \tag{2.17a}$$

$$G^0 = \eta_1, \; A_D = \eta_2, \tag{2.17b}$$

$$G^{\pm} = \phi^{\pm}_1, \; H^{\pm}_D = \phi^{\pm}_2. \tag{2.17c}$$

The mass eigenstates G^0 and $G^{\pm}$ come from the SM-like doublet Φ_1 and are the Goldstone bosons. The mass eigenstates H_D, A_D and $H^{\pm}_D$ come from the dark doublet Φ_2 and form the dark sector of the DDP. The mass matrices of the CP-odd and charged fields can thus be expressed as

$$M^{\eta} = diag(0, m^2_{A_D}), \tag{2.18a}$$

$$M^{\pm} = diag(0, m^2_{H^{\pm}_D}). \tag{2.18b}$$

With respect to the CP-even sector, the mass matrix is not diagonal due to the mixing between the fields ρ_1 and ρ_S. Since we already established that the dark CP-even field H_D is a mass eigenstate, the CP-even mass matrix can be reduced to a 2×2 matrix referring only to the masses of the fields ρ_1 and ρ_S. This mass matrix has the explicit form

$$M^{\rho} = \begin{pmatrix} v^2\lambda_1 & vv_S\lambda_7 \\ vv_S\lambda_7 & v^2_S\lambda_6 \end{pmatrix}, \tag{2.19}$$

where we used the minimum conditions in equation 2.15 to write the parameters m^2_{11} and m^2_S as functions of the VEVs and the λ parameters. The diagonalization of the CP-even mass matrix is performed, using the rotation matrix $R(\alpha)$, defined explicitly as

$$R(\alpha) = \begin{pmatrix} c_\alpha & s_\alpha \\ -s_\alpha & c_\alpha \end{pmatrix}, \tag{2.20}$$

where c_α and s_α represent the cosine and sine of the mixing angle α, respectively. The CP-even mass matrix is then diagonalized through the relation

$$R(\alpha) M^{\rho} R(\alpha)^T = D^2 = diag(m^2_{H_1}, m^2_{H_2}), \tag{2.21}$$

where m_{H_1} and m_{H_2} represent the masses of the visible CP-even mass eigenstates labeled H_1 and H_2. By convention, the visible CP-even physical fields are ordered by ascending mass

$$m^2_{H_1} \leq m^2_{H_2}. \tag{2.22}$$

The CP-even fields in the gauge basis ρ_1 and ρ_S are related to their mass basis counterparts H_1 and H_2 through the same rotation martix that we use to diagonalize the CP-even mass matrix. This relation is expressed as

$$\begin{pmatrix} H_1 \\ H_2 \end{pmatrix} = R(\alpha)^T \begin{pmatrix} \rho_1 \\ \rho_S \end{pmatrix}, \tag{2.23}$$

meaning that the CP-even mass eigenstates H_1 and H_2 are linear combinations of the fields ρ_1 and ρ_S that are written explicitly as

$$H_1 = \rho_1 c_\alpha - \rho_S s_\alpha, \tag{2.24a}$$

$$H_2 = \rho_1 s_\alpha + \rho_S c_\alpha. \tag{2.24b}$$

Like mentioned earlier, this rotation from the gauge basis to the mass basis leads to a reparameterization of the potential. In this reparameterization we choose as independent parameters of the scalar potential in the mass basis the following set

$$\{m^2_{H_1},\ m^2_{H_2},\ m^2_{H_D},\ m^2_{A_D},\ m^2_{H^\pm_D},\ v,\ v_S,\ \alpha,\ m^2_{22},\ \lambda_2,\ \lambda_8\}. \tag{2.25}$$

The relations between the parameters in the gauge and mass basis are given in Appendix A.1.

2.3.2 Higgs Decays to Dark Matter Candidates

The goal of this project, is to study the possible decays of the SM Higgs boson to the dark matter candidates. In the DDP of the N2HDM, either of the two visible CP-even mass eigenstates H_1 and H_2 can be identified as the SM Higgs boson. Therefore, we want to study the decays of both of these fields to the dark matter candidates.

To be considered dark matter, a particle must meet certain requirements. Two of those requirements that are relevant to us are that the particle must have no electric charge [16] and it must be stable [17]. From the particles that form the dark sector of the DDP, only H_D and A_D meet the first requirement. The stability requirement, means that the dark matter particle must be the lightest of the two particles. Since we cannot establish a mass ordering between H_D and A_D, both particles can be DM candidates, depending on which has the smaller mass. In this work, we will focus on the case where $m_{H_D} < m_{A_D}$, meaning that H_D is our dark matter candidate. However, we checked the results for the case in which A_D is the dark matter particle and obtained very similar results.

We can then identify two possible decays within the DDP that may represent the decay of the SM Higgs boson to a pair of dark matter particles. These decays are

$$H_1 \to H_D H_D, \tag{2.26a}$$

$$H_2 \to H_D H_D. \tag{2.26b}$$

The couplings associated with the interactions between the visible CP-even scalars and the dark neutral scalars are very important for our calculations and are given by

$$\lambda_{H_i H_D H_D} = \frac{R_{i1}}{v}\left[\lambda_8 v_S^2 + 2\left(m_{22}^2 - m_{H_D}^2\right)\right] - R_{i2}\lambda_8 v_S, \tag{2.27a}$$

$$\lambda_{H_i A_D A_D} = \frac{R_{i1}}{v}\left[\lambda_8 v_S^2 + 2\left(m_{22}^2 - m_{A_D}^2\right)\right] - R_{i2}\lambda_8 v_S, \tag{2.27b}$$

with $i \in \{1, 2\}$ and R being the rotation matrix defined in equation 2.20. The full list of the DDP's trilinear scalar couplings is presented in appendix A.2. From equation 2.27, we see that the only difference between the couplings of H_1 and H_2 with H_D and A_D is the masses of the dark particles.

Chapter 3

Renormalization of the N2HDM

When dealing with perturbative corrections in Quantum Field Theories (QFT), it is inevitable that one faces divergent integrals at some point. These integrals usually arise from Feynman diagrams containing loops such as the ones depicted in figure 3.1. As an example, let us consider the typical loop integral

$$\int_0^\infty \frac{d^4q}{(2\pi)^4}\frac{1}{q^2-m^2}, \tag{3.1}$$

where q is the loop momentum and m is the mass of the loop particle. It is clear that, for $q \to \infty$ the integral diverges. These types of divergences are called ultraviolet (UV) divergences because they are associated with high loop momentum. If we make $m = 0$, we see that another divergence arises for $q \to 0$. These are called infrared (IR) divergences because they are associated with low loop momentum. If we expect to be able to draw physically relevant conclusions from the model, we need to treat these divergences. Both types of divergences have to be treated separately. In this project, we address only the UV divergences since none of the processes that we are interested in contains IR divergences at one-loop.

3.1 Renormalization and Regularization

Before we can renormalize the model we need to isolate the divergences. This is achieved through the process of regularization. While there are several methods of regularization, one of the most common is dimensional regularization[1] [18]. In dimensional regularization, the divergent integrals are solved in general D dimensions instead of four space-time dimensions. This turns the divergent integrals into well defined, solvable integrals. D is commonly defined as

$$D = 4 - 2\epsilon, \tag{3.2}$$

[1] Dimensional regularization preserves the gauge structure of Green's functions at one-loop.

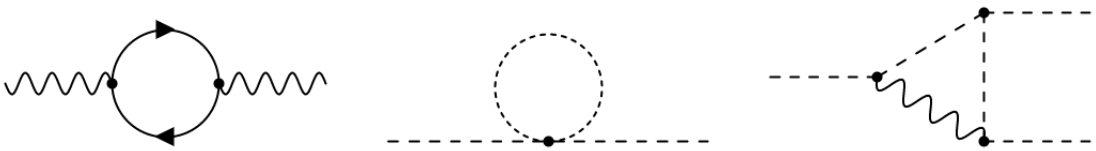

Figure 3.1: Loop diagrams. Some examples of possible Feynman loop diagrams.

with ϵ being the regulator. Solving the loop integral in equation 3.1 using dimensional regularization, isolates the divergent part (as well as a finite part that comes with it) in the term

$$\Delta = \frac{1}{\epsilon} - \gamma_E + \ln 4\pi, \tag{3.3}$$

where γ_E is the Euler-Mascheroni constant. In the limit $\epsilon \to 0$, we recover the physical dimension $D = 4$ and the divergence becomes explicit.

With the loop integrals regularized, we can treat the UV divergences by renormalizing the model. In the process of renormalization, we assume that each of the parameters of the model is a bare parameter. This bare parameter ρ_0 is infinite by definition and can be decomposed into a finite part ρ and an infinite part $\delta\rho$ such that

$$\rho_0 = \rho + \delta\rho. \tag{3.4}$$

The finite term is the renormalized parameter and can be identified as the physical parameter. The infinite term is the counter-term of the parameter. These counter-terms must then be fixed in such way as to cancel out the divergent parts of the loop integrals [19]. For n independent parameters, n renormalization conditions are needed to fix all the counter-terms.

If we want not only a finite S matrix but also finite Green's functions, a similar procedure must be applied to the fields' wave-functions. We decompose the bare wave-function ϕ_0 into a renormalized wave-function ϕ and a wave-function renormalization constant (WFRC) $\delta\phi$ by scaling them as

$$\phi_0 = \sqrt{Z_\phi}\phi \approx \left(1 + \frac{\delta Z_\phi}{2}\right)\phi, \tag{3.5}$$

where the factor $\sqrt{Z_\phi}$ is the field strength renormalization constant. The WFRC in the last step of equation 3.5 is obtained through an expansion of the square-root around unity, up to NLO. In a similar way to the renormalization of the parameters, for m fields, m renormalization conditions are needed in order to fix all the WFRCs. The renormalization conditions for parameters and wave-functions are determined using renormalization schemes. The schemes used in this project are discussed in the next sections.

After all parameters and wave-functions are renormalized, all divergences vanish and all experimentally measurable results are finite, allowing us to calculate higher order corrections to the observable quantities of the model. Since we are only interested in studying the processes in equation 2.26, we do

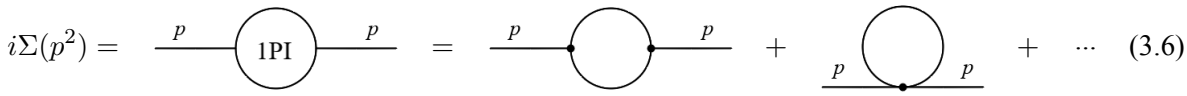

(3.6)

Figure 3.2: One-particle irreducible Feynman diagrams for the propagator. The 1PI Feynman diagrams for the propagator are the set of loop diagrams that cannot be reduced to simpler loop diagrams by a simple cut. These types of loop Feynman diagrams, with only one initial and final states are called the self-energies of the field.

not need to renormalize the entire model. Instead, we only need to renormalize the parameters appearing in equation 2.27 as well as the fields H_1, H_2, H_D and A_D[2].

3.2 On-Shell Renormalization Scheme

One of the more common renormalization schemes is the On-Shell (OS) renormalization scheme. In the OS scheme, it is assumed that all particles of the model are on their mass-shell. This means that the particles obey the condition $p^2 = m^2$ and are therefore physical. Using this renormalization scheme we are able to fix all mass and WFRCs.

To better understand the OS scheme, let us consider a scalar particle ϕ of mass m. The motion of this particle through space-time is ruled by a function G of its momentum called the propagator. This propagator is a Green's function of the field's equations of motion. At all orders in perturbation theory, the propagator can be defined as a geometric series

$$\begin{aligned} G(p^2) &= \int d^4x \, \langle 0|T\phi(x)\phi^*(0)|0\rangle \\ &= \frac{i}{p^2-m^2} + \frac{i}{p^2-m^2} i\Sigma_\phi(p^2) \frac{i}{p^2-m^2} + \frac{i}{p^2-m^2}\left(i\Sigma_\phi(p^2)\frac{i}{p^2-m^2}\right)^2 + \dots \\ &= \frac{i}{p^2-m^2}\sum_{n=0}^{\infty}\left(\frac{-\Sigma_\phi(p^2)}{p^2-m^2}\right)^n = \frac{i}{p^2-m^2+\Sigma_\phi(p^2)}, \end{aligned} \tag{3.7}$$

where p is the momentum of the field, $|0\rangle$ represents the vacuum state, T is the time-ordering operator and $i\Sigma_\phi(p^2)$ represents the sum of all the field's truncated one-particle irreducible (1PI) Feynman diagrams, as shown in figure 3.2. A 1PI Feynman diagram is any diagram that cannot be separated into two distinct diagrams by removing a single line [19]. The sum of the 1PI diagrams with two external fields, may also be referred to as a self-energy.

[2] Although the processes we are studying do not involve the field A_D, its renormalization is needed for the renormalization of the processes $H_i \to H_D H_D$. This is discussed in subsection 3.7.2. Moreover, to calculate the branching ratio at NLO we would also need to renormalize the process $H_i \to A_D A_D$.

The goal of the OS scheme is to keep the form of the propagator at the next order in perturbation theory. This will fix the mass and WFRCs. We start with the bare propagator G_0 which is defined at the lowest order. Using the definition of the propagator in equation 3.7 we obtain

$$\begin{aligned} G_0 &= \int d^4x \, \langle 0|T\phi_0(x)\phi_0^*(0)|0\rangle = \frac{i}{p^2 - m_0^2 + \Sigma_\phi(p^2)} \\ &\Rightarrow \sqrt{Z_\phi}^* \int d^4x \, \langle 0|T\phi(x)\phi^*(0)|0\rangle \sqrt{Z_\phi} = \frac{i}{p^2 - m^2 + \Sigma_\phi(p^2) + \delta m^2} \\ &\Rightarrow \int d^4x \, \langle 0|T\phi(x)\phi^*(0)|0\rangle = \frac{i}{\sqrt{Z_\phi}^* \left(p^2 - m^2 + \Sigma_\phi(p^2) + \delta m^2\right) \sqrt{Z_\phi}} \\ &\Rightarrow G(p^2) \approx \frac{i}{p^2 - m^2 + \hat{\Sigma}_\phi(p^2)}, \end{aligned} \tag{3.8}$$

where $G(p^2)$ is now the renormalized propagator and $\hat{\Sigma}_\phi(p^2)$ represents the renormalized self-energy. In the last step of equation 3.8 we ignore all terms of order $\mathcal{O}\left(\delta^2\right)$ and above. The renormalized self-energy is thus written as

$$\hat{\Sigma}_\phi(p^2) = \Sigma_\phi(p^2) - \delta m^2 + \frac{\delta Z_\phi^*}{2}(p^2 - m^2) + (p^2 - m^2)\frac{\delta Z_\phi}{2}, \tag{3.9}$$

where we used the expansion in equation 3.5.

As mentioned earlier, the fixing of the counter-terms is achieved by setting conditions for the renormalized propagator in equation 3.8. This translates into conditions for the renormalized self-energy. The application of these conditions is, in general, straightforward. However, we are faced with some subtleties that we must deal with, due to the mixing of the fields at one-loop. In the next subsections we discuss the application of these conditions in the cases of non-mixing and mixing fields.

3.2.1 Renormalization Conditions for Non-mixing Fields

In the OS scheme, there are two main conditions that are applied to the renormalized propagator: (1) the renormalized mass of the field must be the pole of the propagator and (2) the residue of the field's propagator must be fixed at i. The first condition, means that the mass must be physical and, therefore, the field must be on its mass shell. From the renormalized propagator in equation 3.8, we easily conclude that for the renormalized mass to be the pole of the propagator, the renormalized self-energy, must vanish at the pole $p^2 = m^2$. Evaluating the expression in equation 3.9 at the pole and setting it equal to zero, we get the expression

$$\delta m^2 = \Sigma_\phi(m^2), \tag{3.10}$$

fixing the mass counter-term for the field.

To use the second condition, we need to go through a few more steps. First, we must preform a Taylor

expansion, up to NLO, of the denominator of the renormalized propagator around the pole

$$\begin{aligned} iG^{-1}(p^2) &= p^2 - m^2 + \hat{\Sigma}_\phi(p^2) \\ &\approx \left(1 + \frac{\partial \hat{\Sigma}_\phi(p^2)}{\partial p^2}\bigg|_{p^2=m^2}\right)(p^2 - m^2). \end{aligned} \tag{3.11}$$

Then we take the residue of the propagator at the pole. Since it is a simple pole, the residue is given by

$$\begin{aligned} Res(G(p^2), m^2) &= \lim_{p^2 \to m^2} \left[(p^2 - m^2) i \left(1 + \frac{\partial \hat{\Sigma}_\phi(p^2)}{\partial p^2}\bigg|_{p^2=m^2}\right)^{-1} (p^2 - m^2)^{-1}\right] \\ &= i \left(1 + \frac{\partial \hat{\Sigma}_\phi(p^2)}{\partial p^2}\bigg|_{p^2=m^2}\right)^{-1}. \end{aligned} \tag{3.12}$$

Requiring the residue in equation 3.12 to be i, yields the condition

$$\frac{\partial \hat{\Sigma}_\phi(p^2)}{\partial p^2}\bigg|_{p^2=m^2} = 0. \tag{3.13}$$

Using the renormalized self-energy expression in equation 3.9, and applying the condition in equation 3.13, we obtain the expression

$$\delta Z_\phi = -\,\mathrm{Re}\left\{\frac{\partial \Sigma_\phi(p^2)}{\partial p^2}\bigg|_{p^2=m^2}\right\}, \tag{3.14}$$

fixing the WFRC.

For a non-mixing field at one-loop, the WFRC and the mass counter-term are fixed through the expressions in equations 3.10 and 3.14 respectively. For a set of mixing fields, although the process is very similar, some changes must be made.

3.2.2 Renormalization Conditions for Mixing Fields

Let us consider two mixing fields ϕ_1 and ϕ_2 with masses m_1 and m_2 respectively, containing the same quantum numbers. They can be paired into a vector Φ such that

$$\Phi = \begin{pmatrix} \phi_1 \\ \phi_2 \end{pmatrix}. \tag{3.15}$$

The renormalization of the vector's wave-function can be done through a decomposition analogous to the one in equation 3.5. Defining Φ_0 as the bare wave-function, we obtain the expression

$$\Phi_0 = \begin{pmatrix} \phi_{1,0} \\ \phi_{2,0} \end{pmatrix} \approx \left(\mathbb{I}_{2\times 2} + \frac{\delta Z_\Phi}{2}\right) \begin{pmatrix} \phi_1 \\ \phi_2 \end{pmatrix}, \tag{3.16}$$

where $\mathbb{I}_{2\times2}$ is the 2×2 identity matrix and δZ_Φ is a 2×2 matrix containing the WFRCs, written as

$$\delta Z_\Phi = \begin{pmatrix} \delta Z_{\phi_1\phi_1} & \delta Z_{\phi_1\phi_2} \\ \delta Z_{\phi_2\phi_1} & \delta Z_{\phi_2\phi_2} \end{pmatrix}. \tag{3.17}$$

The renormalized propagator for the doublet Φ can be defined in an analogous way to the one in equation 3.8 and is best expressed through its inverse

$$G_\Phi^{-1}(p^2) = -i\left(p^2\mathbb{I}_{2\times2} - M^2 + \hat{\Sigma}_\Phi(p^2)\right), \tag{3.18}$$

where M^2 is the diagonal matrix containing the squared masses for the fields ϕ_1 and ϕ_2 and $\hat{\Sigma}_\Phi(p^2)$ is a symmetric 2×2 matrix containing the renormalized self-energies for the mixing fields. The renormalized self-energy matrix elements are defined in a similar way to the expression in equation 3.9

$$\hat{\Sigma}_{\phi_i\phi_j}(p^2) = \Sigma_{\phi_i\phi_j}(p^2) - \delta M_{ij}^2 + \frac{\delta Z^*_{\phi_j\phi_i}}{2}(p^2 - M_{jj}^2) + (p^2 - M_{ii}^2)\frac{\delta Z_{\phi_i\phi_j}}{2}, \tag{3.19}$$

with $i, j \in \{1, 2\}$ and where $\Sigma_{\phi_i\phi_j}(p^2)$ represents the sum of the 1PI self-energy Feynman diagrams with ϕ_i in the initial state and ϕ_j in the final state and δM^2 is a symmetric 2×2 matrix containing the mass counter-terms[3].

The renormalization conditions introduced in subsection 3.2.1 still apply in the case of mixing fields. In this context, condition 1 means that for $p^2 = m_i^2$, the i-th diagonal element of the propagator should vanish. This translates into the following set of conditions

$$\hat{\Sigma}_{\phi_i\phi_i}(m_i^2) = 0. \tag{3.20}$$

Applying the set of conditions in equation 3.20 to the diagonal renormalized self-energy elements using the expression in equation 3.19, we are able to obtain the diagonal mass counter-terms

$$\delta M_{ii}^2 = \Sigma_{\phi_i\phi_i}(m_i^2). \tag{3.21}$$

Condition 2 can be applied in a way equivalent to the non-mixing case. By expanding the inverted propagator in equation 3.18 around the pole $p^2\mathbb{I}_{2\times2} - M^2$ and requiring the residue of the i-th diagonal element to be i at $p^2 = m_i^2$. This produces the set of conditions

$$\left.\frac{\partial\hat{\Sigma}_{\phi_i\phi_i}(p^2)}{\partial p^2}\right|_{p^2=m_i^2} = 0. \tag{3.22}$$

The set of conditions in equation 3.22 enables us to obtain the diagonal WFRCs

$$\delta Z_{\phi_i\phi_i} = -\,\mathrm{Re}\left\{\left.\frac{\partial\Sigma_{\phi_i\phi_i}(p^2)}{\partial p^2}\right|_{p^2=m_i^2}\right\}. \tag{3.23}$$

[3]The matrix δM^2 is, in general, not diagonal.

The main difference between the non-mixing and the mixing cases is the off-diagonal elements of both δM^2 and δZ_Φ matrices. In general, these elements are not zero and contribute to the renormalization of the model, meaning that they must be calculated as well. In the context of the OS scheme, a third set of conditions needs to be applied when dealing with mixing fields. Since we assume that particles are on their mass shell, no mixing should be allowed when $p^2 = m_i^2$. This means, that both off-diagonal self-energies should vanish at both $p^2 = m_1^2$ and $p^2 = m_2^2$, which results in the four conditions

$$\begin{aligned} \hat{\Sigma}_{\phi_i\phi_j}(m_i^2) &= 0, \\ \hat{\Sigma}_{\phi_i\phi_j}(m_j^2) &= 0, \end{aligned} \tag{3.24}$$

with $i \neq j$. These four conditions can be used to obtain expressions for both the off-diagonal counter-terms and their complex conjugates. However, from equation 3.19 and based on the fact that both $\Sigma_\Phi(p^2)$ and δM^2 are symmetric matrices, we conclude that $\delta Z_{\phi_i\phi_j} = \delta Z^*_{\phi_i\phi_j}$, meaning that $\delta Z_{\phi_i\phi_j}$ must be real. This reduces the initial set of four conditions to only two

$$\hat{\Sigma}_{\phi_i\phi_j}(m_j^2) = 0. \tag{3.25}$$

The conditions in equation 3.25 result in the expressions for the off-diagonal WFRCs

$$\delta Z_{\phi_i\phi_j} = \frac{2}{m_i^2 - m_j^2} \operatorname{Re}\{\Sigma_{\phi_i\phi_j}(m_j^2) - \delta M_{ij}^2\}. \tag{3.26}$$

However, we are yet to fix the off-diagonal mass counter-terms. The expressions for these counter-terms depend on the renormalization scheme used for the so-called tadpole terms. This is discussed in detail in the next section.

3.3 Tadpole Renormalization

In general, the N2HDM scalar potential contains terms that are linear in the CP-even fields ρ_1, ρ_2 and ρ_S. These terms are called the tadpole terms because they are represented by Feynman diagrams like the ones in figure 3.3, which resemble a tadpole. These tadpole terms can be obtained through the relation

$$T_i = \left\langle \frac{\partial V}{\partial \rho_i} \right\rangle, \tag{3.27}$$

with $i \in \{1, 2, S\}$. Recalling the vacuum stability conditions in equation 2.8, we realize that those are just the result of the conditions

$$T_i = 0. \tag{3.28}$$

At tree level, these conditions are necessary to make sure that the vacuum is fixed at the proper value, meaning that the tadpole terms should vanish at the vacuum state.

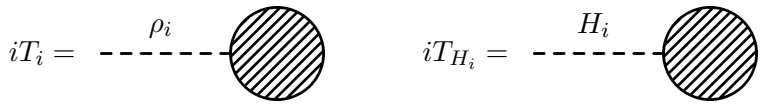

(a) (b)

Figure 3.3: Tadpole diagrams. Feynman diagram representation of the linear terms in the fields in the (a) gauge basis and in the (b) mass basis, at one-loop.

In the case of the DDP, the stability conditions are reduced to their form in equation 2.15. Therefore, we can define the DDP tadpole terms as[4]

$$T_1 = \frac{1}{2}(v^2\lambda_1 + v_S^2\lambda_7) + m_{11}^2, \tag{3.29a}$$

$$T_S = \frac{1}{2}(v^2\lambda_7 + v_S^2\lambda_6) + m_S^2. \tag{3.29b}$$

At one-loop, the tadpole terms suffer a shift analogous to the parameter shift in equation 3.4. After the shift, the vacuum must remain fixed at the proper value, meaning that the bare tadpole term $T_{i,0}$ must obey the condition

$$T_{i,0} = T_i + \delta T_i = 0, \tag{3.30}$$

with $i \in \{1, S\}$ and where T_i is now the renormalized tadpole and δT_i is the tadpole counter-term. From equation 3.30 we obtain the set of tadpole renormalization conditions

$$\delta T_i = -T_i. \tag{3.31}$$

There are two options regarding the application of the renormalization condition in equation 3.31. One approach is to renormalize the tadpole terms, maintaining the tree-level relations between the VEVs and the masses [20–22]. The second approach, consists in renormalizing the VEVs themselves. In this project, we follow the second method, known as the Alternative Tadpole (AT) scheme [23–25]. The AT scheme, has the advantage of producing gauge-independent counter-terms for the physical parameters. However, this is not true for the WFRCs, as we will see in section 3.6.

In the AT scheme, we identify the VEVs of the model as being the bare VEVs v_0 and $v_{S,0}$ that must be corrected at one-loop, through the shift

$$\begin{aligned} v_0 &= v + \delta v, \\ v_{S,0} &= v_S + \delta v_S. \end{aligned} \tag{3.32}$$

[4] If we take the parameter m_{12}^2 to be identically zero in the DDP, the minimum condition corresponding to the field ρ_2 vanishes since the doublet Φ_2 has zero VEV.

In this case, the tadpole shifts in equation 3.30 are the result of the shifts in the VEVs in equation 3.32. These tadpole shifts can be obtained as a function of the VEV counter-terms by

$$\delta T_1 = \frac{\partial T_1}{\partial v}\delta v + \frac{\partial T_1}{\partial v_S}\delta v_S, \tag{3.33a}$$

$$\delta T_S = \frac{\partial T_S}{\partial v}\delta v + \frac{\partial T_S}{\partial v_S}\delta v_S, \tag{3.33b}$$

where the tree-level minimum conditions in equation 2.15 can be used to substitute m_{11}^2 and m_S^2. The derivatives in equation 3.33, correspond to the elements of the CP-even mass matrix M^ρ. Therefore, the relation between the tadpole counter-terms and the VEV counter-terms can be expressed as

$$\begin{pmatrix} \delta T_1 \\ \delta T_S \end{pmatrix} = M^\rho \begin{pmatrix} \delta v \\ \delta v_S \end{pmatrix}. \tag{3.34}$$

It is easier to work with the tadpole counter-terms in the mass basis. For this reason it is convenient to obtain a relation between the VEV counter-terms and the mass basis tadpole counter-terms. This can be achieved by multiplying both sides of equation 3.34 by the inverse of the mass matrix and then use the rotation matrix in equation 2.20 to rotate the tadpole counter-term side to the mass basis

$$\begin{aligned} \begin{pmatrix} \delta v \\ \delta v_S \end{pmatrix} &= R(\alpha)R(\alpha)^T(M^\rho)^{-1}R(\alpha)R(\alpha)^T \begin{pmatrix} \delta T_1 \\ \delta T_S \end{pmatrix} \\ &= R(\alpha)(D^2)^{-1} \begin{pmatrix} \delta T_{H_1} \\ \delta T_{H_2} \end{pmatrix}. \end{aligned} \tag{3.35}$$

Using the tadpole renormalization condition set in equation 3.31, we can substitute the tadpole counter-terms in equation 3.35 by the tadpole terms. Therefore, the explicit relation between the VEVs and the mass basis tadpole terms becomes

$$\begin{pmatrix} \delta v \\ \delta v_S \end{pmatrix} = \begin{pmatrix} -c_\alpha \frac{T_{H_1}}{m_{H_1}^2} - s_\alpha \frac{T_{H_2}}{m_{H_2}^2} \\ s_\alpha \frac{T_{H_1}}{m_{H_1}^2} - c_\alpha \frac{T_{H_2}}{m_{H_2}^2} \end{pmatrix}. \tag{3.36}$$

From equation 3.36 we can see that the VEV counter-terms are given by the linear combination of the tadpole terms refering to the mass eigenstates H_1 and H_2 devided by their corresponding squared masses. This leads to an interesting conclusion. Using as an example the expression for δv, we see that

$$\delta v = c_\alpha \frac{i}{m_{H_1}^2} iT_{H_1} + s_\alpha \frac{i}{m_{H_2}^2} iT_{H_2}. \tag{3.37}$$

If we use the tadpole diagram representation in figure 3.3, we can see that each of the terms of equation 3.37 can be represented by a tadpole diagram. However, we can take this interpretation further by noting that the factors $i/m_{H_j}^2$ can be interpreted as scalar propagators with zero momentum transfer. This turns

the truncated tadpole diagrams from figure 3.3 into connected tadpole diagrams. Therefore, the VEV counter-terms in 3.36 can be represented as a combination of Feynman diagrams of the form

$$\delta v_i = R_{i1}$$ 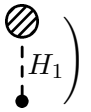 $$+ R_{i2}$$ 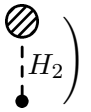 $$, \tag{3.38}$$

where $i \in \{1, 2\}$ with δv_2 corresponding to δv_S. The dot in each diagram indicates that it is a connected diagram.

Since the masses depend on the VEVs, the shifts in equation 3.32 have an effect in the mass renormalization. In addition to the mass counter-terms coming from the bare mass decomposition, an additional term appears due to the VEV counter-term contribution

$$m_0^2 = m^2 + \delta m^2 + \Delta m^2, \tag{3.39}$$

where the term Δm^2 represents the contribution coming from the VEV renormalization. For the case of two mixing fields like the ones in subsection 3.2.2, an analogous contribution appears in the form of a matrix

$$M_0^2 = M^2 + \begin{pmatrix} \delta m_{\phi_1}^2 & 0 \\ 0 & \delta m_{\phi_2}^2 \end{pmatrix} + \begin{pmatrix} \Delta M_{\phi_1\phi_1}^2 & \Delta M_{\phi_1\phi_2}^2 \\ \Delta M_{\phi_2\phi_1}^2 & \Delta M_{\phi_2\phi_2}^2 \end{pmatrix}. \tag{3.40}$$

The elements $\Delta M_{\phi_i\phi_j}^2$ are functions of the VEV counter-terms and, therefore, contain the combination of diagrams that we found in equation 3.38. In general, they are of the form

$$\Delta M_{\phi_i\phi_j}^2 = i\lambda_{H_1\phi_i\phi_j}$$ 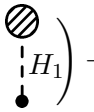 $$+ i\lambda_{H_2\phi_i\phi_j}$$ 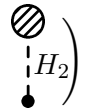 $$, \tag{3.41}$$

where $\lambda_{H_1\phi_i\phi_j}$ and $\lambda_{H_2\phi_i\phi_j}$ represent the trilinear couplings for the vertices $H_1\phi_i\phi_j$ and $H_2\phi_i\phi_j$ respectively. From equation 3.41, we conclude that the additional mass counter-terms $\Delta M_{\phi_i\phi_j}^2$ resulting from the renormalization of the VEVs, have the form of self-energy diagrams and can be represented as

$$\Delta M_{\phi_i\phi_j}^2 = i$$ 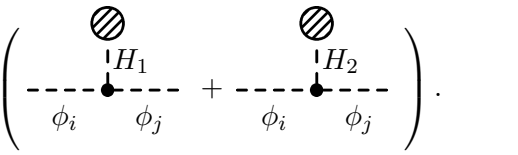 $$. \tag{3.42}$$

By comparing the counter-term matrices in equation 3.40 with the mass counter-term matrix δM^2 in equation 3.19, we are able to deduce the explicit form of the δM^2 matrix as

$$\delta M_{ij}^2 = \delta m_i^2 \delta_{ij} + \Delta M_{\phi_i\phi_j}^2. \tag{3.43}$$

Furthermore, since the mass counter-terms resulting from the VEV renormalization have self-energy form, we can define a modified self-energy $i\Sigma_{\phi_i\phi_j}^{Tad}$ such that

$$i\Sigma_{\phi_i\phi_j}^{Tad}(p^2) = i\Sigma_{\phi_i\phi_j}(p^2) - i\Delta M_{\phi_i\phi_j}^2, \tag{3.44}$$

$$i\Sigma^{Tad}(p^2) =$$ 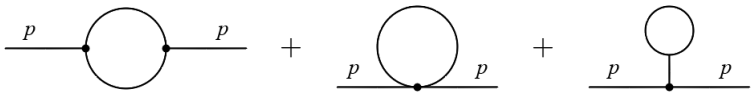 (3.46)

Figure 3.4: Modified self-energy in the AT scheme. In the alternative tadpole scheme, the particle self-energy includes the so-called tadpole contributions. These contributions, are the result of the renormalization of the VEVs.

where $i\Sigma^{Tad}_{\phi_i\phi_j}$ contains not only the sum of the 1PI diagrams between ϕ_i and ϕ_j but also the tadpole contributions from equation 3.42, as shown in figure 3.4. With this definition, the renormalized self-energy can be expressed as

$$\hat{\Sigma}_{\phi_i\phi_j}(p^2) = \Sigma^{Tad}_{\phi_i\phi_j}(p^2) - \delta m_i^2\delta_{ij} + \frac{\delta Z^*_{\phi_j\phi_i}}{2}(p^2 - M_{jj}^2) + (p^2 - M_{ii}^2)\frac{\delta Z_{\phi_i\phi_j}}{2}, \tag{3.45}$$

where δ_{ij} is the Kronecker delta function. The renormalized self-energy for the case of the non-mixing fields has an analogous form to equation 3.45.

With the self-energy definition in equation 3.45 we can now express the mass counter-terms and the WFRCs in their final form. In the non-mixing fields case, the mass counter-term and WFRC definitions in equations 3.10 and 3.14 become

$$\delta m^2 = \Sigma^{Tad}_{\phi}(m^2), \tag{3.47a}$$

$$\delta Z_\phi = -\,\mathrm{Re}\left\{\frac{\partial\Sigma^{Tad}_{\phi}(p^2)}{\partial p^2}\bigg|_{p^2=m^2}\right\}. \tag{3.47b}$$

In the case of mixing fields, the mass counter-terms and WFRCs definitions in equations 3.21, 3.23 and 3.26 become

$$\delta m_i^2 = \Sigma^{Tad}_{\phi_i\phi_i}(m_i^2), \tag{3.48a}$$

$$\delta Z_{\phi_i\phi_i} = -\,\mathrm{Re}\left\{\frac{\partial\Sigma^{Tad}_{\phi_i\phi_i}(p^2)}{\partial p^2}\bigg|_{p^2=m_i^2}\right\}, \tag{3.48b}$$

$$\delta Z_{\phi_i\phi_j} = \frac{2}{m_i^2 - m_j^2}\,\mathrm{Re}\Big\{\Sigma^{Tad}_{\phi_i\phi_j}(m_j^2)\Big\}, \tag{3.48c}$$

with $i, j \in \{1, 2\}$

There are some additional effects under the AT scheme. From equation 2.27, we realize that the trilinear couplings for our processes have dependencies on v and v_S. By renormalizing the VEVs, additional terms appear that depend on the VEV counter-terms. Using, once again, the Feynman diagram

representation of the VEV counter-terms, we can write these additional terms as

$$\Delta\lambda_{H_iH_DH_D} = \lambda_{H_iH_iH_DH_D}\left(\quad H_i\right) + \lambda_{H_iH_jH_DH_D}\left(\quad H_j\right), \tag{3.49}$$

with $i, j \in \{1, 2\}$. Similarly to what happens with the additional mass counter-terms in equation 3.41, the terms in equation 3.49 can be interpreted as a set of extra diagrams of the model

$$\Delta\lambda_{H_iH_DH_D} = \left(\begin{array}{ccc} H_i & & H_D \\ & \diagup\!\!\diagdown & \\ H_i & & H_D \end{array} \quad + \quad \begin{array}{ccc} H_j & & H_D \\ & \diagup\!\!\diagdown & \\ H_i & & H_D \end{array} \right). \tag{3.50}$$

The diagrams in equation 3.50 will contribute to the renormalization of the process amplitude, which is discussed in section 3.7.

3.4 Scalar Masses and Fields

The renormalization of the scalar masses and fields of the N2HDM is done using the OS scheme along with the AT scheme discussed in sections 3.2 and 3.3 respectively. Like we discussed in subsection 3.2.2, some fields are allowed to mix at one-loop. In the N2HDM, this is the case of the CP-even fields H_1 and H_2. Therefore, to renormalize the fields we must group them in a bare vector as per equation 3.16, resulting in

$$\begin{pmatrix} H_{1,0} \\ H_{2,0} \end{pmatrix} = \begin{pmatrix} 1 + \frac{\delta Z_{H_1H_1}}{2} & \frac{\delta Z_{H_1H_2}}{2} \\ \frac{\delta Z_{H_2H_1}}{2} & 1 + \frac{\delta Z_{H_2H_2}}{2} \end{pmatrix} \begin{pmatrix} H_1 \\ H_2 \end{pmatrix}. \tag{3.51}$$

We then use equations 3.48b and 3.48c to obtain the expressions for the WFRCs

$$\delta Z_{H_1H_1} = -\,\mathrm{Re}\left\{ \frac{\partial \Sigma^{Tad}_{H_1H_1}(p^2)}{\partial p^2}\bigg|_{p^2=m^2_{H_1}} \right\}, \tag{3.52a}$$

$$\delta Z_{H_2H_2} = -\,\mathrm{Re}\left\{ \frac{\partial \Sigma^{Tad}_{H_2H_2}(p^2)}{\partial p^2}\bigg|_{p^2=m^2_{H_2}} \right\}, \tag{3.52b}$$

$$\delta Z_{H_1H_2} = \frac{2}{m^2_{H_1} - m^2_{H_2}}\,\mathrm{Re}\Big\{ \Sigma^{Tad}_{H_1H_2}(m^2_{H_2}) \Big\}, \tag{3.52c}$$

$$\delta Z_{H_2H_1} = \frac{2}{m^2_{H_2} - m^2_{H_1}}\,\mathrm{Re}\Big\{ \Sigma^{Tad}_{H_1H_2}(m^2_{H_1}) \Big\}. \tag{3.52d}$$

To renormalize the masses, we first identify them as bare parameters as in equation 3.4. This results in the shifts

$$m^2_{H_1,0} = m^2_{H_1} + \delta m^2_{H_1}, \tag{3.53a}$$

$$m^2_{H_2,0} = m^2_{H_2} + \delta m^2_{H_2}. \tag{3.53b}$$

The counter-terms in equation 3.53 are then fixed using equation 3.48a, resulting in

$$\delta m^2_{H_1} = \mathrm{Re}\Big\{\Sigma^{Tad}_{H_1H_1}(m^2_{H_1})\Big\}, \tag{3.54a}$$
$$\delta m^2_{H_2} = \mathrm{Re}\Big\{\Sigma^{Tad}_{H_2H_2}(m^2_{H_2})\Big\}. \tag{3.54b}$$

The remaining scalar fields H_D and A_D are non-mixing fields. As such, their renormaliztion is straightforward. The fields are renormalized by identifying them as bare fields and using the definition in equation 3.5, from which we get

$$H_{D,0} = \left(1 + \frac{\delta Z_{H_D}}{2}\right) H_D, \tag{3.55a}$$
$$A_{D,0} = \left(1 + \frac{\delta Z_{A_D}}{2}\right) A_D. \tag{3.55b}$$

The WFRCs are fixed using equation 3.47b, giving us the expressions

$$\delta Z_{H_D} = -\,\mathrm{Re}\left\{\left.\frac{\partial \Sigma^{Tad}_{H_D}(p^2)}{\partial p^2}\right|_{p^2=m^2_{H_D}}\right\}, \tag{3.56a}$$
$$\delta Z_{A_D} = -\,\mathrm{Re}\left\{\left.\frac{\partial \Sigma^{Tad}_{A_D}(p^2)}{\partial p^2}\right|_{p^2=m^2_{A_D}}\right\}. \tag{3.56b}$$

The squared masses for H_D and A_D are treated in the same way as in the case of the mixing fields H_1 and H_2, meaning that the bare squared masses are given by

$$m^2_{H_D,0} = m^2_{H_D} + \delta m^2_{H_D}, \tag{3.57a}$$
$$m^2_{A_D,0} = m^2_{A_D} + \delta m^2_{A_D}. \tag{3.57b}$$

Using equation 3.47a, we obtain the expression for the squared mass counter-terms as

$$\delta m^2_{H_D} = \mathrm{Re}\Big\{\Sigma^{Tad}_{H_D}(m^2_{H_D})\Big\}, \tag{3.58a}$$
$$\delta m^2_{A_D} = \mathrm{Re}\Big\{\Sigma^{Tad}_{A_D}(m^2_{A_D})\Big\}. \tag{3.58b}$$

3.5 Electroweak Parameters

In section 2.3, we established the VEVs as independent parameters of the potential, in the mass basis. However, we would like to express our calculation in terms of measurable quantities. We can achieve

this, by expressing the VEVs as functions of these quantities. With respect to the VEV v, it can be defined at tree-level by the expression

$$v = \frac{2m_W\sqrt{m_Z^2 - m_W^2}}{e\, m_Z}. \tag{3.59}$$

Since we are working in the AT scheme, the renormalized VEV is fixed as the tree-level VEV. Therefore, the reparameterization in equation 3.59 leads to additional terms due to the VEV renormalization. These additional terms labeled Δv, are obtained through the relation

$$\Delta v = \frac{\partial v}{\partial m_W^2}\delta m_W^2 + \frac{\partial v}{\partial m_Z^2}\delta m_Z^2 + \frac{\partial v}{\partial e}\delta e. \tag{3.60}$$

Applying equation 3.60 to the relation in equation 3.59, we get the explicit form of Δv as

$$\Delta v = \frac{2m_W\sqrt{m_Z^2 - m_W^2}}{e\, m_Z}\left(\frac{1}{2(m_Z^2 - m_W^2)}\left[\frac{m_Z^2}{m_W^2}\delta m_W^2 - \frac{m_W^2}{m_Z^2}\delta m_Z^2\right] + \delta Z_e\right), \tag{3.61}$$

where we used the substitution $\delta e = e\delta Z_e$. We should note that Δv is not related to the VEV counter-term δv. In fact, this procedure would not be necessary if we had expressed the potential as a function of e, m_Z^2 and m_W^2 from the beginning. However, if we had done that, the tadpole renormalization would have been slightly more complicated and not as elegant.

An equivalent argument can be made in the case of the VEV v_S. This is addressed in subsection 3.7.1.

From equation 3.61 we get three additional counter-terms that we must fix: the charge counter-term δZ_e and the counter-terms for the masses of the W and Z bosons.

3.5.1 $W^\pm$ and Z Boson Masses

The renormalization of the gauge boson masses can be done using the OS scheme along with the AT scheme in a similar way to what was done to the scalar masses in section 3.4. However, since we are dealing with vector fields, their propagator has a different form. The propagator for a generic vector field V in the general R_ξ gauge is given by

$$G_{\mu\nu}(p^2) = \left(-g_{\mu\nu} + \frac{p_\mu p_\nu}{p^2}\right)G^T(p^2) - i\frac{p_\mu p_\nu}{p^2}\frac{\xi_V}{p^2 - \xi_V m_V^2}, \tag{3.62}$$

where $g_{\mu\nu}$ is the metric tensor and ξ_V is the gauge-fixing parameter. The last term of equation 3.62 is the longitudinal part of the propagator and will not be used in our calculations. The remaining term of equation 3.62 is the transverse part of the propagator and contains the scalar function G^T which is a Green's function that can be defined at all orders of perturbation theory as

$$G^T(p^2) = \frac{i}{p^2 - m_V^2 + \Sigma_V^T(p^2)}, \tag{3.63}$$

where $i\Sigma_V^T$ represents the sum of all truncated 1PI Feynman diagrams for the vector field. Equation 3.63 is therefore equivalent to the scalar propagator definition in equation 3.7, meaning the OS scheme can be applied to the vector fields in the exact same way as we did for the scalar fields. Therefore, the mass counter-terms for the W boson can be fixed using the expression in equation 3.47a

$$\delta m_W^2 = \mathrm{Re}\Big\{\Sigma_W^{Tad,T}(m_W^2)\Big\}. \tag{3.64}$$

At one-loop, the Z boson mixes with the photon, due to both having the same quantum numbers. This means that we must treat the Z boson and the photon as mixing fields in the context of the OS scheme. Therefore, we can define a self-energy matrix $\Sigma^{Tad,T}(p^2)$ such that

$$\Sigma^{Tad,T}(p^2) = \begin{pmatrix} \Sigma_{ZZ}^{Tad,T}(p^2) & \Sigma_{Z\gamma}^{T}(p^2) \\ \Sigma_{\gamma Z}^{T}(p^2) & \Sigma_{\gamma\gamma}^{T}(p^2) \end{pmatrix}, \tag{3.65}$$

where each self-energy contains the sum of all 1PI Feynman diagrams between each combination of fields, including the tadpole contributions according to the AT scheme. The self-energy diagrams involving the photon do not have tadpole contributions since the photon does not couple to the CP-even scalar fields H_1 and H_2. The mass counter-term for the Z boson is then given by equation 3.48a as

$$\delta m_Z^2 = \mathrm{Re}\Big\{\Sigma_{ZZ}^{Tad,T}(m_Z^2)\Big\}. \tag{3.66}$$

3.5.2 Electric Charge

The physical value of the electric charge is fixed in the Thomson limit which is the limit of zero photon momentum in the Thomson scattering between an electron and a photon. To renormalize the electric charge, we assume a bare charge e_0 that can be decomposed as

$$e_0 = (1 + \delta Z_e)e, \tag{3.67}$$

where e becomes the renormalized electric charge and δZ_e is the charge counter-term. The charge counter-term is fixed by the condition that all corrections to the $ee\gamma$ vertex must vanish when the external particles are on their mass-shell. Due to a Ward identity originating from the gauge invariance of the model, the charge counter-term can be expressed simply as a function of the photon and Z boson self-energies, defined in equation 3.65 [20]. Explicitly, the charge counter-term has the form

$$\delta Z_e^{\alpha(0)} = \frac{1}{2}\frac{\partial \Sigma_{\gamma\gamma}^T(p^2)}{\partial p^2}\bigg|_{p^2=0} + \frac{s_W}{c_W}\frac{\Sigma_{\gamma Z}^T(0)}{m_Z^2}, \tag{3.68}$$

where c_W and s_W are respectively the cosine and sine of the Weinberg angle and the superscript $\alpha(0)$ denotes that we are considering the fine-structure constant α at the zero mass scale. However, the counter-term in equation 3.68 contains large logarithmic corrections due to the small fermion masses ($f \neq t$).

To minimize the effect of these undesired contributions, we use the so-called "G_μ scheme" [20, 26] in which α is derived from the Fermi constant G_μ as

$$\alpha_{G_\mu} = \frac{\sqrt{2} G_\mu m_W^2}{\pi} \left(1 - \frac{m_W^2}{m_Z^2}\right). \tag{3.69}$$

This leads to a large part of the $\mathcal{O}(\alpha)$ corrections being absorbed in the LO decay width and allows us to take into consideration the running of the fine-structure constant from the zero mass scale to the electroweak scale. Since these corrections are included in the LO width, we must subtract them from the explicit $\mathcal{O}(\alpha)$ corrections to avoid double counting. This is done by subtracting the weak corrections to the muon decay Δr from the counter-term in equation 3.68. Therefore, the electric charge counter-term becomes

$$\delta Z_e\big|_{G_\mu} = \delta Z_e^{\alpha(0)} - \frac{1}{2}(\Delta r)_{\text{1-loop}}, \tag{3.70}$$

with $(\Delta r)_{\text{1-loop}}$ being the one-loop expression for Δr given by

$$\begin{aligned}(\Delta r)_{\text{1-loop}} = {} & \left.\frac{\partial \Sigma_{\gamma\gamma}^T(p^2)}{\partial p^2}\right|_{p^2=0} - \frac{c_W^2}{s_W^2}\left(\frac{\Sigma_{ZZ}^{Tad,T}(m_Z^2)}{m_Z^2} - \frac{\Sigma_W^{Tad,T}(m_W^2)}{m_W^2}\right) + \frac{\Sigma_W^{Tad,T}(0) - \Sigma_W^{Tad,T}(m_W^2)}{m_W^2} \\ & - 2\frac{c_W}{s_W}\frac{\Sigma_{\gamma Z}^T(0)}{m_Z^2} + \frac{\alpha}{4\pi s_W^2}\left(6 + \frac{7 - 4s_W^2}{2s_W^2}\log c_W^2\right).\end{aligned} \tag{3.71}$$

Through the expression in equation 3.70 we see that the first term of equation 3.68, which contains the undesired corrections, cancels against the first term of equation 3.71. From this point on, whenever we mention the counter-term δZ_e we will be referring to the definition in equation 3.70.

3.6 Mixing Angle α

As an independent parameter of the model, the mixing angle α must also be renormalized. To do this, we must choose in which basis we wish to do it, as it will lead to different paths of renormalization. If we perform the renormalization in the gauge basis, α has to be renormalized as a function of the gauge basis parameters and not as a mixing angle. If instead we perform the renormalization after the rotation to the mass basis, α must be renormalized as a mixing angle. The difference between the two approaches is that in the first case, the rotation angle is the renormalized parameter, while in the second case it the bare parameter α_0 that is used to rotate to the mass basis. In this project, we use the second approach, to which we refer as the KOSY scheme [21, 22].

In a similar fashion to the other physical parameters, we start by defining the bare mixing angle α_0, which is decomposed as

$$\alpha_0 = \alpha + \delta\alpha, \tag{3.72}$$

where α is the renormalized mixing angle and $\delta\alpha$ is the mixing angle counter-term. As mentioned in the beginning of the section, we use the bare mixing angle to perform the rotation between the gauge and mass basis. Using the decomposition in equation 3.72 with the rotation matrix R, we get

$$R(\alpha_0) = \begin{pmatrix} \cos\alpha_0 & \sin\alpha_0 \\ -\sin\alpha_0 & \cos\alpha_0 \end{pmatrix} = \begin{pmatrix} \cos(\alpha+\delta\alpha) & \sin(\alpha+\delta\alpha) \\ -\sin(\alpha+\delta\alpha) & \cos(\alpha+\delta\alpha) \end{pmatrix} = R(\alpha)R(\delta\alpha). \tag{3.73}$$

We can then use the rotation matrix in equation 3.73, to perform the rotation of the bare fields between the gauge and mass basis , resulting in the expression

$$\begin{aligned} \begin{pmatrix} H_{1,0} \\ H_{2,0} \end{pmatrix} &= R(\alpha_0)^T \begin{pmatrix} \rho_{1,0} \\ \rho_{S,0} \end{pmatrix} \\ &= R(\delta\alpha)^T R(\alpha)^T \sqrt{Z_\rho} \begin{pmatrix} \rho_1 \\ \rho_S \end{pmatrix} \\ &= R(\delta\alpha)^T R(\alpha)^T \sqrt{Z_\rho} R(\alpha) R(\alpha)^T \begin{pmatrix} \rho_1 \\ \rho_S \end{pmatrix} \\ &= \sqrt{Z_H} \begin{pmatrix} H_1 \\ H_2 \end{pmatrix}, \end{aligned} \tag{3.74}$$

where $\sqrt{Z_\rho}$ and $\sqrt{Z_H}$ represent the field strength renormalization constant matrices in the gauge and mass basis, respectively. The matrix $\sqrt{Z_\rho}$ is a real symmetric matrix. Therefore, at NLO, we may use the following parameterization for $\sqrt{Z_H}$

$$\begin{aligned} \sqrt{Z_H} &= R(\delta\alpha)^T \begin{pmatrix} 1+\frac{\delta Z_{H_1H_1}}{2} & \delta C \\ \delta C & 1+\frac{\delta Z_{H_2H_2}}{2} \end{pmatrix} \\ &\approx \begin{pmatrix} 1+\frac{\delta Z_{H_1H_1}}{2} & \delta C+\delta\alpha \\ \delta C-\delta\alpha & 1+\frac{\delta Z_{H_2H_2}}{2} \end{pmatrix}, \end{aligned} \tag{3.75}$$

where we use the approximations $\cos\delta\alpha \approx 1$ and $\sin\delta\alpha \approx \delta\alpha$ and discard all terms of order $\mathcal{O}(\delta^2)$. For the renormalization to be consistent, the relation for the field renormalization that we obtained in equation 3.74 must be equivalent to the one we obtained previously with the OS scheme. Therefore, comparing equations 3.51 and 3.75, we obtain the relations

$$\frac{\delta Z^{OS}_{H_1H_2}}{2} = \delta C + \delta\alpha, \tag{3.76a}$$

$$\frac{\delta Z^{OS}_{H_2H_1}}{2} = \delta C - \delta\alpha, \tag{3.76b}$$

where the superscript OS denotes that the counter-term comes from the OS scheme. Solving this system

of equations for $\delta\alpha$ and δC, results in

$$\delta\alpha = \frac{\delta Z^{OS}_{H_1H_2} - \delta Z^{OS}_{H_2H_1}}{4}, \tag{3.77a}$$

$$\delta C = \frac{\delta Z^{OS}_{H_1H_2} + \delta Z^{OS}_{H_2H_1}}{4}. \tag{3.77b}$$

The counter-term δC is not used and may be ignored. Finally, we can replace $\delta Z^{OS}_{H_1H_2}$ and $\delta Z^{OS}_{H_2H_1}$ by their expressions in equations 3.52c and 3.52d. With this substitution, we obtain the final expression for the mixing angle counter-term as

$$\delta\alpha = \frac{1}{2(m^2_{H_1} - m^2_{H_2})} \mathrm{Re}\Big\{\Sigma^{Tad}_{H_1H_2}(m^2_{H_1}) + \Sigma^{Tad}_{H_1H_2}(m^2_{H_2})\Big\}. \tag{3.78}$$

There is a problem with the expression that we just derived. The amplitudes of some diagrams contributing to the self-energies in equation 3.78 are not gauge-independent. This would not be a problem as long as the gauge-dependence vanishes in the final amplitude calculation. However, it has been shown that when using the KOSY scheme for the angular counter-terms, the final amplitudes remain gauge-dependent [24]. If we wish to make physically relevant calculations, the total amplitude of the processes cannot depend on the gauge. Therefore, we must find a way to make equation 3.78 gauge-independent. In the next subsection, we discuss a method to obtain gauge-independent self-energies.

3.6.1 Pinch Technique

One way of making the self-energies in equation 3.78 gauge-independent is using the pinch technique. An extensive discussion of the method and its applications can be found in [27]. While a detailed description of the technique is outside the scope of this thesis, we describe the basic procedure.

As an example, let us consider the amplitude $\mathcal{M}$ for a generic scattering process between two fermions. By definition, the amplitude of the process must be gauge-independent at all orders of perturbation theory. However, at NLO, the total amplitude will contain contributions of self-energy, triangle and box diagrams that might be individually gauge-dependent, as shown in figure 3.5. In order to keep the total amplitude gauge-independent, the gauge-dependent terms from the individual classes of diagrams must cancel out. This can be demonstrated by separating the total amplitude into sub-amplitudes representing the contributions of each class of diagrams

$$\mathcal{M}(s,t,m_i) = \mathcal{M}_{\text{self}}(t,\xi) + \mathcal{M}_{\text{tri}}(t,m_i,\xi) + \mathcal{M}_{\text{box}}(t,s,m_i,\xi), \tag{3.79}$$

where s and t are the Mandelstam variables, obeying the relation $s + t + u = 2(m_1^2 + m_2^2)$ with m_i representing the masses of the external particles. ξ is the gauge-fixing parameter and $\mathcal{M}_{\text{self}}$, $\mathcal{M}_{\text{tri}}$ and $\mathcal{M}_{\text{box}}$ are the amplitudes of the one-loop contributions from self-energy, triangle and box diagrams respectively. If we take the derivative with respect to ξ and s on both sides of equation 3.79, we can easily

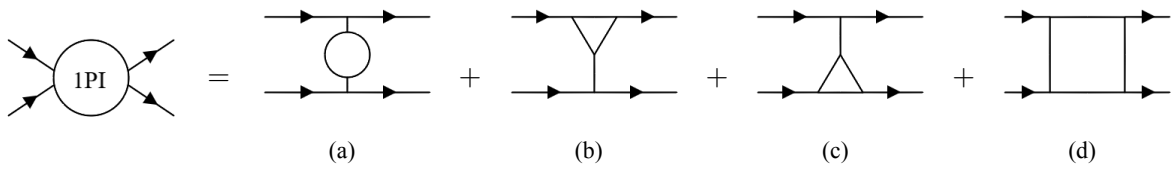

Figure 3.5: One-loop contributions to a scattering process. At one-loop, the contributions for a general scattering process can be separated in (a) self-energy contributions, (b) and (c) triangle contributions and (d) box contributions. The sum of the amplitudes of all contributions must be gauge-independent.

see that

$$\frac{\partial^2 \mathcal{M}_{\text{box}}}{\partial \xi \partial s} = 0, \tag{3.80}$$

which means that $\mathcal{M}_{\text{box}}$ can be split into two independent functions, depending on ξ and s separately

$$\mathcal{M}_{\text{box}} = \hat{\mathcal{M}}_{\text{box}}(t, s, m_i) + h(t, m_i, \xi), \tag{3.81}$$

where $\hat{\mathcal{M}}_{\text{box}}$ is gauge-independent. Since they have the same variable dependency, we can add the gauge-dependent function h to $\mathcal{M}_{\text{tri}}$ defining a new triangle sub-amplitude $\tilde{\mathcal{M}}_{\text{tri}}$

$$\tilde{\mathcal{M}}_{\text{tri}}(t, m_i, \xi) = \mathcal{M}_{\text{tri}}(t, m_i, \xi) + h(t, m_i, \xi). \tag{3.82}$$

Replacing $\mathcal{M}_{\text{box}}$ in equation 3.79 by the expression in equation 3.81 and using the definition in equation 3.82, we now have

$$\mathcal{M}(s, t, m_i) = \mathcal{M}_{\text{self}}(t, \xi) + \tilde{\mathcal{M}}_{\text{tri}}(t, m_i, \xi) + \hat{\mathcal{M}}_{\text{box}}(t, s, m_i). \tag{3.83}$$

We can then repeat the process taking the derivative with respect to ξ and m_i on both sides of equation 3.83, obtaining

$$\frac{\partial^2 \tilde{\mathcal{M}}_{\text{tri}}}{\partial \xi \partial m_i} = 0, \tag{3.84}$$

which means that similarly to $\mathcal{M}_{\text{box}}$, we can decompose $\tilde{\mathcal{M}}_{\text{tri}}$ into two independent functions, depending on ξ and m_i separately

$$\tilde{\mathcal{M}}_{\text{tri}} = \hat{\mathcal{M}}_{\text{tri}}(t, m_i) + f(t, \xi), \tag{3.85}$$

where, once again, $\hat{\mathcal{M}}_{\text{tri}}$ is gauge-independent. The function f has the same dependency as the sub-amplitude $\mathcal{M}_{\text{self}}(t, \xi)$ which means that we can define a new sub-amplitude $\hat{\mathcal{M}}_{\text{self}}$ as

$$\hat{\mathcal{M}}_{\text{self}}(t, \xi) = \mathcal{M}_{\text{self}}(t, \xi) + f(t, \xi). \tag{3.86}$$

We were able to isolate all gauge dependencies inside the sub-amplitude $\hat{\mathcal{M}}_{\text{self}}$. However, since the total amplitude must be gauge-independent, $\hat{\mathcal{M}}_{\text{self}}$ must also be gauge-independent, meaning that the all gauge-dependencies have to cancel out inside $\hat{\mathcal{M}}_{\text{self}}$. Therefore, the total amplitude can be expressed as the sum of individually gauge-independent contributions

$$\mathcal{M}(s,t,m_i) = \hat{\mathcal{M}}_{\text{self}}(t) + \hat{\mathcal{M}}_{\text{tri}}(t,m_i) + \hat{\mathcal{M}}_{\text{box}}(t,s,m_i). \tag{3.87}$$

This procedure illustrates the essence of the pinch technique at one-loop: the gauge-dependent terms of the triangle and box diagram contributions can be "pinched out" and eventually canceled at the level of the self-energies. In fact, the gauge-dependent terms that are extracted from the triangle and box diagrams, can be represented as self-energy diagrams that cancel out the gauge-dependent terms of the original self-energy contributions. Therefore, we can define a new gauge-independent "pinched" self-energy given by

$$\Sigma^{PT}(p^2) = \Sigma^{Tad}(p^2)\big|_{\xi=1} + \Sigma^{Add}(p^2), \tag{3.88}$$

where $\Sigma^{Tad}(p^2)\big|_{\xi=1}$ is the original AT scheme self-energy contribution evaluated in the Feynman gauge ($\xi = 1$) and $\Sigma^{Add}(p^2)$ represents additional gauge-independent terms, leftover from the pinch technique.

Applying this to the mixing angle counter-term in equation 3.78, we get the expression

$$\begin{aligned}\delta\alpha &= \frac{\text{Re}\{\Sigma^{PT}_{H_1H_2}(m^2_{H_1}) + \Sigma^{PT}_{H_1H_2}(m^2_{H_2})\}}{2(m^2_{H_1} - m^2_{H_2})} \\ &= \frac{\text{Re}\Big\{\left[\Sigma^{Tad}_{H_1H_2}(m^2_{H_1}) + \Sigma^{Tad}_{H_1H_2}(m^2_{H_2})\right]_{\xi=1} + \Sigma^{Add}_{H_1H_2}(m^2_{H_1}) + \Sigma^{Add}_{H_1H_2}(m^2_{H_2})\Big\}}{2(m^2_{H_1} - m^2_{H_2})},\end{aligned} \tag{3.89}$$

where $\Sigma^{Add}_{H_1H_2}$ has the explicit form

$$\begin{aligned}\Sigma^{Add}_{H_1H_2}(p^2) = -\frac{g_Y^2}{32\pi^2 c_W^2} c_\alpha s_\alpha \left(p^2 - \frac{m^2_{H_1} - m^2_{H_2}}{2}\right) \\ \times \left[B_0(p^2, m_Z, m_Z) + 2c_W^2 B_0(p^2, m_W, m_W)\right],\end{aligned} \tag{3.90}$$

where g_Y is the $U(1)_Y$ coupling constant, c_W is the cosine of the Weinberg angle and B_0 is a Passarino-Veltman function. The expression in equation 3.89 was obtained from the calculations for the counter-terms of the mixing angles for the broken phase of the N2HDM in [25]. To obtain the equivalent expression for the DDP, we used the replacement

$$(\beta - \alpha_1, \alpha_2, \alpha_3) \to (\alpha, 0, 0), \tag{3.91}$$

and the fact that (A_D, Z) and ($H_D^\pm$, W) loop contributions do not exist in the DDP due to A_D and $H_D^\pm$ belonging to the dark sector.

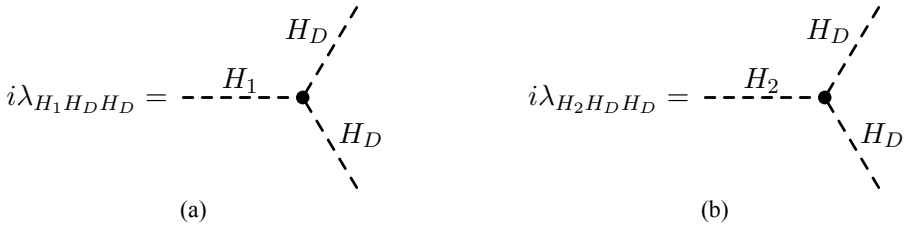

Figure 3.6: Tree-level Higgs decay Feynman diagrams. Tree-level Feynman diagrams for the possible decays of (a) H_1 and (b) H_2 to the dark matter candidate H_D

3.7 Amplitude Renormalization

In general, the observable quantities related to a given process depend on the quantum mechanical probability associated with that process. This probability is represented by the probability amplitude $\mathcal{M}$ of the process. In terms of Feynman diagrams, the amplitude is defined by the sum of the amplitudes of all possible diagrams with the same initial and final states. Since we are only interested in decay processes like the ones in equation 2.26, we will be limiting this discussion to the case of one-to-two particle processes. These decay processes are represented at tree-level by a single Feynman diagram as shown in figure 3.6. In general, the leading order probability amplitude of a decay process involving only scalar fields, is given by

$$\mathcal{M}^{\text{LO}} = \lambda, \tag{3.92}$$

where λ represents the coupling between the fields involved in the process.

When we consider the one-loop corrections to the amplitude of the process, several additional contributions have to be considered. In general, these contributions can be separated into classes of Feynman diagrams as shown in figure 3.7. Diagrams (a), (b) and (c) represent corrections to the external legs. These self-energy like contributions should vanish under the OS scheme, since they are accounted for in the propagator renormalization. Diagram (d) represents the vertex correction contributions. These include all 1PI Feynman diagrams with the same initial and final states, including the vertex tadpole contributions defined in equation 3.50. Diagram (e) represents the counter-term contributions. These contributions appear due to the additional terms resulting from the renormalization of the parameters and fields. The sum of all these one-loop corrections, can be expressed as a total amplitude $\mathcal{M}^{\text{1-loop}}$, expressed as

$$\mathcal{M}^{\text{1-loop}} = \mathcal{M}^{\text{VC}} + \mathcal{M}^{\text{CT}}, \tag{3.93}$$

where $\mathcal{M}^{\text{VC}}$ represents the amplitude of the vertex correction contributions and $\mathcal{M}^{\text{CT}}$ represents the amplitude associated with the counter-term contributions. If we ignore all the terms of order $\mathcal{O}(\delta^2)$, the counter-term amplitude can be separated into terms coming from the renormalization of the parameters

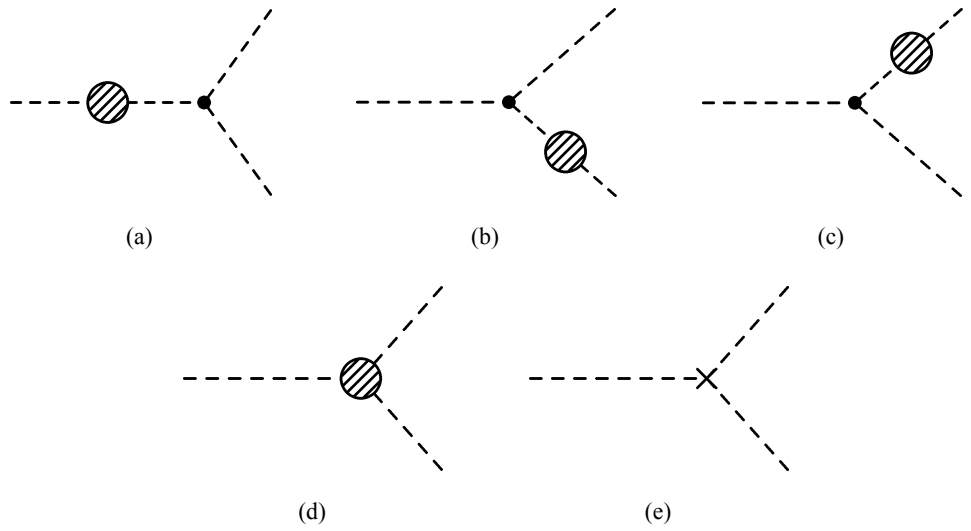

Figure 3.7: One-loop corrections to the amplitude. The one-loop corrections to the amplitude of a decay process can be represented by classes of Feynman diagrams containing (a), (b) and (c) external leg correction contributions, (d) vertex correction contributions and (e) counter-term contributions.

and terms coming from the renormalization of the wave-functions, such that

$$\mathcal{M}^{\text{CT}} = \delta\lambda^{\text{P}} + \delta\lambda^{\text{WF}}, \tag{3.94}$$

where the superscript P and WF indicate the parameter and wave-function contributions respectively. The term representing the parameter renormalization contribution, can be interpreted as being a counter-term for the coupling of the process that results from the renormalization of the parameters. The explicit form of this counter-term can be obtained by calculating the shift in the coupling as a result of the shift in the parameters of the model

$$\delta\lambda^{\text{P}} = \sum_i \frac{\partial\lambda}{\partial\rho_i}\delta\rho_i, \tag{3.95}$$

where the ρ represents the set of independent parameters of the model and $\delta\rho$ their corresponding counter-terms.

The term representing the wave-function renormalization contributions, results from the additional Lagrangian terms that appear due to the WFRCs. The explicit form depends on the mixing nature of the fields involved in the process and can generally be expressed, at one-loop, as

$$\delta\lambda^{\text{WF}} = \lambda\sum_i \frac{\delta Z_{X_i}}{2} + \delta Z_{mix}, \tag{3.96}$$

where X represents the set of fields interacting in the process and δZ_{mix} represents the terms containing off-diagonal WFRCs coming from the renormalization of mixing fields.

The total NLO amplitude of a process $\mathcal{M}^{\text{NLO}}$, is given by the sum of the leading order amplitude defined in equation 3.92 with the one-loop corrections that we have defined in equation 3.93, such that

$$\mathcal{M}^{\text{NLO}} = \mathcal{M}^{\text{LO}} + \mathcal{M}^{\text{1-loop}}. \tag{3.97}$$

In order to calculate the counter-term contributions for the amplitude as defined in equation 3.95, we must fix the counter-terms of all parameters that appear in the coupling of the process. From equation 2.27, we see that the couplings of the processes that we want to study, contain dependencies in the parameters m_{22}^2, λ_8 and v_S. However, we are yet to fix the expressions for the counter-terms δm_{22}^2 and $\delta\lambda_8$ and the form of Δv_S. These counter-terms cannot be calculated using any of the renormalization schemes discussed so far, meaning that we must find alternative schemes through which we can fix the remaining counter-terms. In the next subsections, we discuss two renormalization schemes that will allow us to complete the renormalization of our processes.

3.7.1 Minimal Subtraction Scheme

The minimal subtraction (MS) scheme, is a widely used renormalization scheme. In general, it uses the fact that, after regularization, the divergences of one-loop integrals appear isolated as poles in the regulator ϵ like described in subsection 3.1. After fixing all possible counter-terms for the fields and parameters using other renormalization schemes, the remaining counter-terms are fixed such that they exactly cancel the remaining divergencies.

A much more common form of the MS scheme is the modified minimal substraction scheme ($\overline{\text{MS}}$), also known as MS-bar. In the $\overline{\text{MS}}$ scheme, the counter-terms cancel not only the divergent parts of the integrals, but the full Δ terms as defined in equation 3.3.

We use the $\overline{\text{MS}}$ scheme to find the counter-terms for the parameters m_{22}^2 and λ_8. We do this by first, finding the β functions for the parameters. The β function is a measure of the dependence of the parameter on the renormalization scale μ introduced by the dimensional regularization and is defined as

$$\beta_\rho^{(1)} = 32\pi^2 \frac{\partial \rho}{\partial \ln \mu}, \tag{3.98}$$

where ρ represents the parameter and the superscript (1) indicates that it is the one-loop β function. The β function is related to the parameter counter-term by

$$\delta\rho = \frac{1}{32\pi^2}\beta_\rho^{(1)}\Delta, \tag{3.99}$$

with Δ being defined in equation 3.3. Applying this to the parameters m_{22}^2 and λ_8, we get the expressions for their the counter-terms as

$$\delta m_{22}^2 = \frac{1}{32\pi^2}\beta_{m_{22}^2}^{(1)}\Delta, \tag{3.100a}$$

$$\delta\lambda_8 = \frac{1}{32\pi^2}\beta_{\lambda_8}^{(1)}\Delta, \tag{3.100b}$$

where the functions $\beta^{(1)}_{m^2_{22}}$ and $\beta^{(1)}_{\lambda_8}$, given in terms of the gauge basis parameters, have the explicit form

$$\beta^{(1)}_{m^2_{22}} = 2\lambda_4 m^2_{11} + 4\lambda_3 m^2_{11} + 6\lambda_2 m^2_{22} - \frac{45}{30} g^2_Y m^2_{22} - \frac{9}{2} g^2_L m^2_{22} + \lambda_8 m^2_S, \tag{3.101a}$$

$$\beta^{(1)}_{\lambda_8} = 2\lambda_4\lambda_7 + 4\lambda_3\lambda_7 + \frac{\lambda_8}{10}\left(30\lambda_6 + 40\lambda_8 - 45 g^2_L + 60\lambda_2 - \frac{45}{3} g^2_Y\right), \tag{3.101b}$$

where g_Y and g_L are the $U(1)_Y$ and $SU(2)_L$ gauge couplings, respectively. These expressions were obtained using the `Mathematica` package `SARAH 4.14.2` [28–32].

With the expressions in equation 3.100, we would expect the renormalization process to be complete. However, when we check the total amplitude of the renormalized process with respect to its finiteness, we notice that some divergent terms remain. In the beginning of section 3.5, we mentioned that the explicit form of the term Δv_S was unknown. We see now that, since our couplings depend on v_S, we need to fix Δv_S in order to cancel all the divergent terms and make the process amplitudes UV finite. Under the $\overline{\text{MS}}$ scheme, we can simply define Δv_S in such way that it absorbs the remaining divergent terms. By doing this, we obtain the expression

$$\Delta v_S = -\left(s_\alpha \frac{T_{H_1}}{m^2_{H_1}} + c_\alpha \frac{T_{H_2}}{m^2_{H_2}}\right)_{\text{div}}, \tag{3.102}$$

where the subscript 'div' denotes that we take only the divergent part of the expression. The explicit calculation of Δv_S is presented in appendix B.1.

With the expression in equation 3.102, we have fixed all the counter-terms that are involved in our process, meaning that we now have finite NLO amplitudes.

3.7.2 Process-Dependent Scheme

A different way to obtain the expressions for the counter-terms of m^2_{22} and λ_8 is to use a process-dependent scheme. This scheme has the advantage of defining the parameter counter-terms in a more physical way. The process-dependent scheme consists of taking a set of different processes, containing couplings which depend on the parameters that are to be renormalized, and requiring that their partial decay widths are the same at both LO and NLO. This results in the condition

$$\Gamma^{\text{LO}}_{\text{Aux}} = \Gamma^{\text{NLO}}_{\text{Aux}}, \tag{3.103}$$

where the subscript Aux indicates that the partial decay widths refer to the auxiliary processes. The explicit form of the partial decay width at both LO and NLO is derived in section 4.1. In practice, the condition in equation 3.103 is equivalent to saying that the absolute square of the amplitude of the auxiliary process must be the same at LO and NLO, resulting in the expression

$$\left|\mathcal{M}^{\text{LO}}_{\text{Aux}}\right|^2 = \left|\mathcal{M}^{\text{NLO}}_{\text{Aux}}\right|^2. \tag{3.104}$$

Using the definition in equation 3.97 and expanding the absolute square of the amplitude at NLO we get

$$\begin{aligned}\left|\mathcal{M}^{\text{NLO}}_{\text{Aux}}\right|^2 &= \left(\mathcal{M}^{\text{NLO}}_{\text{Aux}}\right)^* \mathcal{M}^{\text{NLO}}_{\text{Aux}} \\ &= \left(\mathcal{M}^{\text{LO}} + \mathcal{M}^{\text{1-loop}}_{\text{Aux}}\right)^* \left(\mathcal{M}^{\text{LO}}_{\text{Aux}} + \mathcal{M}^{\text{1-loop}}_{\text{Aux}}\right) \\ &= \left|\mathcal{M}^{\text{LO}}_{\text{Aux}}\right|^2 + \left(\left(\mathcal{M}^{\text{LO}}_{\text{Aux}}\right)^* \mathcal{M}^{\text{1-loop}}_{\text{Aux}} + \mathcal{M}^{\text{LO}}_{\text{Aux}} \left(\mathcal{M}^{\text{1-loop}}_{\text{Aux}}\right)^*\right) + \mathcal{O}(\text{NNLO}) \\ &\approx \left|\mathcal{M}^{\text{LO}}_{\text{Aux}}\right|^2 + 2\,\text{Re}\Big\{\left(\mathcal{M}^{\text{LO}}_{\text{Aux}}\right)^* \mathcal{M}^{\text{1-loop}}_{\text{Aux}}\Big\}.\end{aligned} \tag{3.105}$$

If we substitute the result from equation 3.105 in equation 3.104, we get the condition

$$2\,\text{Re}\Big\{\left(\mathcal{M}^{\text{LO}}_{\text{Aux}}\right)^* \mathcal{M}^{\text{1-loop}}_{\text{Aux}}\Big\} = 0. \tag{3.106}$$

The renormalization condition can be simplified further by noticing that, according to equation 3.92, the LO amplitude $\mathcal{M}^{\text{LO}}_{\text{Aux}}$ is just the coupling associated with the auxiliary process. Therefore, our final renormalization condition becomes

$$\text{Re}\Big\{\mathcal{M}^{\text{1-loop}}_{\text{Aux}}\Big\} = 0. \tag{3.107}$$

Applying this condition to all the auxiliary processes, results in a system of equations that can be solved in order to obtain expressions for the counter-terms we want to fix. Usually, we would need as many auxiliary processes as the counter-terms we want to obtain. However, in the specific case of the processes we are studying, we only need one auxiliary process to fix both counter-terms δm_{22}^2 and $\delta\lambda_8$.

From the scalar trilinear couplings listed in appendix A.2, we see that there are two decay processes with couplings that have the exact same dependence on m_{22}^2 and λ_8 as the coupling of our process. These processes are

$$H_i \to H_D^+ H_D^-, \tag{3.108a}$$

$$H_i \to A_D A_D. \tag{3.108b}$$

The process in equation 3.108a should be avoided, since the vertex corrections included in the amplitude one-loop correction will contain IR divergences due to diagrams with photons in the loop. Therefore, we are left with the process $H_i \to A_D A_D$ as our auxiliary process. Applying the condition for the process-dependent scheme in equation 3.107 to our auxiliary process and using the one-loop amplitude definition in equation 3.93, we get the expression

$$\mathcal{M}^{\text{1-loop}}_{H_i\to A_D A_D} = \mathcal{M}^{\text{VC}}_{H_i\to A_D A_D} + \mathcal{M}^{\text{CT}}_{H_i\to A_D A_D}\Big|_{\delta m_{22}^2,\delta\lambda_8=0} + \mathcal{M}^{\delta m_{22}^2,\delta\lambda_8}_{H_i\to A_D A_D} = 0, \tag{3.109}$$

where we split the counter-term contribution to the amplitude, into a term containing only the contributions due to the counter-terms δm_{22}^2 and $\delta\lambda_8$ in the term and a term containing the remaining counter-term contributions. Since both the main process and the auxiliary process have the same dependence on the

parameters m_{22}^2 and λ_8, the contribution to their corresponding one-loop amplitudes due to the counter-terms δm_{22}^2 and $\delta\lambda_8$ should also be the same, leading to the relation

$$\mathcal{M}^{\delta m_{22}^2,\delta\lambda_8}_{H_i\to H_D H_D} = \mathcal{M}^{\delta m_{22}^2,\delta\lambda_8}_{H_i\to A_D A_D}. \tag{3.110}$$

Using equation 3.110, we can solve equation 3.109 in order to obtain the solution

$$\mathcal{M}^{\delta m_{22}^2,\delta\lambda_8}_{H_i\to H_D H_D} = -\mathcal{M}^{\text{VC}}_{H_i\to A_D A_D} - \mathcal{M}^{\text{CT}}_{H_i\to A_D A_D}\Big|_{\delta m_{22}^2,\delta\lambda_8=0}. \tag{3.111}$$

Using this result, we can finally write the complete one-loop amplitude correction for our main process as

$$\begin{aligned}\mathcal{M}^{\text{1-loop}}_{H_i\to H_D H_D} = \mathcal{M}^{\text{VC}}_{H_i\to H_D H_D} + \mathcal{M}^{\text{CT}}_{H_i\to H_D H_D}\Big|_{\delta m_{22}^2,\delta\lambda_8=0} \\ - \mathcal{M}^{\text{VC}}_{H_i\to A_D A_D} - \mathcal{M}^{\text{CT}}_{H_i\to A_D A_D}\Big|_{\delta m_{22}^2,\delta\lambda_8=0}.\end{aligned} \tag{3.112}$$

Process-dependent schemes are usually accompanied by a physical constraint on the auxiliary process. More commonly, it is required that the auxiliary process occurs strictly on-shell. This is equivalent to saying that the auxiliary process must be physical. This requirement, constrains the mass of the auxiliary dark particle A_D, resulting in the condition

$$m_{A_D} \leq \frac{m_{H_i}}{2}. \tag{3.113}$$

This condition, restricts the parameter space as the allowed mass range for the auxiliary particle is limited. For the rest of this thesis, this approach will be referred as the OS process-dependent scheme.

An alternative approach, is to set the external momenta of the auxiliary process to zero. We refer to this approach as the zero external momentum (ZEM) process-dependent scheme. This method has the advantage of not constraining the mass of the auxiliary dark particle, allowing for a wider scan of the parameter space.

Both the OS and the ZEM process-dependent schemes are represented in figure 3.8 in the form of Feynman diagrams. The vertex corrections contained in the third term of equation 3.112, depends on which approach we choose. This means that each scheme will produce different one-loop corrections to the amplitude of the main process. In section 6.4, we compare how the different process-dependent schemes affect the final numerical results.

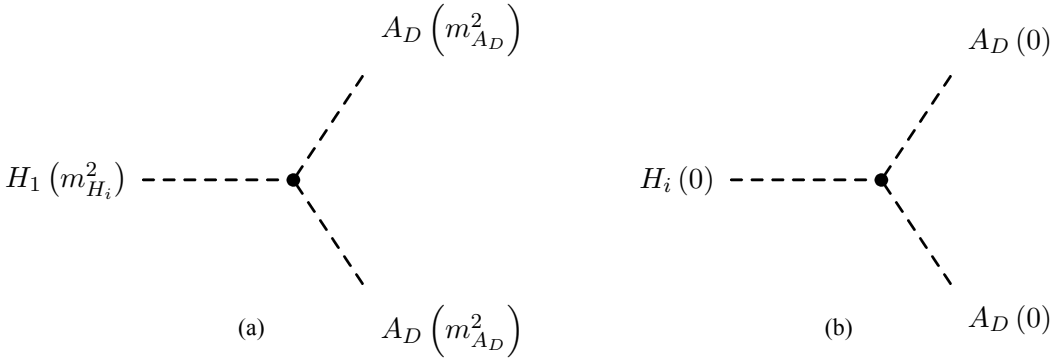

Figure 3.8: Process-dependent schemes. Feynamn diagram representation of the two process-dependent schemes. In the (a) OS process-dependent scheme the auxiliary process happens when the external momenta obey $p_i^2 = m_i^2$. In the (b) ZEM process-dependent scheme, all external momenta are set to zero.

Chapter 4

Observables at Next-to-Leading Order

In order to make theoretical predictions that can be tested in an experimental setting, we need to link the results of the quantum mechanical quantities to observable quantities. In this project we are specially interested in calculating the NLO corrections to two measurable quantities with respect to the processes in equation 2.26: the partial decay width and the branching ratio. The calculation of each of these quantities at NLO is discussed in the next sections.

4.1 Partial Decay Width

When a particle is unstable, it may decay into different sets of other particles. We refer to each of these decays as decay channels or decay modes. Often, the different decay modes of a particle differ in terms of their dependence on conserved quantities, coupling constants or other parameters of the model. For this reason, each decay mode has an associated probability of occurring, that may differ from the remaining modes. One way of measuring the probability associated with a certain decay is through the decay's partial decay width. The partial decay width of a process is related to its probability amplitude by Fermi's Golden Rule [33]. Explicitly, if we assume a decay from an initial state i of mass m_i to a set of n final states $\{f_1, f_2, ..., f_n\}$ of masses $\{m_1, m_2, ..., m_n\}$, the differential partial decay width of the process is given by

$$d\Gamma_{i\to f_1 f_2 ... f_n} = \frac{1}{2m_i}\left(\prod_{k=1}^{n}\frac{d^3\vec{p}_k}{(2\pi)^3 2E_k}\right)(2\pi)^4\delta^{(4)}(p_i - \sum_{k=1}^{n} p_k) S \sum_{d.o.f} \left|\mathcal{M}_{i\to f_1 f_2 ... f_n}\right|^2, \tag{4.1}$$

where p_i is the momentum of the initial state, E_k and p_k are the energy and momentum of the k-th final state, $\delta^{(4)}$ is the Dirac delta function, S is a product of statistical factors $1/m!$ for each group of m identical final states and $\mathcal{M}_{i\to f_1 f_2 ... f_n}$ is the amplitude for the decay as defined in section 3.7. Note that in equation 4.1 the absolute square of the amplitude is being summed over all possible degrees of freedom allowed by the initial and final states, e.g. spins, polarizations, etc. In the processes that we wish to study, all external

particles are scalars, meaning that for all initial and final states, there is only one degree of freedom. This allows us to simply drop the sum over the degrees of freedom in our calculations. Assuming that the probability amplitude of the process is independent of the final momenta, we can integrate equation 4.1 for a two-body decay over all final momenta, in order to obtain the general expression for the partial decay width as

$$\Gamma_{i\to f_1 f_2} = \frac{S}{16\pi m_i^3}\lambda(m_i^2, m_{f_1}^2, m_{f_2}^2)\left|\mathcal{M}_{i\to f_1 f_2}\right|^2, \tag{4.2}$$

where the function λ is the Källén triangle function defined as

$$\lambda(x, y, z) = \sqrt{x^2 + y^2 + z^2 - 2xy - 2xz - 2yz}. \tag{4.3}$$

We have seen that the partial decay width of a process is proportional to the absolute square of its probability amplitude. Therefore, when we take into consideration the one-loop corrections to the amplitude of the process, this also affects its partial decay width. By substituting the absolute square of the amplitude in equation 4.2 by the NLO expansion in equation 3.105, we obtain the expression for the partial decay width at NLO as

$$\begin{aligned}\Gamma^{\text{NLO}}_{i\to f_1 f_2} &= S\frac{\lambda(m_i^2, m_{f_1}^2, m_{f_2}^2)}{16\pi m_i^3}\left(\left|\mathcal{M}^{\text{LO}}_{i\to f_1 f_2}\right|^2 + 2\,\text{Re}\Big\{\left(\mathcal{M}^{\text{LO}}_{i\to f_1 f_2}\right)^* \mathcal{M}^{\text{1-loop}}_{i\to f_1 f_2}\Big\}\right)\\ &= \Gamma^{\text{LO}}_{i\to f_1 f_2} + S\frac{\lambda(m_i^2, m_{f_1}^2, m_{f_2}^2)}{8\pi m_i^3}\,\text{Re}\Big\{\left(\mathcal{M}^{\text{LO}}_{i\to f_1 f_2}\right)^* \mathcal{M}^{\text{1-loop}}_{i\to f_1 f_2}\Big\},\end{aligned} \tag{4.4}$$

where the second term of the last step represents the one-loop correction to the LO partial decay width.

Another important quantity that will be useful in our analysis, is the relative size of the one-loop correction to the partial decay width. This quantity helps us gauge how large the one-loop corrections are with respect to the LO partial decay width and is defined as

$$\frac{\Gamma^{\text{NLO}}_{i\to f_1 f_2} - \Gamma^{\text{LO}}_{i\to f_1 f_2}}{\Gamma^{\text{LO}}_{i\to f_1 f_2}}. \tag{4.5}$$

The sum of the partial decay widths of all the decay modes of a certain particle, is called the total decay width of the particle [33]. The total decay width of a particle i, is defined as

$$\Gamma_i = \sum_f \Gamma_{i\to f}, \tag{4.6}$$

where f represents the possible decay modes of the particle i. For any simple extension of the SM, like the N2HDM, the total decay width of a particle can be separated into a part containing the partial decay widths of decays to SM particles and a part containing the partial decay widths of the decays to the new particles introduced by the model, such that

$$\Gamma_i = \Gamma_{i\to\text{SM}} + \Gamma_{i\to\text{New}}. \tag{4.7}$$

It is clear that the one-loop corrections to the partial decay widths also affect the total decay width. The total decay width at NLO, is obtained by replacing the partial decay widths in equation 4.8 by the corresponding NLO widths. Therefore, we can write the total decay width as

$$\Gamma_i^{\text{NLO}} = \Gamma_{i\to\text{SM}}^{\text{NLO}} + \Gamma_{i\to\text{New}}^{\text{NLO}}. \tag{4.8}$$

Now that we have defined the partial and total decay widths of a decay process, we have all the tools necessary to calculate the second measurable quantity of interest to us.

4.2 Branching Ratio

The branching ratio, also known as the branching fraction, represents the relative frequency of a particular decay mode [33]. In other words, the branching ratio represents what fraction from a set of n identical particles, will decay through that specific decay mode. Like the name suggests, it is the ratio between the partial decay width of the decay mode and the total decay width of the decaying particle. For a particle i decaying to a set of particles $\{f_1, f_2\}$, the branching ratio of the decay is given by

$$BR(i \to f_1 f_2) = \frac{\Gamma_{i\to f_1 f_2}}{\Gamma_i}. \tag{4.9}$$

We can isolate the decay process in question in the total decay width, obtaining

$$BR(i \to f_1 f_2) = \frac{\Gamma_{i\to f_1 f_2}}{\Gamma_{i\to\text{other}} + \Gamma_{i\to f_1 f_2}}, \tag{4.10}$$

where the subscript 'other' denotes that this term contains the sum of the partial decay widths of all the remaining decay modes of i. This decomposition is useful in showing how we include the one-loop corrections in the branching ratio. If we use the one-loop corrected partial decay widths in equation 4.10, we obtain the expression for the NLO branching ratio as

$$BR^{\text{NLO}}(i \to f_1 f_2) = \frac{\Gamma_{i\to f_1 f_2}^{\text{NLO}}}{\Gamma_{i\to\text{other}}^{\text{NLO}} + \Gamma_{i\to f_1 f_2}^{\text{NLO}}}. \tag{4.11}$$

In a similar fashion to the partial decay widths, we can analyse how large the one-loop corrections to the branching ratio are, by calculating their relative size with respect to the LO branching ratio. This quantity is defined as

$$\frac{BR^{\text{NLO}}(i \to f_1 f_2) - BR^{\text{LO}}(i \to f_1 f_2)}{BR^{\text{LO}}(i \to f_1 f_2)}. \tag{4.12}$$

As we will see in section 6.4, the branching ratios of the Higgs boson decays to the dark matter candidates are our main tool to study the parameter space of the DDP of the N2HDM.

Chapter 5

The Higgs Decays to Dark Matter

The main goal of this thesis is to study, at NLO, the possible decays of the Higgs boson to the dark matter candidates in the context of the DDP of the N2HDM. Like we mentioned in subsection 2.3.2, both mass eigenstates H_1 and H_2 can be identified with the SM Higgs boson. This results in two separate scenarios for the Higgs boson decays to the dark matter candidates, due to different couplings between the two mass eigenstates and the dark particles as well as the mass ordering convention introduced in equation 2.22. In the next subsections, we discuss each scenario with more detail. From equation 2.27, we see that the couplings for the two dark matter candidates differ only in mass of the dark particle. Therefore, we can limit the following discussion to the case in which H_D is considered the dark matter particle.

5.1 Light Higgs Decay

The first scenario we are considering, is the one in which the SM Higgs boson is identified with the CP-even neutral scalar H_1. Due to the mass ordering condition in equation 2.22, this means that the SM Higgs is the lightest of the two visible CP-even scalar particles in the model. For this reason, we refer to this scenario as the Light Higgs scenario. In this case, the explicit coupling to the dark matter candidate H_D is written, using the appropriate elements from the rotation matrix R in equation 2.27a, as

$$\lambda_{H_1 H_D H_D} = \frac{2c_\alpha}{v}\left(\frac{\lambda_8 v_S^2}{2} + m_{22}^2 - m_{H_D}^2\right) - s_\alpha \lambda_8 v_S. \tag{5.1}$$

Like we discussed in section 3.7, to calculate the one-loop corrections to the amplitude of the process, we must calculate the vertex correction contributions and the counter-term contributions. For the vertex contributions, we must sum the amplitudes of all 1PI Feynman diagrams with H_1 in the initial state and a H_D pair in the final state. All included diagram classes are shown, in figure 5.1.

With regards to the calculation of the counter-term contributions, we refer to the expression in equation 3.94. For the parameter contributions to the counter-term amplitude, we use the expression in equa-

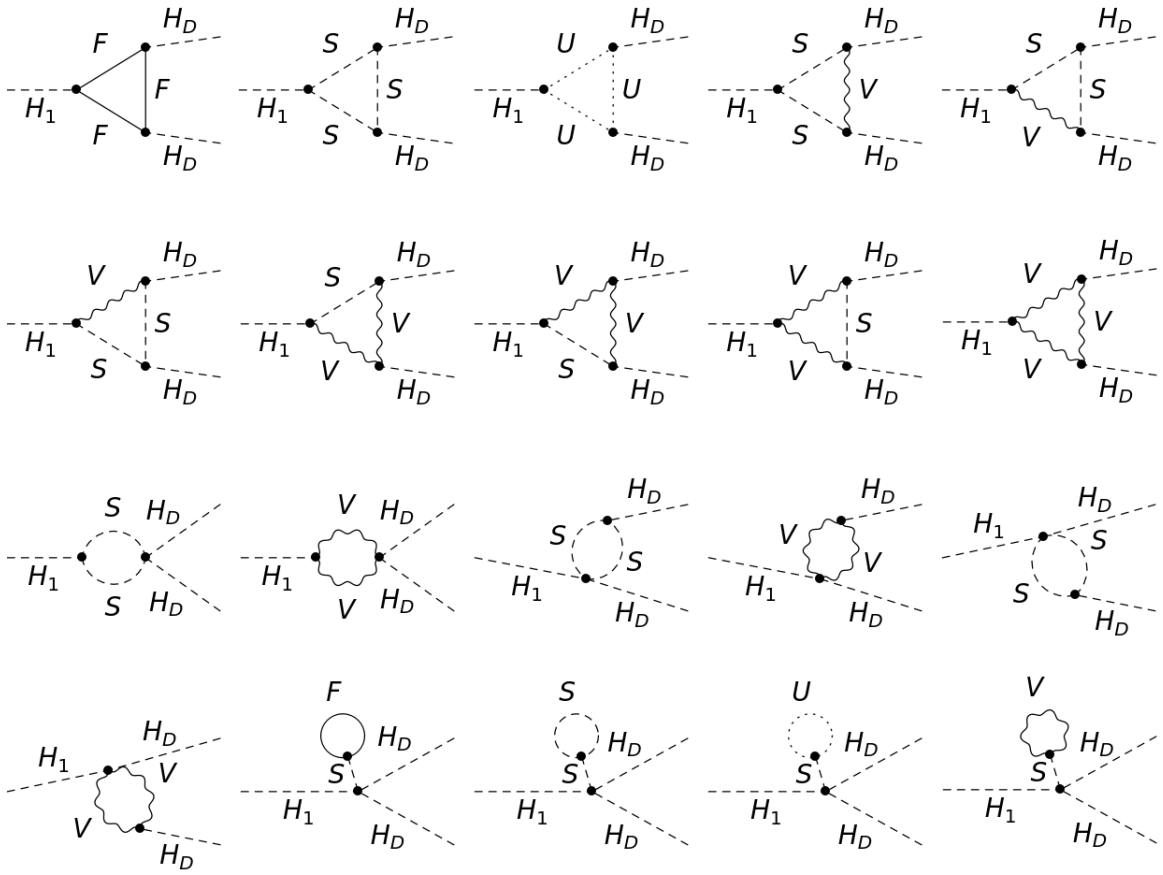

Figure 5.1: Vertex corrections for the Light Higgs scenario. Vertex corrections to the amplitude of the process $H_1 \to H_D H_D$, in the Light Higgs scenario. Notice the last four classes of diagrams are the additional vertex diagrams that result from the ATS.

tion 3.95, obtaining the expression

$$\begin{aligned}\delta\lambda^{\mathrm{P}}_{H_1H_DH_D} = &\frac{2c_\alpha}{v^2}\left(m^2_{H_D} - m^2_{22} - \frac{\lambda_8 v_S^2}{2}\right)\Delta v - \frac{2c_\alpha}{v}\delta m^2_{H_D} \\ &+ \left(\frac{2s_\alpha}{v}\left(m^2_{H_D} - m^2_{22} - \frac{\lambda_8 v_S^2}{2}\right) - c_\alpha\lambda_8 v_S\right)\delta\alpha \\ &+ \frac{2c_\alpha}{v}\delta m^2_{22} + \left(\frac{c_\alpha}{v}v_S^2 - s_\alpha v_S\right)\delta\lambda_8 + \left(\frac{2c_\alpha}{v}\lambda_8 v_S - s_\alpha\lambda_8\right)\Delta v_S.\end{aligned} \tag{5.2}$$

For the WFRC contribution, we use the expression in equation 3.96. Taking into consideration the fact

that H_1 and H_2 mix at one-loop, the WFRC contribution to the vertex has the form

$$\begin{aligned}\delta\lambda^{\text{WF}}_{H_1H_DH_D} &= \lambda_{H_1H_DH_D}\left(\frac{\delta Z_{H_1H_1}}{2}+\delta Z_{H_D}\right)+\lambda_{H_2H_DH_D}\frac{\delta Z_{H_2H_1}}{2}\\ &=\left(\frac{2c_\alpha}{v}\left(\frac{\lambda_8 v_S^2}{2}+m_{22}^2-m_{H_D}^2\right)-s_\alpha\lambda_8 v_S\right)\left(\frac{\delta Z_{H_1H_1}}{2}+\delta Z_{H_D}\right)\\ &-\left(\frac{2s_\alpha}{v}\left(\frac{\lambda_8 v_S^2}{2}+m_{22}^2-m_{H_D}^2\right)+c_\alpha\lambda_8 v_S\right)\frac{\delta Z_{H_2H_1}}{2}.\end{aligned} \tag{5.3}$$

Using equations 5.2 and 5.3, we can write the full counter-term amplitude contribution as

$$\begin{aligned}\mathcal{M}^{\text{CT}}_{H_1\to H_DH_D} &= \frac{2c_\alpha}{v^2}\left(m_{H_D}^2-m_{22}^2-\frac{\lambda_8 v_S^2}{2}\right)\Delta v-\frac{2c_\alpha}{v}\delta m_{H_D}^2\\ &+\frac{2c_\alpha}{v}\delta m_{22}^2+\left(\frac{c_\alpha}{v}v_S^2-s_\alpha v_S\right)\delta\lambda_8+\left(\frac{2c_\alpha}{v}\lambda_8 v_S-s_\alpha\lambda_8\right)\Delta v_S\\ &+\left(\frac{2s_\alpha}{v}\left(m_{H_D}^2-m_{22}^2-\frac{\lambda_8 v_S^2}{2}\right)-c_\alpha\lambda_8 v_S\right)\left(\delta\alpha+\frac{\delta Z_{H_2H_1}}{2}\right)\\ &-\left(\frac{2c_\alpha}{v}\left(m_{H_D}^2-m_{22}^2-\frac{\lambda_8 v_S^2}{2}\right)+s_\alpha\lambda_8 v_S\right)\left(\frac{\delta Z_{H_1H_1}}{2}+\delta Z_{H_D}\right).\end{aligned} \tag{5.4}$$

With the one-loop corrections to the amplitude completely defined, we can now obtain the partial decay width of the process. As discussed in section 4.1, the LO expression for a decay process is given by the expression in equation 4.2. Therefore, for the process we are considering, the LO partial decay width is written as

$$\begin{aligned}\Gamma^{\text{LO}}_{H_1\to H_DH_D} &= S\frac{\lambda(m_{H_1}^2,m_{H_D}^2,m_{H_D}^2)}{16\pi m_{H_1}^3}\left|\mathcal{M}^{\text{LO}}_{H_1\to H_DH_D}\right|^2\\ &=\frac{\sqrt{m_{H_1}^2-4m_{H_D}^2}}{32\pi m_{H_1}^2}\left(\frac{2c_\alpha}{v}\left(\frac{\lambda_8 v_S^2}{2}+m_{22}^2-m_{H_D}^2\right)-s_\alpha\lambda_8 v_S\right)^2,\end{aligned} \tag{5.5}$$

where we used the statistical factor $S=1/2!$ since the decay contains two identical particles in the final state. The expression for the partial decay width at NLO, is obtained through the definition in equation 4.4. Using the expressions previously derived in this section, we write the NLO partial decay width of the decay as

$$\begin{aligned}\Gamma^{\text{NLO}}_{H_1\to H_DH_D} &= \Gamma^{\text{LO}}_{H_1\to H_DH_D}\\ &+\frac{\sqrt{m_{H_1}^2-4m_{H_D}^2}}{16\pi m_{H_1}^2}\,\text{Re}\Big\{\left(\mathcal{M}^{\text{LO}}_{H_1\to H_DH_D}\right)^*\left(\mathcal{M}^{\text{VC}}_{H_1\to H_DH_D}+\mathcal{M}^{\text{CT}}_{H_1\to H_DH_D}\right)\Big\}.\end{aligned} \tag{5.6}$$

Assuming all the counter-terms are fixed, the expression in equation 5.6 should be positive and finite. The form of the NLO partial decay width of the process is independent of the renormalization schemes used to fix the counter-terms.

Like we mentioned before, while we only present the results for the case in which H_D is the dark matter particle, the same procedure can be applied in the case in which A_D is the dark matter particle, yielding similar results.

5.2 Heavy Higgs Decay

The second scenario that we will discuss, is the one in which the SM Higgs boson is identified with the CP-even neutral scalar H_2. Using once again the mass ordering condition in equation 2.22, we see that the SM Higgs becomes the heaviest of the two visible CP-even scalar particles. For this reason, we refer to this case as the Heavy Higgs scenario. One of the main differences between the Heavy Higgs and the Light Higgs scenarios, is that in the Heavy Higgs scenario, the mass ordering leads to an upper bound on the other visible CP-even particle H_1. This constrains the parameters space since $m_{H_1} \leq 125$ GeV. Also, in the Heavy Higgs scenario, an additional contribution to the total decay width of H_2 must be considered due to the process $H_2 \to H_1 H_1$ being kinematically allowed.

In this scenario, the explicit coupling to the dark matter candidate H_D is

$$\lambda_{H_2 H_D H_D} = -\frac{2 s_\alpha}{v}\left(\frac{\lambda_8 v_S^2}{2} + m_{22}^2 - m_{H_D}^2\right) - c_\alpha \lambda_8 v_S. \tag{5.7}$$

Once again, we refer to the discussion in section 3.7 for the calculation of the one-loop corrections to the amplitude. The vertex correction contributions are given by the sum of the amplitudes of all 1PI Feynman diagrams with H_2 in the initial state and a H_D pair in the final state. The considered diagram classes are shown in figure 5.2, where we can see that they are essentially the same as in the Light Higgs scenario.

In a similar fashion to the Light Higgs scenario, we use equation 3.94 to decompose the counter-term contribution to the amplitude, into parameter counter-term contributions and WFRC contributions. For the parameter counter-term contributions, we again use equation 3.95 to obtain the expression

$$\begin{aligned}
\delta\lambda^{\mathrm{P}}_{H_2 H_D H_D} = {} & \frac{2 s_\alpha}{v^2}\left(\frac{\lambda_8 v_S^2}{2} + m_{22}^2 - m_{H_D}^2\right)\Delta v + \frac{2 s_\alpha}{v}\delta m_{H_D}^2 \\
& + \left(\frac{2 c_\alpha}{v}\left(m_{H_D}^2 - m_{22}^2 - \frac{\lambda_8 v_S^2}{2}\right) + s_\alpha \lambda_8 v_S\right)\delta\alpha \\
& - \frac{2 s_\alpha}{v}\delta m_{22}^2 - \left(\frac{s_\alpha}{v} v_S^2 + c_\alpha v_S\right)\delta\lambda_8 - \left(\frac{2 s_\alpha}{v}\lambda_8 v_S + c_\alpha \lambda_8\right)\Delta v_S.
\end{aligned} \tag{5.8}$$

For the WFRC contribution, we refer once again to equation 3.96. Similarly to the Light Higgs scenario, we must take into account the mixing nature of H_2. Therefore, we obtain the expression

$$\begin{aligned}
\delta\lambda^{\mathrm{WF}}_{H_2 H_D H_D} &= \lambda_{H_2 H_D H_D}\left(\frac{\delta Z_{H_2 H_2}}{2} + \delta Z_{H_D}\right) + \lambda_{H_1 H_D H_D}\frac{\delta Z_{H_1 H_2}}{2} \\
&= \left(\frac{2 s_\alpha}{v}\left(m_{H_D}^2 - m_{22}^2 - \frac{\lambda_8 v_S^2}{2}\right) - c_\alpha \lambda_8 v_S\right)\left(\frac{\delta Z_{H_2 H_2}}{2} + \delta Z_{H_D}\right) \\
&\quad - \left(\frac{2 c_\alpha}{v}\left(m_{H_D}^2 - m_{22}^2 - \frac{\lambda_8 v_S^2}{2}\right) + s_\alpha \lambda_8 v_S\right)\frac{\delta Z_{H_1 H_2}}{2}.
\end{aligned} \tag{5.9}$$

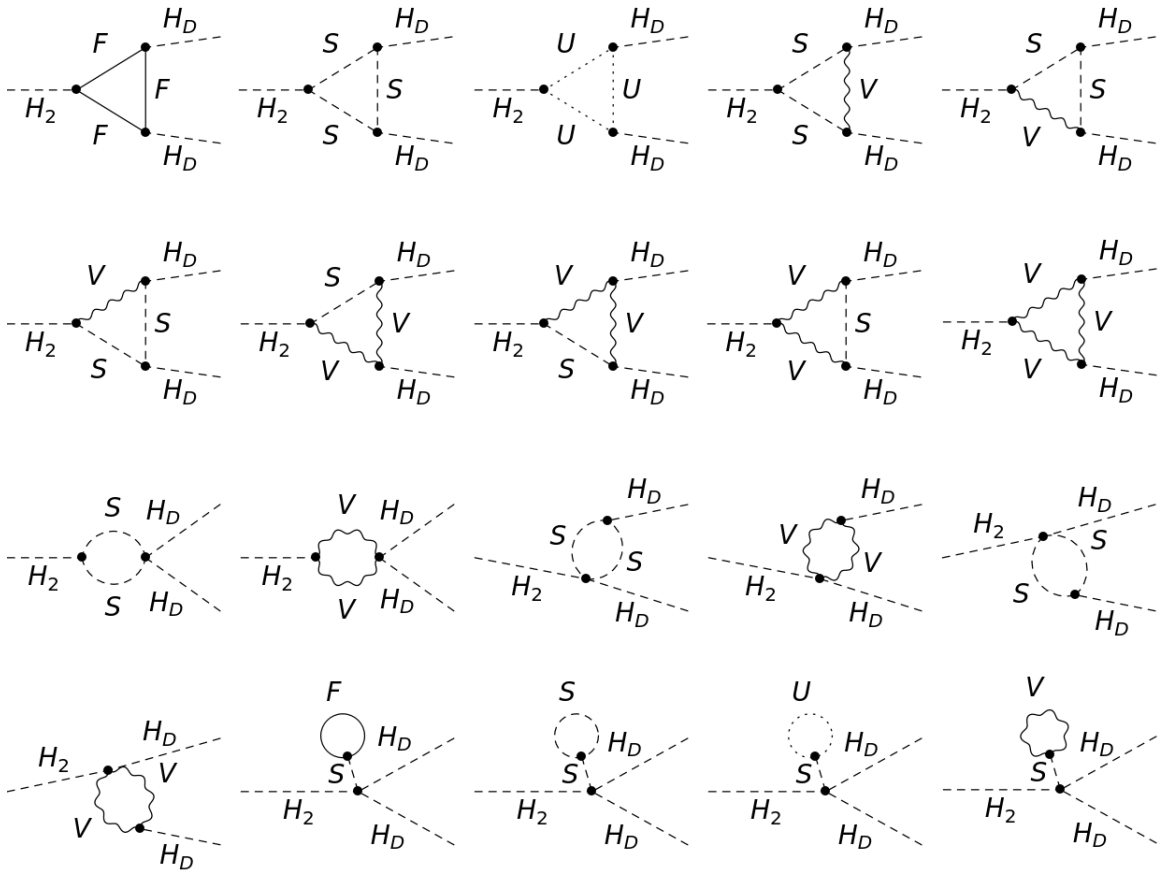

Figure 5.2: Vertex corrections for the Heavy Higgs scenario. Vertex corrections to the amplitude of the process $H_2 \to H_D H_D$, in the Heavy Higgs scenario. Notice the last four classes of diagrams are the additional vertex diagrams that result from the ATS.

Using equations 5.8 and 5.9, we can write the full counter-term amplitude contribution as

$$\begin{aligned}
\mathcal{M}^{\mathrm{CT}}_{H_2 \to H_D H_D} = & \frac{2 s_\alpha}{v^2}\left(\frac{\lambda_8 v_S^2}{2} + m_{22}^2 - m_{H_D}^2\right)\Delta v + \frac{2 s_\alpha}{v}\delta m_{H_D}^2 \\
& - \frac{2 s_\alpha}{v}\delta m_{22}^2 - \left(\frac{s_\alpha}{v} v_S^2 + c_\alpha v_S\right)\delta\lambda_8 - \left(\frac{2 s_\alpha}{v}\lambda_8 v_S + c_\alpha \lambda_8\right)\Delta v_S \\
& + \left(\frac{2 c_\alpha}{v}\left(m_{H_D}^2 - m_{22}^2 - \frac{\lambda_8 v_S^2}{2}\right) + s_\alpha \lambda_8 v_S\right)\left(\delta\alpha - \frac{\delta Z_{H_2 H_1}}{2}\right) \\
& - \left(\frac{2 s_\alpha}{v}\left(m_{H_D}^2 - m_{22}^2 - \frac{\lambda_8 v_S^2}{2}\right) - c_\alpha \lambda_8 v_S\right)\left(\frac{\delta Z_{H_1 H_1}}{2} + \delta Z_{H_D}\right),
\end{aligned} \tag{5.10}$$

The partial decay width of the process at LO is written as

$$\begin{aligned}\Gamma^{\text{LO}}_{H_2\to H_D H_D} &= S\frac{\lambda(m^2_{H_2},m^2_{H_D},m^2_{H_D})}{16\pi m^3_{H_2}}\left|\mathcal{M}^{\text{LO}}_{H_2\to H_D H_D}\right|^2 \\ &= \frac{\sqrt{m^2_{H_2}-4m^2_{H_D}}}{32\pi m^2_{H_2}}\left(\frac{2s_\alpha}{v}\left(m^2_{H_D}-m^2_{22}-\frac{\lambda_8 v_S^2}{2}\right)-c_\alpha\lambda_8 v_S\right)^2,\end{aligned} \tag{5.11}$$

where again we used the statistical factor $S = 1/2!$. Using equation 4.4 along with the expressions already calculated in this section, we get the expression for the partial decay width of the decay at NLO

$$\begin{aligned}\Gamma^{\text{NLO}}_{H_2\to H_D H_D} &= \Gamma^{\text{LO}}_{H_2\to H_D H_D} \\ &+ \frac{\sqrt{m^2_{H_2}-4m^2_{H_D}}}{16\pi m^2_{H_2}}\,\text{Re}\Big\{\left(\mathcal{M}^{\text{LO}}_{H_2\to H_D H_D}\right)^*\left(\mathcal{M}^{\text{VC}}_{H_2\to H_D H_D}+\mathcal{M}^{\text{CT}}_{H_2\to H_D H_D}\right)\Big\}.\end{aligned} \tag{5.12}$$

Similarly to the Light Higgs scenario, the same procedure can be applied in the case in which A_D is the dark matter particle, yielding similar results.

5.3 Total Decay Width and Branching Ratio Calculation

Like we discussed in the end of section 4.1, the total decay width of a particle is defined as the sum of the partial decay widths of all the decay modes of that particle. This means that, if we want to calculate the total decay widths for H_1 and H_2 at NLO, we must consider the one-loop corrections to all the decay modes of these particles. However, in the context of the two scenarios that were described in the previous sections, we use an approximation in which we only consider the one-loop corrections to the Higgs boson decay into dark matter particles. Using the decomposition in equation 4.8, we can express this approximation to the total decay width as

$$\overline{\Gamma}^{\text{NLO}}_{H_i} = \Gamma^{\text{LO}}_{H_i\to SM}+\Gamma^{\text{LO}}_{H_i\to A_D A_D}+\Gamma^{\text{LO}}_{H_i\to H_D^+ H_D^-}+\delta_{i2}\Gamma^{\text{LO}}_{H_2\to H_1 H_1}+\Gamma^{\text{NLO}}_{H_i\to H_D H_D}, \tag{5.13}$$

where the bar indicates an approximated quantity and δ is the Kronecker delta function. Note that in the process-dependent renormalization schemes described in subsection 3.7.2 the second term of equation 5.13 is not an approximation due to the renormalization condition in equation 3.103. This is only a good approximation if the NLO corrections to the partial decay widths of the remaining decay modes are small enough to be ignored. To check the validity of this approximation, we start by noting that in the Light Higgs and Heavy Higgs scenarios we are considering the limits $c_\alpha \to 1$ and $s_\alpha \to 1$ respectively. In these limits the partial decay width of H_1 or H_2 to SM particles approaches the total decay width of the SM Higgs boson. This means that, in these specific scenarios, we may use the SM predictions in order to see how large the NLO corrections to the partial decay widths are. Using the `Fortran` code `HDECAY` [34, 35], we get numerical values for the SM total decay width of the Higgs boson at both LO and NLO. For the

LO total decay width we get $\Gamma^{\text{LO}}_{h_{125}\to SM} = 4.068$ MeV while at NLO we get $\Gamma^{\text{NLO}}_{h_{125}\to SM} = 4.096$ MeV, representing a correction of around 0.7%. We can see that the NLO corrections to the decay widths of the Higgs boson in the SM are very small. Within the DDP, we must take into consideration additional vertex correction diagrams at one-loop that contain loops with particles from the dark sector. This is the case for the decays $H_i \to ZZ$ and $H_i \to WW$ due to the coupling of the W and Z bosons to the dark sector of the DDP. These corrections should be of the same order as the corrections to the vertices $H_i \to H_D H_D$ that we have been studying. These new vertices that modify the decay widths of the Higgs decays to Z and W bosons are already very constrained at tree-level by experimental measurements of the couplings of the Higgs boson. Also, most of the decays contributing to the Higgs boson total decay width remain unaffected by these corrections. Take for example the case of the Higgs' decays to fermions which represent over 65% of the contributions to the Higgs boson total decay width. Since the fermions do not couple to the dark sector of the DDP, the one-loop corrections to these decays should be very close to the SM case. With respect to the NLO corrections to the partial decay widths of the decays of H_1 and H_2 into particles from the dark sector, we can again argue that these decays are very limited by experiment at tree-level and their NLO corrections should be low. Taking all of these points into consideration it is fair to assume that the corrections to the Higgs total decay width will not be too large, meaning that our approximation is reasonable.

Finally, using the approximated total decay width, we define an approximated branching ratio for the decays of H_1 and H_2 into DM particles. For that, we define the quantity $\mathcal{R}_{H_i}$ as the ratio between the actual NLO total decay width and our approximation, written as

$$\mathcal{R}_{H_i} = \frac{\Gamma^{\text{NLO}}_{H_i}}{\overline{\Gamma}^{\text{NLO}}_{H_i}} = \frac{\Gamma^{\text{NLO}}_{H_i}}{\Gamma^{\text{LO}}_{H_i} - \Gamma^{\text{LO}}_{H_i\to H_D H_D} + \Gamma^{\text{NLO}}_{H_i\to H_D H_D}}. \tag{5.14}$$

The approximated branching ratio is then expressed as a function of the exact branching ratio as

$$\begin{aligned} \overline{BR}^{\text{NLO}}(H_i \to H_D H_D) &= \mathcal{R}_{H_i} BR^{\text{NLO}}(H_i \to H_D H_D) \\ &= \frac{\Gamma^{\text{NLO}}_{H_i\to H_D H_D}}{\Gamma^{\text{LO}}_{H_i} - \Gamma^{\text{LO}}_{H_i\to H_D H_D} + \Gamma^{\text{NLO}}_{H_i\to H_D H_D}}. \end{aligned} \tag{5.15}$$

Chapter 6

Numerical Analysis

In the previous chapters we discussed the general construction of the N2HDM and its DDP, described the process of renormalization, defined the form of the observable quantities at NLO and established the scenarios we wish to study. In this chapter, we put everything together and discuss some numerical results. In the next sections, we present the software and inputs used to obtain these results. Then, we discuss how the different renormalization schemes discussed in section 3.7 affect the NLO partial decay width of our processes. Finally, we perform a scan of the allowed parameter space, for both scenarios described in chapter 5, and discuss the results for the branching ratios of the generated points.

6.1 Software

Most of the calculations in this work were done using high energy physics' codes. For the calculation of the one-loop corrections, several `Mathematica` packages were used. The implementation of the model was done using `FeynRules 2.3.35` [36–38]. This package, takes the implementation of a model and outputs all its Feynman rules. `FeynArts 3.11` [39, 40] is a tool that generates Feynman diagrams and their corresponding amplitudes. Using the output from `FeynRules` with `FeynArts` , we obtained all the one-loop amplitudes needed for our calculations. These amplitudes were subjected to a series of simplifications using `FeynCalc 9.3.1` [41, 42]. `FeynCalc` is a package that handles several common algebraic calculations within QFT. Some of these calculations are the contraction of Lorentz indices, the calculation of color factors, tensor and Dirac algebra in D dimensions and the reduction of one-loop integrals to Passarino-Veltman functions.

Other codes were also used to obtain the numerical values that we will be discussing in the following sections. The `Mathematica` package `LoopTools 2.14` [43, 44] was used to obtain the numerical values for the finite parts of the Passarino-Veltman functions contained in the one-loop amplitudes. The scan of the parameter space was performed using the `C++` code `ScannerS` [45, 46]. This code generates parameter space points, taking into consideration the most relevant theoretical and experimental constraints. Regarding the theoretical constraints [7, 8], `ScannerS` tests for perturbative unitarity, boundedness from

below and vacuum stability. As for the experimental constraints, `ScannerS` takes into consideration electroweak precision data, Higgs couplings measurements and scalars exclusion limits and dark matter constraints. `ScannerS` integrates these constraints through an interface with other codes. These include `HiggsBound-5` [47] for the Higgs searches results, `HiggsSignals-2` [48] for the constraints of the SM-like Higgs boson measurements and `MicroOMEGAs-5.2.4` [49–51] for the dark matter relic abundance and the nucleon-DM cross section for direct detection. The dark matter relic abundance has to be below the measurement by the Planck experiment [52] and the nucleon-DM cross section has to be within the bounds imposed by the XENON1T [53] experiment. Finally, we used the `Fortran` code `N2HDECAY` [54], which is an extension for the N2HDM of the original `HDECAY` [34, 35] code, to obtain tree-level total decay widths and branching ratios for the CP-even mass eigenstates H_1 and H_2, including state-of-the-art QCD corrections.

6.2 General Inputs

In order to calculate the numerical values for our observables, we must define the set of values to use as inputs for the parameters of the model. In this section, we present only the values for the parameters that are constant throughout all calculations. These are essentially the SM parameters that include the fermion and gauge boson masses, the CKM matrix elements and the EW coupling constant. The values for the scalar parameters of the DDP, vary depending on which analysis is being performed. Therefore, they will be defined in each of the following sections, as needed.

For the fermion masses, the chosen values are

$$m_u = 2.2 \times 10^{-3}\ \text{GeV}, \qquad m_c = 1.43141297\ \text{GeV}, \qquad m_t = 172.5\ \text{GeV}, \tag{6.1}$$

$$m_d = 4.7 \times 10^{-3}\ \text{GeV}, \qquad m_s = 0.095\ \text{GeV}, \qquad m_b = 4.84141297\ \text{GeV}, \tag{6.2}$$

$$m_e = 0.510998910 \times 10^{-3}\ \text{GeV}, \qquad m_\mu = 0.1056583715\ \text{GeV}, \qquad m_\tau = 1.77682\ \text{GeV}. \tag{6.3}$$

Regarding the masses of the W and Z bosons, we used the following values

$$m_W = 80.35797\ \text{GeV}, \quad m_Z = 91.15348\ \text{GeV}. \tag{6.4}$$

As for the CKM matrix, it is considered to be real in all calculations. Its elements are set as

$$V_{CKM} = \begin{pmatrix} 0.97427 & 0.22534 & 0.00351 \\ 0.2252 & 0.97344 & 0.0412 \\ 0.00867 & 0.0404 & 0.9991 \end{pmatrix}. \tag{6.5}$$

Like we discussed in subsection 3.5.2, we use the G_μ scheme for the renormalization of the electric charge. This means that the value of the EW coupling constant depends on the value of the Fermi constant. This value is very precisely measured and is currently

$$G_F = 1.1663787 \times 10^{-5}\ \text{GeV}^{-2}. \tag{6.6}$$

In subsection 3.5.2 we also mentioned that, in the G_μ scheme, a large part of the corrections is already included at LO. For that reason, the LO results presented in the following discussions are not pure tree-level results.

6.3 Effect of the Renormalization Scheme on the Higgs-to-invisible Decay Rate corrections.

In subsections 3.7.1 and 3.7.2 we discussed three different renormalization schemes that were used to fix the expressions for the counter-terms δm_{22}^2 and $\delta\lambda_8$. We now study the effect that each of these renormalization schemes has on the one-loop corrections to the decay width of the Higgs boson to the dark matter candidates. For this analysis, we focus only on how the one-loop corrections behave with respect to some parameters of the model for each of the different renormalization schemes, ignoring theoretical and experimental constraints.

The DDP can be compared to the IDM [9–12] due to the similar vacuum configuration of the doublets. In fact, we can obtain the IDM as a limit of the DDP by setting the parameters λ_8, α and v_S to

$$\lambda_8 = 0, \quad \alpha = 0, \quad v_S \to \infty, \tag{6.7}$$

in this specific order. This is equivalent to setting m_S^2, λ_6, λ_7 and λ_8 to zero in the potential in equation 2.4. The resulting potential is the IDM potential. By considering this limit, we can use the existing IDM bounds [55] to limit the range of some of our parameters. We will be limiting this discussion to the Light Higgs scenario, as it is the only scenario with a non-vanishing coupling in the IDM limit.

We have to fix the scalar inputs used for the following discussion. Since we are in the Light Higgs scenario, the mass of H_1 is the same as the mass of the SM Higgs boson. Therefore, the masses of the two visible Higgs bosons are fixed as

$$m_{H_1} = 125.09 \text{ GeV}, \quad m_{H_2} = 500 \text{ GeV}. \tag{6.8}$$

As for the dark sector, we assume $m_{A_D} > m_{H_D}$, making H_D the dark matter candidate. We fix the masses of the dark particles m_{H_D} and $m_{H_D^\pm}$ and dark coupling λ_2 as

$$m_{H_D} = 60 \text{ GeV}, \quad m_{H_D^\pm} = 100 \text{ GeV or } 500 \text{ GeV}, \quad \lambda_2 = 0.12, \tag{6.9}$$

while the the mass parameters m_{A_D} and m_{22}^2 are either fixed or scanned over in each analysis. In the the $\overline{\text{MS}}$ scheme, the one-loop corrections to the amplitude of the process depend on the energy scale μ. For this analysis, the energy scale has been chosen as $\mu = m_{H_1}$.

We start by studying how the partial decay width behaves as a function of the coupling of the process. For this analysis, we set m_{A_D} as

$$m_{A_D} = 62 \text{ GeV}. \tag{6.10}$$

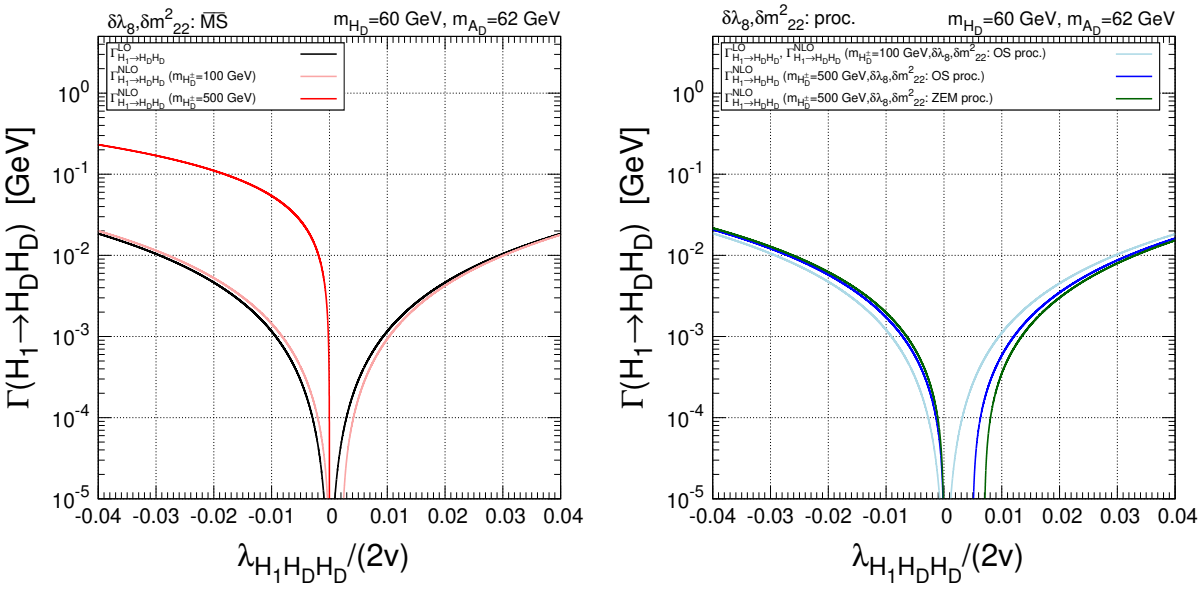

(a) (b)

Figure 6.1: Relation between partial decay width and tree-level coupling. Partial decay width as a function of the tree level coupling in the IDM limit of the DDP, in the (a) $\overline{\text{MS}}$ scheme and in the (b) process-dependent schemes. The NLO partial decay widths are evaluated at $m_{H_D^\pm} = 100$ GeV and 500 GeV.

As for m_{22}^2, we choose a range that respects the current upper bounds on the IDM dark coupling $|\lambda_L| < 0.005$ [55]. This limit, corresponds to the current bound on direct detection of dark matter from the XENON1T experiment [53]. This IDM dark coupling, relates to the coupling of our process in the IDM limit of the DDP as

$$\lambda_L = \frac{\lambda^{\text{IDM}}_{H_1 H_D H_D}}{2v} = \frac{m_{22}^2 - m_{H_D}^2}{v^2}. \tag{6.11}$$

In figure 6.1, we present the correlation between the tree-level coupling in the IDM limit and the partial decay widths of the process $H_1 \to H_D H_D$, at LO and NLO, for different values of the mass of the dark charged scalar. We can see that for both the $\overline{\text{MS}}$ shceme on the left and the process dependent schemes on the right, the partial decay width behaves parabolically at both LO and NLO. This result should be expected, as from the definitions in equations 4.2 and 4.4 we see that the partial decay width depends on the squared amplitude of the process which, in turn, depends on the coupling. An interesting result, is the strong dependence of the one-loop corrections on the mass of the charged scalar in the $\overline{\text{MS}}$ scheme. The corrections in this scheme, can become very large for large values of $m_{H_D^\pm}$. This is not the case for the process-dependent schemes. From the plot on the right, we can see that the corrections are much more reasonable in the process-dependent schemes, even for large values of $m_{H_D^\pm}$.

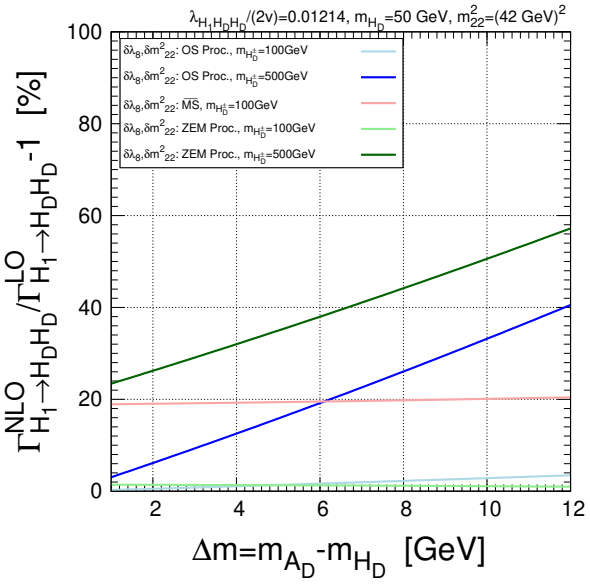

Figure 6.2: Size of the one-loop corrections and scalar mass difference. Relative size of the one-loop corrections as a function of the difference between the masses of H_D and A_D, in all renormalization schemes. In each scheme, the corrections are evaluated for $m_{H_D^\pm} = 100$ GeV and 500 GeV with the exception of the $\overline{\text{MS}}$ scheme which is only presented at $m_{H_D^\pm} = 100$ GeV.

Next, we study how the size of one-loop corrections to the partial decay width evolve with respect to the difference between the masses of the neutral dark scalars H_D and A_D. The relative size of the correction is defined as in equation 4.5. For this analysis, we set $m_{H_D} = 50$ GeV and $m^2_{22} = (42 \text{ GeV})^2$. We also define the difference between the masses of the neutral dark scalars as

$$\Delta m = m_{A_D} - m_{H_D}. \tag{6.12}$$

Due to the limit imposed on m_{A_D} by the OS process-dependent scheme kinematic constraints, we set the upper limit $\Delta m \lessapprox 12$ GeV. In figure 6.2, we present the correlation between the relative corrections to the partial decay width and the difference between the masses of the neutral dark scalars, in each of the renormalization schemes and for different values of $m_{H_D^\pm}$. We notice that the corrections in the $\overline{\text{MS}}$ scheme remain fairly constant with respect to the mass difference, showing that in this scheme the corrections are independent of Δm. This is not true in the case of the process-dependent schemes. We see that for both the OS and ZEM process-dependent schemes, the corrections are larger for higher values of the mass difference, ranging between 0% and 4% for $m_{H_D^\pm} = 100$ GeV. For larger values of $m_{H_D^\pm}$ these corrections become larger, ranging between 4% and 40% for the OS process-dependent scheme and between 24% and 57% for the ZEM process-dependent scheme, for $m_{H_D^\pm} = 500$ GeV. We notice again the dependence of all renormalization schemes on the mass of the charged Higgs. This is specially true

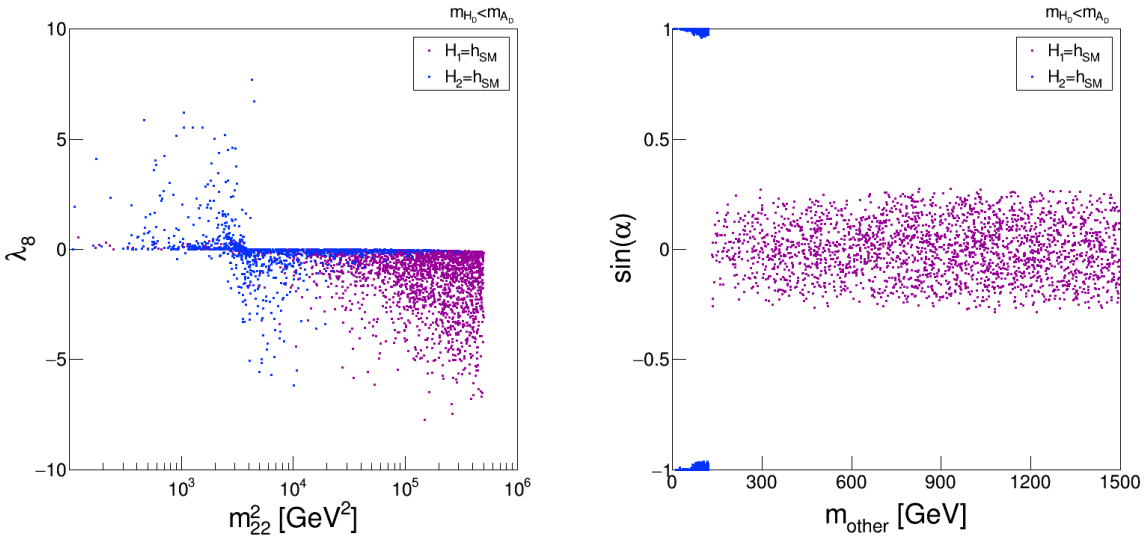

(a) (b)

Figure 6.3: Parameter space projections. Projections of the parameter space of the generated points on the (a) (m^2_{22}, λ_8) plane and on the (b) $(m_{\text{other}}, \sin\alpha)$ plane for both the Light Higgs scenario (purple) and the Heavy Higgs scenario (blue). The mass m_{other} represents the mass of the non-SM Higgs boson field in each scenario.

in the $\overline{\text{MS}}$ scheme, as the size of the corrections go from 19% for $m_{H_D^\pm} = 100$ GeV to well above 100% for $m_{H_D^\pm} = 500$ GeV.

6.4 Scan Analysis of the Parameter Space.

In chapter 4, we presented the definition of the partial decay width and the branching ratio, as well as their form at both LO and NLO. Our main goal is to scan the allowed parameter space of the DDP with respect to the one-loop corrected partial decay width for the SM-like Higgs decays to the dark matter candidates. We want to calculate the NLO branching ratio as defined in equation 5.15, and compare it with the current limit on the SM Higgs-to-invisible decay with the objective of trying to constrain the parameter space of the DDP. In the following discussion, we discuss the scan results for both observable quantities and how the different renormalization schemes discussed in section 3.7 affect these results.

In order to perform the scan of the parameter space, we must define ranges for the parameters. Like we discussed in chapter 5, in the Light Higgs scenario, we identify H_1 as being the SM Higgs boson.

Therefore, we choose the following values for the scan

$$\begin{aligned} m_{H_1} &= 125.09 \text{ GeV}, \\ 130 \text{ GeV} < m_{H_2} &< 1500 \text{ GeV}. \end{aligned} \tag{6.13}$$

In the Heavy Higgs scenario, we identify H_2 with the SM Higgs boson instead. Therefore, the chosen values are

$$\begin{aligned} 62 \text{ GeV} < m_{H_1} &< 120 \text{ GeV}, \\ m_{H_2} &= 125.09 \text{ GeV}. \end{aligned} \tag{6.14}$$

For both scenarios, the following ranges are used for the values of the remaining scalar parameters

$$\begin{gathered} 1 \text{ GeV} < m_{H_D} < 62 \text{ GeV}, \quad 1 \text{ GeV} < m_{A_D} < 1400 \text{ GeV}, \quad 65 \text{ GeV} < m_{H_D^\pm} < 1400 \text{ GeV}, \\ 10^{-3} \text{ GeV}^2 < m_{22}^2 < 10^6 \text{ GeV}^2, \quad 0 < \lambda_2 < 4\pi, \quad -4\pi < \lambda_8 < 4\pi, \\ 1 \text{ GeV} < v_S < 5000 \text{ GeV}, \quad -\frac{\pi}{2} < \alpha < \frac{\pi}{2}. \end{gathered} \tag{6.15}$$

Using `ScannerS` with these input ranges, we generate parameter points for each scenario, applying all theoretical and experimental constraints. In figure 6.3 we show the parameter space projected onto two planes: on the left, we have the projection onto the (m_{22}^2, λ_8) plane and on the right we have the projection onto the $(m_{\text{other}}, \sin\alpha)$ where m_{other} represents the mass of H_2 in the Light Higgs scenario or the mass of H_1 in the Heavy Higgs scenario. In the first projection, we can see that most of the allowed values for the coupling λ_8 are very close to zero in the Light Higgs scenario, while on the Heavy Higgs scenario, they are more frequent for higher values of m_{22}^2 and are mostly negative. In the second projection, we can see that $\sin\alpha$ is either close to zero or close to ± 1, depending on the scenario. This results from the constraint that in each scenario, the visible CP-even scalar identified as the SM Higgs boson must have a very SM-like behaviour. With respect to m_{other}, it is clear that, as discussed in chapter 5, the Light Higgs scenario contains a much larger parameter space in comparison with the Heavy Higgs scenario.

We now discuss how the NLO partial decay widths for each scenario compare across the different renormalization schemes for the dark parameters m_{22}^2 and λ_8. In figure 6.4, we present the correlation plots between the NLO and LO partial decay widths for the Higgs boson decays to the dark matter candidate H_D, in the $\overline{\text{MS}}$ scheme and in the OS process dependent scheme. Since we are considering the field H_D as our dark matter particle, we choose only points where $m_{A_D} > m_{H_D}$. Also, due to the mass constraints discussed in subsection 3.7.2, we only consider points where $m_{A_D} \leq 125/2$ GeV for the OS process dependent scheme. In both scenarios, we notice that the values for the LO partial decay widths have a boundary at around 4×10^{-4} GeV. This is the result of experimental constraints on the Higgs boson couplings to SM particles. These measurements are done with very high precision and limit the allowed values for the partial decay widths of the Higgs boson decays to new particles. For the NLO partial decay widths we can clearly see that the $\overline{\text{MS}}$ scheme and the OS process dependent scheme have very different behaviours. For the $\overline{\text{MS}}$ scheme, we see that for both scenarios, most of the NLO partial decay widths are several orders of magnitude larger than the corresponding widths at LO, meaning that

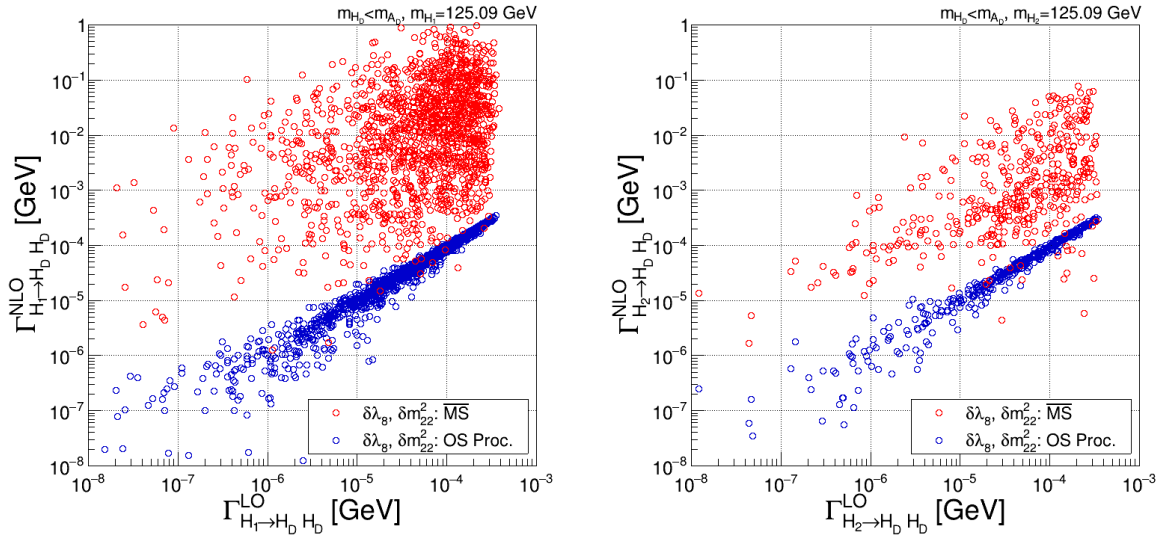

(a) (b)

Figure 6.4: Partial decay width in the $\overline{\text{MS}}$ and OS process-dependent schemes. Correlation between the NLO and LO partial decay widths for the (a) Light Higgs scenario and the (b) Heavy Higgs scenario, in the $\overline{\text{MS}}$ (red) and OS process dependent (blue) renormalization schemes.

the one-loop corrections to the partial decay width in the $\overline{\text{MS}}$ scheme are very large. For the OS process dependent scheme, the values for the partial decay widths are much more well-behaved. This is due to the relation between the one-loop corrections to the decay width and the difference between the masses of H_D and A_D, discussed in section 6.3. For the allowed points in the OS process dependent scheme, the mass differences between the DM candidates are very low with $|\Delta m| \lesssim 6$ GeV. This produces small corrections to the partial decay widths, leading to the more consistent behaviour of this renormalization scheme.

We can do the same analysis for the ZEM process dependent scheme. Like we discussed in subsection 3.7.2, the ZEM process dependent scheme does not have the mass constraints that the OS process dependent scheme does. We can use this feature to create two different sets of parameter points: one for $m_{A_D} \leq 125/2$ GeV and another for $125/2 \leq m_{A_D} \leq 1500$ GeV. In figure 6.5 we present once more the correlation between the NLO and the LO partial decay widths but this time, for the ZEM process dependent scheme. We can see that for $m_{A_D} \leq 125/2$ GeV (grey points) the partial decay widths have a similar behavior to those in the OS process dependent scheme, meaning that the values for the partial decay widths at NLO are reasonably close to the values at LO. However, it is also clear that the corrections are larger in the ZEM process dependent scheme since there is a wider distribution of the points with respect to the line $\Gamma^{\text{NLO}} = \Gamma^{\text{LO}}$. For the case with $125/2 \leq m_{A_D} \leq 1400$ GeV, we see a com-

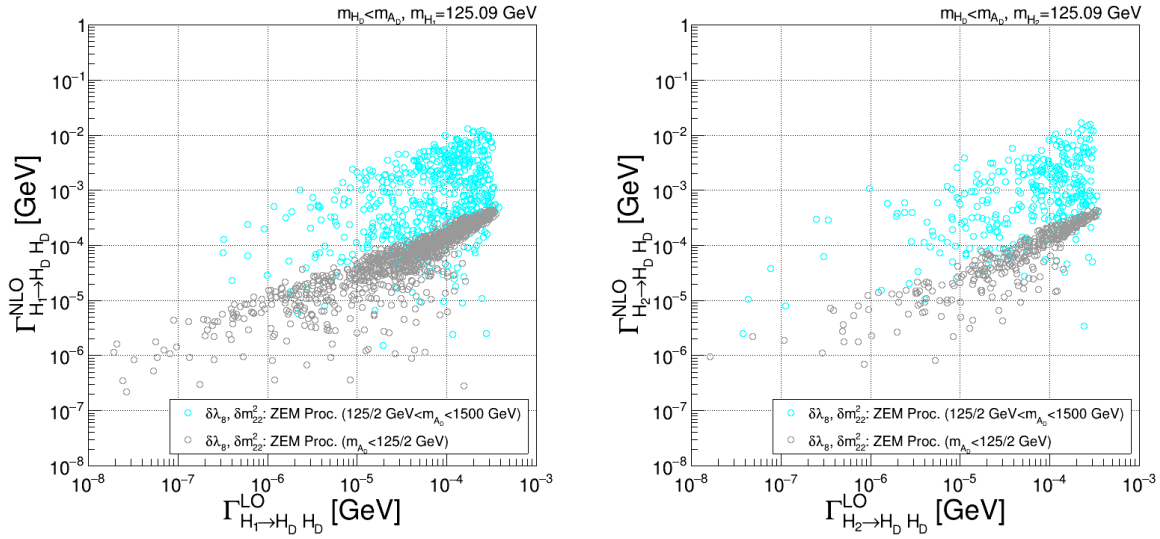

(a) (b)

Figure 6.5: Partial decay width in the ZEM process-dependent scheme. Correlation between the NLO and LO partial decay widths for the (a) Light Higgs scenario and the (b) Heavy Higgs scenario, in the ZEM process dependent scheme. The parameter points are separated into two samples: one for $m_{A_D} < 125/2$ GeV (grey) and another for $125/2$ GeV $< m_{A_D} < 1500$ GeV (cyan).

pletely different behavior. The NLO partial decay widths reach very high values similar to what happens in the $\overline{\text{MS}}$ scheme. This is again the result of the dependence of the amplitudes in the process dependent schemes on the difference between the masses of the DM candidates H_D and A_D. In this sample, the allowed mass differences are bigger, leading to much higher corrections on the observables.

To better understand how the different renormalization schemes influence the size of the corrections, we present in figure 6.6, plots of the relative size of the correction to the partial decay width, as defined in equation 4.5, as a function of the LO partial decay width in each renormalization scheme, for each scenario. In order to compare the same set of parameter points in all renormalization schemes, we limit our samples to points where $m_{A_D} \leq 125/2$ GeV which is the limit for the OS process dependent scheme. The black line indicates the 100% value for the corrections. We can see from the plots that the OS process dependent scheme is the most stable of the three schemes, with the corrections staying mostly between -100% and 100%. While some points in this scheme can reach values as high as 500%, these occur only for small values of the LO partial decay width, meaning that the values for NLO partial decay width of these points can still be within the experimental limit. For the ZEM process dependent scheme, we can see that a considerable amount of points have corrections above 100%, making this renormalization scheme much less stable than its OS counterpart. The $\overline{\text{MS}}$ renormalization scheme is the most unstable

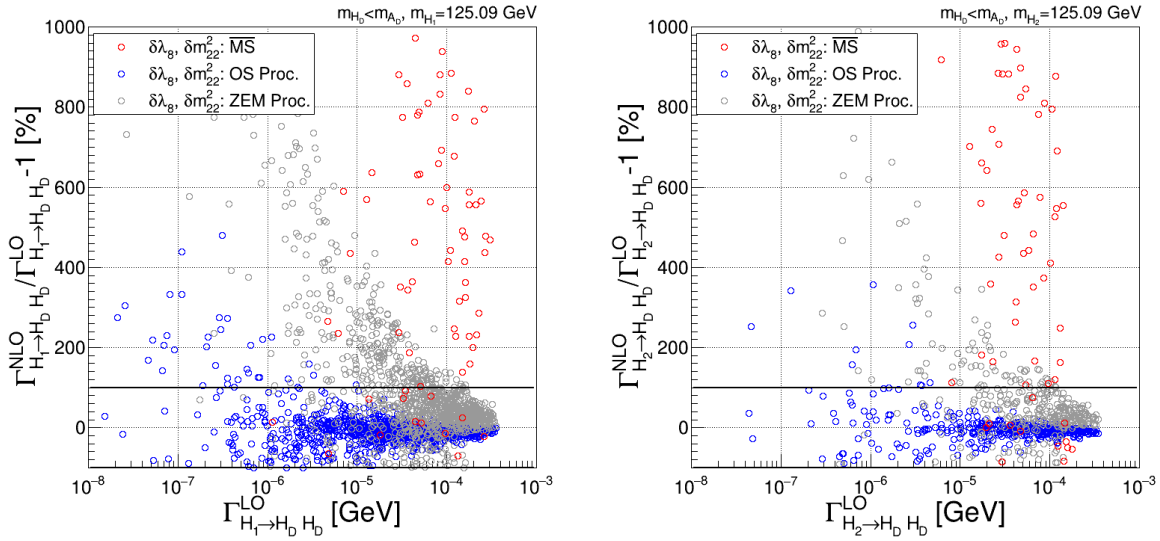

(a) (b)

Figure 6.6: NLO corrections to the partial decay width. One-loop corrections to the partial decay width as a function of the LO partial decay width for the (a) Light Higgs scenario and the (b) Heavy Higgs scenario in the $\overline{\text{MS}}$ (red), OS process-dependent (blue) and ZEM process-dependent (grey) renormalization schemes. The black line indicates the $\pm 100\%$ value for the corrections.

of the three, producing the highest corrections for all values of the LO partial decay widths.

Since the corrections in the $\overline{\text{MS}}$ scheme depend on the choice of the renormalization scale, this could become a source of instability. For all previous calculations we chose $\mu = 125.09$ GeV as the renormalization scale. To understand if this value is adequate, we studied how the size of the correction to the partial decay width of random parameter points depends on the renormalization scale. The points were selected in two extremes: the 'low' points were selected from all the points with $\Gamma^{\text{Rel}} < 50\%$ and the 'high' points were selected from the points with $\Gamma^{\text{Rel}} > 100000\%$, both at $\mu = 125.09$ GeV. In figure 6.7, we show the results for two of the parameter points. The plot on the left shows the result for one of the 'low' points, while the plot on the right shows the result for one of the 'high' points. We can see that, in both cases, the smallest correction occurs at very different renormalization scales. For the 'low' point, the minimum correction occurs in the vicinity of our chosen renormalization scale, becoming increasingly large for higher renormalization scales. Similar behaviours were observed for the other 'low' points. For the 'high' point, the correction is very large at the original renormalization scale, decreasing substantially until reaching its minimum value at around $\mu = 780$ GeV. The general behaviour is the same for the other 'high' points. However, the renormalization scale at which each point reaches the minimum correction varies greatly. Based on this analysis, we can conclude that the instability of the

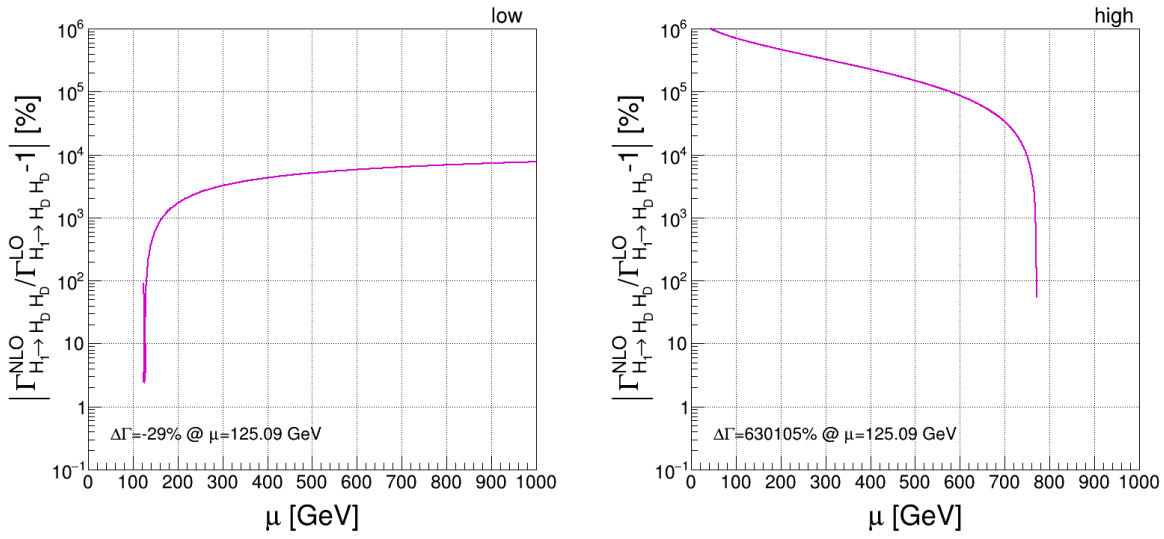

(a) (b)

Figure 6.7: Renormalization scale dependence in the $\overline{\text{MS}}$ scheme. Absolute size of the corrections as a function of the renormalization scale for two random parameter points in the extremes of the corrections size (at $\mu = 125.09$ GeV). For the (a) parameter point with low correction, the minimum correction occurs at a very different renormalization scale than that of the (b) high correction parameter point. While the size of the correction was evaluated for the full range 0 GeV $< \mu < 1000$ GeV, we only show the curve in the interval of μ for which the NLO partial decay width is physical ($\Gamma^{\text{NLO}} > 0$).

corrections in the $\overline{\text{MS}}$ scheme, are not the result of the choice of renormalization scale and that the $\overline{\text{MS}}$ scheme is simply not a good renormalization scheme for this particular application.

Finally, we consider the approximated NLO branching ratios for the generated points. To do that, we use equation 5.13 to calculate the approximated total decay width of H_1 and H_2 in the Light Higgs and Heavy Higgs scenarios respectively. As mentioned in section 6.1, we use the `N2HDECAY` code to get the LO total decay widths of H_1 and H_2. To obtain the approximated NLO total decay width, we perform the calculation

$$\overline{\Gamma}^{\text{NLO}}_{H_i} = \Gamma^{\text{N2HDECAY}}_{H_i} - \Gamma^{\text{LO}}_{H_i \to H_D H_D} + \Gamma^{\text{NLO}}_{H_i \to H_D H_D}, \tag{6.16}$$

with $i \in \{1, 2\}$ and where $\Gamma^{\text{N2HDECAY}}_{H_i}$ represents the LO total decay width for H_i coming from `N2HDECAY` . This calculation, replaces the LO partial decay width of the process $H_i \to H_D H_D$ coming from the `N2HDECAY` with the calculated one-loop corrected partial decay width.

Within the context of perturbation theory, it is fair to assume that very high NLO corrections are not realistic, meaning that we should obtain more trustworthy results by setting an upper limit on these corrections. In figure 6.8, we present the correlation between the NLO and LO branching ratios for both

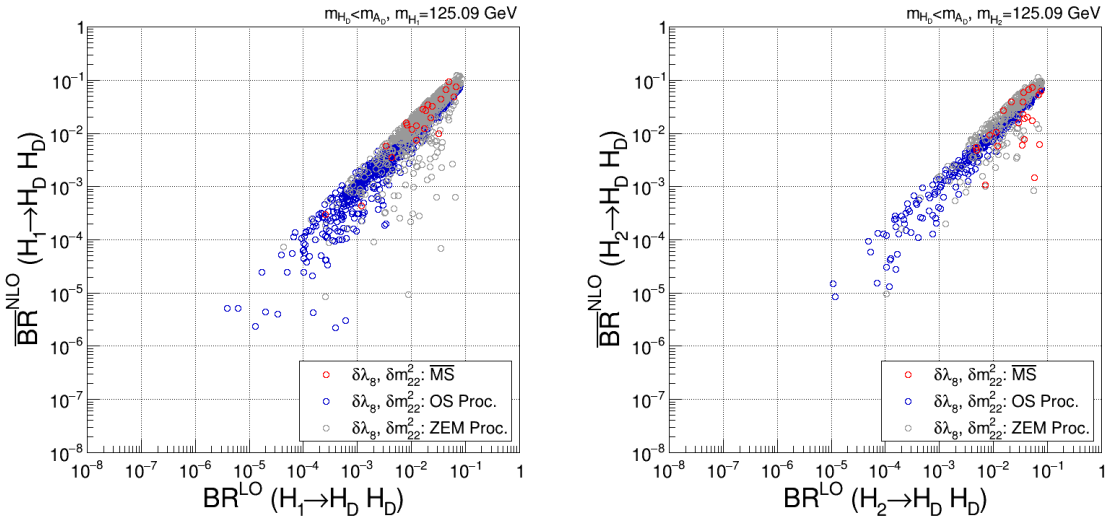

(a) (b)

Figure 6.8: Branching ratios with small corrections. Correlation between the approximated branching ratio at NLO and the LO branching ratio for the (a) Light Higgs scenario and the (b) Heavy Higgs scenario, for parameter points with one-loop corrections to the partial decay width below 100%. The red, blue and grey points, correspond to the $\overline{\text{MS}}$, OS process-dependent and ZEM process-dependent schemes, respectively.

scenarios in the three renormalization schemes. For all samples, we consider only points where the NLO corrections are below 100%. We can see that all the surviving points still have NLO branching ratios below the experimental limit. While no constraints on the parameter space can be obtained from these results, we managed to establish a range of allowed values for the NLO corrections. As the measurements on the Higgs couplings become increasingly precise and the limit on the branching ratio of the Higgs-to-invisible decay improves, we are certain that these results will lead to constraints on the parameter space.

With regards to the cases in which A_D is the dark matter particle, we performed the exact same analysis and obtained identical results in both the Light Higgs scenario and the Heavy Higgs scenario.

Chapter 7

Conclusions

In this work, we calculated the one-loop electroweak corrections to the amplitude of the SM Higgs boson decay into dark matter candidates, in the context of the N2HDM in its DDP. We started by presenting the scalar and Yukawa sectors of the N2HDM. The N2HDM is a simple extension of the SM with two weak isospin doublets and a singlet. The scalar potential of the N2HDM contains two $\mathbb{Z}_2$ symmetries. The N2HDM allows for the existence of different vacuum configurations or phases, one of which is the DDP. In the DDP, one of the doublets and the singlet have non vanishing VEVs, conserving only one of the $\mathbb{Z}_2$ symmetries. This results in two distinct sectors: a visible sector, composed of two neutral CP-even Higgs bosons and a dark sector composed of a neutral CP-even, a neutral CP-odd and two charged Higgs bosons. The DDP provides four distinct processes that could possibly represent the decay of the SM Higgs boson into a pair of dark matter particles. These processes are represented in the N2HDM as $H_i \to H_D H_D$ and $H_i \to A_D A_D$ with $i \in \{1, 2\}$.

In order to calculate the one-loop corrections to the amplitudes of the processes under study, we performed the renormalization of the scalar and gauge sectors of the model. The masses and the field wave-functions were renormalized using the OS renormalization scheme, in which the form of the particles' propagators at higher orders is fixed as being equal to the tree-level propagator. Along with the OS scheme, we also used the AT scheme for the renormalization of the VEVs. In the AT scheme, the VEVs suffer a shift, resulting in additional self-energy and vertex correction diagrams that contribute to the one-loop corrections of the amplitude of the processes. The electric charge was renormalized using the G_μ scheme, which deals with undesirable logarithmic corrections due to the low fermion masses compared to the electroweak energy scale. The CP-even mixing angle was renormalized using the KOSY scheme along with the pinch technique to ensure the gauge-independence of the corrected amplitudes. The remaining parameters m_{22}^2 and λ_8, related to the dark couplings, were renormalized using three distinct schemes: the $\overline{\text{MS}}$ scheme and two process-dependent schemes. We concluded that only in the $\overline{\text{MS}}$ scheme does the expression of the additional VEV counter-term Δv_S needs to be fixed. In both process-dependent schemes, we used $H_i \to A_D A_D$ as the auxiliary processes to renormalize the amplitude of the processes $H_i \to H_D H_D$. One of the process-dependent schemes is the OS process-dependent scheme,

where the particles interacting in the auxiliary process are required to be on their mass shell. The second process-dependent scheme is the ZEM process-dependent scheme, where the external particles of the auxiliary process are required to have zero momentum.

With the renormalization of the processes completed, we discussed the observable quantities that we wished to calculate. We started by defining the concepts of partial decay width and total decay width of a process. For both observables, we derived their general expressions at both LO and NLO. We then presented the concept of branching ratio and calculated its expressions at LO and NLO.

We presented two possible scenarios for the decay of the SM Higgs into a pair of dark matter particles, within the DDP of the N2HDM. These scenarios result from the mass ordering between the two visible CP-even Higgs bosons of the DDP. In the first scenario, the Light Higgs scenario, the SM Higgs is identified with the lightest visible neutral CP-even field, H_1. In the second scenario, the Heavy Higgs scenario, the SM Higgs is identified with the heaviest of the two visible Higgs bosons of the DDP, H_2. For each scenario, we presented the explicit one-loop corrections to the amplitude of the process, as well as the expressions for both the partial decay width and the branching ratio, at NLO. Several differences were pointed out between both scenarios. These differences are the larger parameter space in the Heavy Higgs scenario and the additional contribution to the total decay width due to the kinematically allowed process $H_2 \to H_1 H_1$, also in the Heavy Higgs scenario.

Two numerical studies were performed. In the first study, we observed how the different renormalization schemes used to fix the counter-terms for m_{22}^2 and λ_8, behave with respect to some parameters of the model. First, we discussed the relation between the partial decay width and the dark coupling $\lambda_{H_1 H_D H_D}$ in the IDM limit. We observed that the $\overline{\text{MS}}$ scheme is very sensitive to the mass of the charged Higgs boson, producing very high corrections to the partial decay width for higher masses of the charged Higgs boson. We observed that this is not the case for the process-dependent schemes, in which the corrections are much smaller even for higher charged Higgs mass. We also studied the relation between the size of the corrections to the partial decay width and the difference between the masses of the neutral dark scalars. We concluded that the corrections become larger in the process-dependent schemes as the mass difference increases, while in the case of the $\overline{\text{MS}}$ scheme, the size of the corrections remain fairly constant with respect to the mass difference.

The second numerical study that we performed, was a scan over the parameter space. We used `ScannerS` to generate parameter points for each scenario, taking into consideration the most relevant theoretical and experimental constraints. For each parameter point, we calculated the NLO branching ratio for the decay of the Higgs into a pair of dark matter particles, in the $\overline{\text{MS}}$ scheme and both process-dependent schemes. We concluded that of the three renormalization schemes, the OS process-dependent scheme is the most stable of the three, while the $\overline{\text{MS}}$ scheme is very unstable. We concluded that the instability of the $\overline{\text{MS}}$ scheme cannot be explained by the choice of renormalization scale and that it is simply not a good renormalization scheme in this particular case. We also concluded that the stability of the process-dependent schemes is related to the upper limit of 10 GeV on the mass difference between the neutral dark particles. Finally, we compared the results of the branching ratios with the current upper

limit on the Higgs-to-invisible branching ratio, $BR(h_{125} \to \text{invisible}) < 0.11$, excluding all points with corrections to the partial decay width larger than 100%. We concluded that, if we require that the one-loop corrections are not unphysically large, most of the NLO branching ratios from our sample, calculated on each process-dependent scheme, are at or below the experimental limit. We also observed that, for lower values of LO branching ratio, the NLO corrections become very large. This means that, as the branching ratio becomes more constrained, the NLO corrections will become more unstable.

With some experiments being updated like the LHC run 3 and new experiments being developed, we expect that in the next few years we will have access to increasingly precise measurements of the Higgs couplings and Higgs-to-invisible decay. These measurements may very well be our only tool to probe the dark sectors of many SM extensions, as the dark couplings of these models are only accessible through processes involving dark matter particles. Even though we were not able to extract any constraints to the parameter space of the N2HDM in its DDP, we can see that the presented results are already very close to the current experimental limit. We are certain that as this limit improves, our work will prove very usefull in limiting the parameter space of the DDP of the N2HDM.

References

[1] ATLAS collaboration, *Observation of a new particle in the search for the Standard Model Higgs boson with the ATLAS detector at the LHC*, *Phys. Lett. B* **716** (2012) 1 [1207.7214]. 1

[2] CMS collaboration, *Observation of a New Boson at a Mass of 125 GeV with the CMS Experiment at the LHC*, *Phys. Lett. B* **716** (2012) 30 [1207.7235]. 1

[3] G. Bertone and D. Hooper, *History of dark matter*, *Rev. Mod. Phys.* **90** (2018) 045002 [1605.04909]. 1

[4] C.-Y. Chen, M. Freid and M. Sher, *Next-to-minimal two Higgs doublet model*, *Phys. Rev. D* **89** (2014) 075009 [1312.3949]. 1, 3, 5

[5] A. Drozd, B. Grzadkowski, J.F. Gunion and Y. Jiang, *Extending two-Higgs-doublet models by a singlet scalar field - the Case for Dark Matter*, *JHEP* **11** (2014) 105 [1408.2106].

[6] Y. Jiang, L. Li and R. Zheng, *Boosted scalar confronting 750 GeV di-photon excess*, 1605.01898.

[7] M. Muhlleitner, M.O.P. Sampaio, R. Santos and J. Wittbrodt, *The N2HDM under Theoretical and Experimental Scrutiny*, *JHEP* **03** (2017) 094 [1612.01309]. 1, 51

[8] I. Engeln, P. Ferreira, M.M. Mühlleitner, R. Santos and J. Wittbrodt, *The Dark Phases of the N2HDM*, *JHEP* **08** (2020) 085 [2004.05382]. 1, 3, 5, 51

[9] N.G. Deshpande and E. Ma, *Pattern of Symmetry Breaking with Two Higgs Doublets*, *Phys. Rev. D* **18** (1978) 2574. 1, 53

[10] E. Ma, *Verifiable radiative seesaw mechanism of neutrino mass and dark matter*, *Phys. Rev. D* **73** (2006) 077301 [hep-ph/0601225].

[11] R. Barbieri, L.J. Hall and V.S. Rychkov, *Improved naturalness with a heavy Higgs: An Alternative road to LHC physics*, *Phys. Rev. D* **74** (2006) 015007 [hep-ph/0603188].

[12] L. Lopez Honorez, E. Nezri, J.F. Oliver and M.H.G. Tytgat, *The Inert Doublet Model: An Archetype for Dark Matter*, *JCAP* **02** (2007) 028 [hep-ph/0612275]. 1, 53

[13] ATLAS collaboration, *Combination of searches for invisible Higgs boson decays with the ATLAS experiment*, Tech. Rep. ATLAS-CONF-2020-052, CERN, Geneva (Oct, 2020). 2

[14] D. Azevedo, P. Gabriel, M. Muhlleitner, K. Sakurai and R. Santos, *One-loop Corrections to the Higgs Boson Invisible Decay in the Dark Doublet Phase of the N2HDM*, 2104.03184. 2

[15] S. Glashow and S. Weinberg, *Natural conservation laws for neutral currents*, *Phys. Rev. D* **15** (1977) . 6

[16] S.D. McDermott, H.-B. Yu and K.M. Zurek, *Turning off the lights: How dark is dark matter?*, *Physical Review D* **83** (2011) [1011.2907]. 8

[17] B. Audren, J. Lesgourgues, G. Mangano, P.D. Serpico and T. Tram, *Strongest model-independent bound on the lifetime of dark matter*, *Journal of Cosmology and Astroparticle Physics* **2014** (2014) 028–028 [1407.2418]. 8

[18] C.G. Bollini and J.J. Giambiagi, *Dimensional Renormalization: The Number of Dimensions as a Regularizing Parameter*, *Nuovo Cim. B* **12** (1972) 20. 11

[19] M. Peskin and D. Schroeder, *An Introduction to Quantum Field Theory*, Westview Press (1995). 12, 13

[20] A. Denner, *Techniques for calculation of electroweak radiative corrections at the one loop level and results for W physics at LEP-200*, *Fortsch. Phys.* **41** (1993) 307 [0709.1075]. 18, 25, 26

[21] S. Kanemura, Y. Okada, E. Senaha and C.-P. Yuan, *Higgs coupling constants as a probe of new physics*, *Physical Review D* **70** (2004) [hep-ph/0408364]. 26

[22] S. Kanemura, M. Kikuchi and K. Yagyu, *Fingerprinting the extended higgs sector using one-loop corrected higgs boson couplings and future precision measurements*, *Nuclear Physics B* **896** (2015) 80–137 [1502.07716]. 18, 26

[23] J. Fleischer and F. Jegerlehner, *Radiative corrections to higgs-boson decays in the weinberg-salam model*, *Phys. Rev. D* **23** (1981) 2001. 18

[24] M. Krause, R. Lorenz, M. Muhlleitner, R. Santos and H. Ziesche, *Gauge-independent Renormalization of the 2-Higgs-Doublet Model*, *JHEP* **09** (2016) 143 [1605.04853]. 28

[25] M. Krause, D. Lopez-Val, M. Muhlleitner and R. Santos, *Gauge-independent Renormalization of the N2HDM*, *JHEP* **12** (2017) 077 [1708.01578]. 18, 30

[26] A. Bredenstein, A. Denner, S. Dittmaier and M.M. Weber, *Precise predictions for the Higgs-boson decay H —> WW/ZZ —> 4 leptons*, *Phys. Rev. D* **74** (2006) 013004 [hep-ph/0604011]. 26

[27] D. Binosi and J. Papavassiliou, *Pinch technique: Theory and applications*, *Physics Reports* **479** (2009) 1–152 [0909.2536]. 28

[28] F. Staub, *From Superpotential to Model Files for FeynArts and CalcHep/CompHep*, *Comput. Phys. Commun.* **181** (2010) 1077 [0909.2863]. 34

[29] F. Staub, *Automatic Calculation of supersymmetric Renormalization Group Equations and Self Energies*, *Comput. Phys. Commun.* **182** (2011) 808 [1002.0840].

[30] F. Staub, *SARAH 3.2: Dirac Gauginos, UFO output, and more*, *Comput. Phys. Commun.* **184** (2013) 1792 [1207.0906].

[31] F. Staub, *SARAH 4 : A tool for (not only SUSY) model builders*, *Comput. Phys. Commun.* **185** (2014) 1773 [1309.7223].

[32] F. Staub, *Exploring new models in all detail with SARAH*, *Adv. High Energy Phys.* **2015** (2015) 840780 [1503.04200]. 34

[33] M. Thomson, *Modern particle physics*, Cambridge University Press, New York (2013). 39, 40, 41

[34] A. Djouadi, J. Kalinowski and M. Spira, *HDECAY: A Program for Higgs boson decays in the standard model and its supersymmetric extension*, *Comput. Phys. Commun.* **108** (1998) 56 [hep-ph/9704448]. 48, 52

[35] A. Djouadi, J. Kalinowski, M. Muehlleitner and M. Spira, *HDECAY: Twenty$_{++}$ years after*, *Comput. Phys. Commun.* **238** (2019) 214 [1801.09506]. 48, 52

[36] N.D. Christensen and C. Duhr, *FeynRules - Feynman rules made easy*, *Comput. Phys. Commun.* **180** (2009) 1614 [0806.4194]. 51

[37] C. Degrande, C. Duhr, B. Fuks, D. Grellscheid, O. Mattelaer and T. Reiter, *UFO - The Universal FeynRules Output*, *Comput. Phys. Commun.* **183** (2012) 1201 [1108.2040].

[38] A. Alloul, N.D. Christensen, C. Degrande, C. Duhr and B. Fuks, *FeynRules 2.0 - A complete toolbox for tree-level phenomenology*, *Comput. Phys. Commun.* **185** (2014) 2250 [1310.1921]. 51

[39] J. Kublbeck, M. Bohm and A. Denner, *Feyn Arts: Computer Algebraic Generation of Feynman Graphs and Amplitudes*, *Comput. Phys. Commun.* **60** (1990) 165. 51

[40] T. Hahn, *Generating Feynman diagrams and amplitudes with FeynArts 3*, *Comput. Phys. Commun.* **140** (2001) 418 [hep-ph/0012260]. 51

[41] R. Mertig, M. Bohm and A. Denner, *FEYN CALC: Computer algebraic calculation of Feynman amplitudes*, *Comput. Phys. Commun.* **64** (1991) 345. 51

[42] V. Shtabovenko, R. Mertig and F. Orellana, *New Developments in FeynCalc 9.0*, *Comput. Phys. Commun.* **207** (2016) 432 [1601.01167]. 51

[43] T. Hahn and M. Perez-Victoria, *Automatized one loop calculations in four-dimensions and D-dimensions*, *Comput. Phys. Commun.* **118** (1999) 153 [hep-ph/9807565]. 51

[44] G.J. van Oldenborgh and J.A.M. Vermaseren, *New Algorithms for One Loop Integrals*, *Z. Phys. C* **46** (1990) 425. 51

[45] R. Coimbra, M.O.P. Sampaio and R. Santos, *ScannerS: Constraining the phase diagram of a complex scalar singlet at the LHC*, *Eur. Phys. J. C* **73** (2013) 2428 [1301.2599]. 51

[46] M. Mühlleitner, M.O.P. Sampaio, R. Santos and J. Wittbrodt, *ScannerS: Parameter Scans in Extended Scalar Sectors*, 2007.02985. 51

[47] P. Bechtle, D. Dercks, S. Heinemeyer, T. Klingl, T. Stefaniak, G. Weiglein et al., *HiggsBounds-5: Testing Higgs Sectors in the LHC 13 TeV Era*, 2006.06007. 52

[48] P. Bechtle, S. Heinemeyer, T. Klingl, T. Stefaniak, G. Weiglein and J. Wittbrodt, *HiggsSignals-2: Probing new physics with precision Higgs measurements in the LHC 13 TeV era*, *Eur. Phys. J. C* **81** (2021) 145 [2012.09197]. 52

[49] G. Belanger, F. Boudjema, A. Pukhov and A. Semenov, *MicrOMEGAs 2.0: A Program to calculate the relic density of dark matter in a generic model*, *Comput. Phys. Commun.* **176** (2007) 367 [hep-ph/0607059]. 52

[50] G. Belanger, F. Boudjema, A. Pukhov and A. Semenov, *Dark matter direct detection rate in a generic model with micrOMEGAs 2.2*, *Comput. Phys. Commun.* **180** (2009) 747 [0803.2360].

[51] G. Bélanger, F. Boudjema, A. Goudelis, A. Pukhov and B. Zaldivar, *micrOMEGAs5.0 : Freeze-in*, *Comput. Phys. Commun.* **231** (2018) 173 [1801.03509]. 52

[52] Planck collaboration, *Planck 2018 results. VI. Cosmological parameters*, *Astron. Astrophys.* **641** (2020) A6 [1807.06209]. 52

[53] XENON collaboration, *Dark Matter Search Results from a One Ton-Year Exposure of XENON1T*, *Phys. Rev. Lett.* **121** (2018) 111302 [1805.12562]. 52, 54

[54] I. Engeln, M. Mühlleitner and J. Wittbrodt, *N2HDECAY: Higgs Boson Decays in the Different Phases of the N2HDM*, *Comput. Phys. Commun.* **234** (2019) 256 [1805.00966]. 52

[55] G. Arcadi, A. Djouadi and M. Raidal, *Dark Matter through the Higgs portal*, *Phys. Rept.* **842** (2020) 1 [1903.03616]. 53, 54

Appendix A

Dark Doublet Phase

In this appendix we present additional information, regarding the reparameterization and the couplings of the Dark Doublet Phase of the N2HDM.

A.1 Reparametrization

In subsection 2.3.1, we described the process by which we rotate the system from the gauge basis to the mass basis, and the associated reparameterization. Here, we shall explicitly derive the relations between the gauge basis parameters and the mass basis parameters.

We start by expressing the mass parameters m_{11}^2 and m_S^2 as a function of the VEVs v and v_S by using the DDP stationary conditions in equation 2.15 such that

$$m_{11}^2 = -\frac{1}{2}(v_1^2\lambda_1 + v_S^2\lambda_7) \tag{A.1a}$$

$$m_S^2 = -\frac{1}{2}(v_1^2\lambda_7 + v_S^2\lambda_6) \tag{A.1b}$$

From the diagonalization of the CP-even mass matrix, presented in equation 2.21, we get the following conditions

$$m_{H_1}^2 = v^2\lambda_1 \cos\alpha^2 + v_S^2\lambda_6 \sin\alpha^2 + vv_S\lambda_7 \sin 2\alpha \tag{A.2a}$$

$$m_{H_2}^2 = v^2\lambda_1 \sin\alpha^2 + v_S^2\lambda_6 \cos\alpha^2 - vv_S\lambda_7 \sin 2\alpha \tag{A.2b}$$

$$0 = -v^2\lambda_1 \cos\alpha \sin\alpha + v_S^2\lambda_6 \cos\alpha \sin\alpha + vv_S\lambda_7 \cos 2\alpha \tag{A.2c}$$

The dark sector fields are already mass eigenstates and their masses are given by

$$m_{H_D}^2 = \frac{1}{2}(2m_{22}^2 + v^2(\lambda_3 + \lambda_4 + \lambda_5) + v_S^2\lambda_8) \tag{A.3a}$$

$$m_{A_D}^2 = \frac{1}{2}(2m_{22}^2 + v^2(\lambda_3 + \lambda_4 - \lambda_5) + v_S^2\lambda_8) \tag{A.3b}$$

$$m_{H_D^\pm}^2 = \frac{1}{2}(2m_{22}^2 + v^2\lambda_3 + v_S^2\lambda_8) \tag{A.3c}$$

Using the conditions from equations A.1, A.2 and A.3, we solve a system of equations that allows us to write the gauge basis parameters as functions of the mass basis parameters. The resulting relations are

$$\lambda_1 = \frac{1}{v^2}\left(m_{H_1}^2 \cos^2\alpha + m_{H_2}^2 \sin^2\alpha\right) \tag{A.4a}$$

$$\lambda_3 = \frac{1}{v^2}\left(2(m_{H_D^\pm}^2 - m_{22}^2) - v_S\lambda_8\right) \tag{A.4b}$$

$$\lambda_4 = \frac{1}{v^2}\left(m_{H_D}^2 + m_{A_D}^2 - 2m_{H_D^\pm}^2\right) \tag{A.4c}$$

$$\lambda_5 = \frac{1}{v^2}\left(m_{H_D}^2 - m_{A_D}^2\right) \tag{A.4d}$$

$$\lambda_6 = \frac{1}{v_S^2}\left(m_{H_1}^2 \sin^2\alpha + m_{H_2}^2 \cos^2\alpha\right) \tag{A.4e}$$

$$\lambda_7 = \frac{1}{vv_S}\left(m_{H_1}^2 - m_{H_2}^2\right)\cos\alpha\sin\alpha \tag{A.4f}$$

Like we mentioned in subsection 2.3.1, the dark parameters m_{22}, λ_2 and λ_8 cannot be expressed as a functions of the physical parameters and are, therefore, included in the mass basis parameter set.

A.2 Scalar Trilinear Couplings

Here we present all scalar trilinear couplings for the DDP of the N2HDM. These trilinear couplings $\lambda_{X_iX_jX_k}$ are given by

$$\lambda_{X_iX_jX_k} = \frac{\partial}{\partial X_i}\frac{\partial}{\partial X_j}\frac{\partial}{\partial X_k}\mathcal{L} \tag{A.5}$$

where $X_{i/j/k}$ represents any scalar field in the mass basis. The DDP contains the following scalar trilinear couplings

$$\lambda_{H_iH_iH_i} = -\frac{3m_{H_i}^2}{vv_S}\left(v_S R_{i1}^3 + vR_{i2}^3\right) \tag{A.6a}$$

$$\lambda_{H_iH_jH_j} = -\frac{2m_{H_i}^2 + m_{H_j}^2}{vv_S}\left(v_S R_{i1}R_{j1}^2 + vR_{i2}R_{j2}^2\right) \tag{A.6b}$$

$$\lambda_{H_iH_DH_D} = \frac{R_{i1}}{v}\left(\lambda_8 v_S^2 + 2\left(m_{22}^2 - m_{H_D}^2\right)\right) - R_{i2}\lambda_8 v_S \tag{A.6c}$$

$$\lambda_{H_iA_DA_D} = \frac{R_{i1}}{v}\left(\lambda_8 v_S^2 + 2\left(m_{22}^2 - m_{A_D}^2\right)\right) - R_{i2}\lambda_8 v_S \tag{A.6d}$$

$$\lambda_{H_iH_D^+H_D^-} = \frac{R_{i1}}{v}\left(\lambda_8 v_S^2 + 2\left(m_{22}^2 - m_{H_D^\pm}^2\right)\right) - R_{i2}\lambda_8 v_S \tag{A.6e}$$

where $i, j \in \{1, 2\}$, $i \neq j$ and R is the rotation matrix defined in equation 2.20. We can see that dark particles always appear in pairs in these couplings. This is due to a conserved "darkness" quantum number that results from the unbroken $\mathbb{Z}_2^{(1)}$ symmetry in equation 2.3a.

A.3 Scalar Quadrilinear Couplings

Here we present all scalar quadrilinear couplings for the DDP of the N2HDM. These quadrilinear couplings $\lambda_{X_iX_jX_kX_l}$ are given by

$$\lambda_{X_iX_jX_kX_l} = \frac{\partial}{\partial X_i}\frac{\partial}{\partial X_j}\frac{\partial}{\partial X_k}\frac{\partial}{\partial X_l}\mathcal{L} \tag{A.7}$$

where $X_{i/j/k/l}$ represents any scalar field in the mass basis. The DDP contains the following scalar quadrilinear couplings

$$\lambda_{H_iH_iH_DH_D} = \frac{R_{i1}^2}{v^2}\left(\lambda_8 v_S^2 + 2\left(m_{22}^2 - m_{H_D}^2\right)\right) - R_{i2}^2\lambda_8 \tag{A.8a}$$

$$\lambda_{H_iH_iA_DA_D} = \frac{R_{i1}^2}{v^2}\left(\lambda_8 v_S^2 + 2\left(m_{22}^2 - m_{A_D}^2\right)\right) - R_{i2}^2\lambda_8 \tag{A.8b}$$

$$\lambda_{H_1H_2H_DH_D} = -\frac{\cos\alpha\sin\alpha}{v^2}\left(\lambda_8(v^2+v_S^2) + 2\left(m_{22}^2 - m_{H_D}^2\right)\right) \tag{A.8c}$$

$$\lambda_{H_1H_2A_DA_D} = -\frac{\cos\alpha\sin\alpha}{v^2}\left(\lambda_8(v^2+v_S^2) + 2\left(m_{22}^2 - m_{A_D}^2\right)\right) \tag{A.8d}$$

where $i \in \{1,2\}$ and R is the rotation matrix defined in equation 2.20. While there are a lot more quadrilinear couplings in the DDP, we present only the relevant ones for this project.

Appendix B

$\overline{\text{MS}}$ Renormalization Scheme

In this appendix we discuss additional details about the $\overline{\text{MS}}$ renormalizations scheme.

B.1 Calculation of Δv_S

In this section we present the explicit calculation of the counter-term Δv_S in the $\overline{\text{MS}}$ scheme. Like we discussed in subsection 3.7.1, this counter-term is necessary in order to obtain a finite one-loop amplitude.

We start by referring to section 3.3, where we discussed the ATS. In the ATS, both the self-energies and the one-loop vertex corrections contain both non-tadpole and tadpole contributions, as represented in figure B.1. We shall refer to the non-tadpole contributions as the usual contributions. If we treat each contribution separately, we realize that the divergences originating from the usual contributions vanish just by using the $\overline{\text{MS}}$ counter-terms δm_{22}^2 and $\delta\lambda_8$. However, this is not the case for the tadpole contributions. In order to cancel the remaining divergences coming from the tadpole contributions, we fix the counter-term Δv_S in such way that it cancels these divergences. For simplicity, we shall present the calculation using the process $H_1 \to H_D H_D$, as the calculation is analogous to all other processes.

We start by expressing analytically the tadpole contributions to the one-loop corrections. Using the definition in equation 3.93, we can represent the tadpole contributions as

$$\mathcal{M}^{\text{1-loop}}_{H_1\to H_D H_D}\big|_{\text{tad}} = \mathcal{M}^{\text{VC}}_{H_1\to H_D H_D}\big|_{\text{tad}} + \mathcal{M}^{\text{CT}}_{H_1\to H_D H_D}\big|_{\text{tad}} \tag{B.1}$$

The tadpole contribution for the vertex correction is given by the expression in equation 3.49, which can be written as

$$\mathcal{M}^{\text{VC}}_{H_1\to H_D H_D}\big|_{\text{tad}} = \lambda_{H_1H_1H_DH_D}\frac{T_{H_1}}{m^2_{H_1}} + \lambda_{H_1H_2H_DH_D}\frac{T_{H_2}}{m^2_{H_2}} \tag{B.2}$$

As for the counter-term amplitude, the tadpole contributions come from the counter-terms appearing in equation 5.4. However, not all counter-terms have tadpole contributions. The $\overline{\text{MS}}$ counter-terms δm_{22}^2 and $\delta\lambda_8$ do not contain any tadpole contributions. The same happens for the counter-terms $\delta Z_{H_1H_1}$ and $\delta Z_{H_DH_D}$. From equations 3.52a and 3.56a, we see that these counter-terms are the derivative with

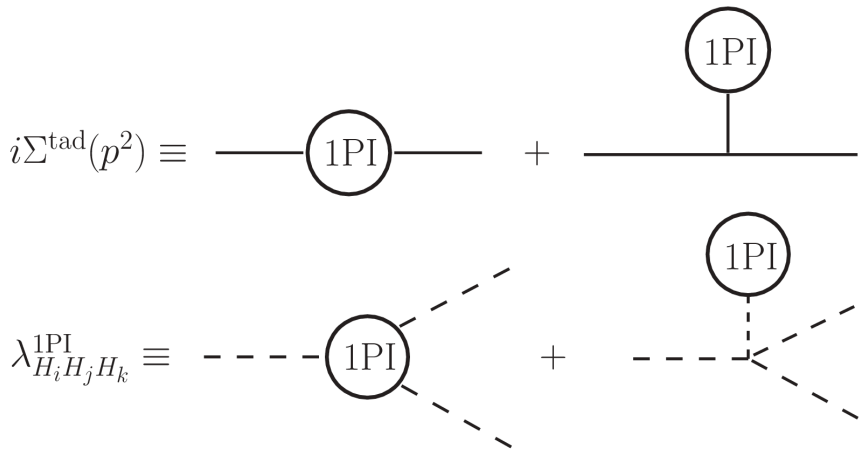

Figure B.1: Tadpole decomposition. Decomposition of the self-energy and vertex correction contributions into usual contributions and tadpole contributions.

respect to the squared external momentum of the self-energies. Since the tadpole contributions to the self-energies do not depend on the external momentum, the tadpole contributions from the counter-terms $\delta Z_{H_1H_1}$ and $\delta Z_{H_DH_D}$ vanish. Therefore, the expression for the tadpole contributions to the counter-term amplitude is given by

$$\begin{aligned}\mathcal{M}^{\text{CT}}_{H_1\to H_DH_D}\big|^{\Delta v_S=0}_{\text{tad}} = \lambda_{H_2H_DH_D}\left(\frac{\delta Z_{H_2H_1}}{2}+\delta\alpha\right)\Big|_{\text{tad}} \\ -\frac{2c_\alpha}{v^2}\left(\frac{v_S\lambda_8}{2}+m^2_{22}-m^2_{H_D}\right)\Delta v\Big|_{\text{tad}} - \frac{2c_\alpha}{v}\delta m^2_{H_D}\Big|_{\text{tad}}\end{aligned} \tag{B.3}$$

where we omitted the term with Δv_S as we only want to identify the leftover divergent terms. The first term of equation B.3 vanishes. This can be demonstrated by using the definitions in equations 3.52d and 3.78, obtaining the result

$$\left(\frac{\delta Z_{H_2H_1}}{2}+\delta\alpha\right)\Big|_{\text{tad}} = \frac{1}{2(m^2_{H_1}-m^2_{H_2})}\left[\Sigma^{Tad}_{H_1H_2}(m^2_{H_2})-\Sigma^{Tad}_{H_1H_2}(m^2_{H_1})\right]\Big|_{\text{tad}} = 0 \tag{B.4}$$

where we used the relation

$$\Sigma^{Tad}_{H_1H_2}(m^2_{H_2})\Big|_{\text{tad}} = \Sigma^{Tad}_{H_1H_2}(m^2_{H_1})\Big|_{\text{tad}} = \lambda_{H_2H_1H_1}\frac{T_{H_1}}{m^2_{H_1}}+\lambda_{H_1H_2H_2}\frac{T_{H_2}}{m^2_{H_2}} \tag{B.5}$$

The tadpole contributions coming from the counter-term $\delta m^2_{H_D}$ are simply written as

$$\delta m^2_{H_D}\big|_{\text{tad}} = \lambda_{H_1H_DH_D}\frac{T_{H_1}}{m^2_{H_1}}+\lambda_{H_2H_DH_D}\frac{T_{H_2}}{m^2_{H_2}} \tag{B.6}$$

Regarding the counter-term Δv, we see from equation 3.61 that its tadpole contributions originate from the electroweak counter-terms discussed in subsections 3.5.1 and 3.5.2. The charge counter-term

δZ_e does not contain any tadpole contributions. Therefore, the only tadpole contributions to Δv come from the mass counter-terms δm_W^2 and δm_Z^2. From equations 3.64 and 3.66, we see that the tadpole contributions from these counter-terms are simply the tadpole diagrams for the W and Z bosons self energies, that can be written generally as

$$\Sigma_{VV}^{Tad,T}\Big|_{\text{tad}} = -\left(c_\alpha \frac{T_{H_1}}{m_{H_1}^2} - s_\alpha \frac{T_{H_2}}{m_{H_2}^2}\right) \tag{B.7}$$

where $V \in \{W, Z\}$. Therefore, we can write the tadpole contribution from the counter-term Δv as

$$\begin{aligned} \frac{\Delta v}{v}\Big|_{\text{tad}} &= \frac{1}{2(m_Z^2 - m_W^2)}\left(\frac{m_Z^2}{m_W^2}\Sigma_W^{Tad,T}\Big|_{\text{tad}} - \frac{m_W^2}{m_Z^2}\Sigma_{ZZ}^{Tad,T}\Big|_{\text{tad}}\right) \\ &= -\frac{1}{v}\left(c_\alpha \frac{T_{H_1}}{m_{H_1}^2} - s_\alpha \frac{T_{H_2}}{m_{H_2}^2}\right) \end{aligned} \tag{B.8}$$

Replacing all the explicit tadpole contributions into equation B.3, we get the expression

$$\begin{aligned} \mathcal{M}^{\text{CT}}_{H_1 \to H_D H_D}\big|_{\text{tad}} &= \left(\lambda_{H_1 H_1 H_D H_D} + \frac{2c_\alpha^2}{v^2}\left(\frac{\lambda_8 v_S}{2} + m_{22}^2 - m_{H_D}^2\right) - \frac{2c_\alpha}{v}\lambda_{H_1 H_D H_D}\right)\frac{T_{H_1}}{m_{H_1}^2} \\ &+ \left(\lambda_{H_1 H_2 H_D H_D} - \frac{2c_\alpha s_\alpha}{v^2}\left(\frac{\lambda_8 v_S}{2} + m_{22}^2 - m_{H_D}^2\right) - \frac{2c_\alpha}{v}\lambda_{H_2 H_D H_D}\right)\frac{T_{H_2}}{m_{H_2}^2} \\ &= \lambda_8\left(\frac{2v_s c_\alpha}{v} - s_\alpha\right)\left(s_\alpha \frac{T_{H_1}}{m_{H_1}^2} + c_\alpha \frac{T_{H_2}}{m_{H_2}^2}\right) \end{aligned} \tag{B.9}$$

The final result contains the tadpole terms T_{H_1} and T_{H_2} that contain divergent terms. We want to fix Δv_S in such way that it cancels the remaining divergence exactly. To achieve this, the term with Δv in equation 5.4, must cancel the divergent part of the result in equation B.9. Therefore, we get the condition

$$\Delta v_S = -\left(s_\alpha \frac{T_{H_1}}{m_{H_1}^2} + c_\alpha \frac{T_{H_2}}{m_{H_2}^2}\right)_{\text{div}} \tag{B.10}$$

This condition ensures that the one-loop corrections to the amplitude of the process is finite, under the $\overline{\text{MS}}$ renormalization scheme.